STOCHASTIC APPROACHES TO HETEROGENEOUS AND COMPLEX REACTION KINETICS

Thesis Submitted for the degree of

Doctor of Philosophy (Sc.)

in

Chemistry (Physical)

by

BISWAJIT DAS

UNIVERSITY OF CALCUTTA

2012

TO MY LATE FATHER

Acknowledgements

Date:

Biswajit Das
Satyendra Nath Bose National Centre for Basic Sciences
Block-JD, Sector-III, Salt Lake, Kolkata, India.

Contents

Chapter 1

Introduction

For the biochemical reactions in living systems, the knotty issues arise due to the accessibility, distribution and orientation of the proteins or enzymes to react with the substrates and the overall reaction dynamics is governed by the the chemical and mechanical steps involved[1, 2, 3]. Heterogeneity is also developed in systems with countably small number of reactants with multiple conformations or with various diffusion mechanisms and in some situations additional complexity comes in due to the diffusion of ions under an applied external field in the environment of proteins[4, 5]. Not only in the bulk but now it is also possible to monitor a single enzyme activity in a heterogeneous and complex environment[1, 2] with the advent of single molecule force-clamp technique like atomic force microscopy[6] and fluorescence imaging techniques like wide-field and confocal microscopy. On the other hand, the study of interfacial enzymatic reaction is gaining increasing attention in biological systems as an enzyme plays a crucial role of lipid metabolism and as mediator of intercellular signalling processes[1, 2, 3, 7]. Even a reaction in a homogeneous solution with very few number of reactants the kinetics can be stochastic in nature where fluctuation of the number of reactants become as important as the mean number and the traditional rate equation picture of kinetics fails miserably [8, 9, 10]. Usually the dynamics of chemical reactions at the level of single or few molecules can be described by the chemical master equation where the time evolution of the number of reactants or conformations is considered as a kind of random-walk process in the population or conformational state space[11, 12, 13, 14, 15]. Further source of statistical inhomogeneity comes in when some non-chemical rate processes are involved namely, due to various diffusive mechanical movement of particles over several phases[1, 2], for different interactions among the conformational states of a reactant [11] and during random as well as biased attachment and detachment of ligands to a receptor[12] with many active sites. In ion channels the complexity comes in due to the movement of the ions through the channels made by the charged proteins with multiple conformations under the biased voltage along with the diffusive motion of the ions[4, 5].

In the proposed thesis, our main motivation is to study the kinetic and thermo-dynamic aspects of some heterogeneous and complex biochemical processes with the emphasis on the enzyme catalysis and ion transport in proteins. To deal with such complex systems, we resort to the master equation approach which offers a general framework to characterize a dynamical system in terms of some rate processes in various time and space scales. From the kinetics of such a process through a master equation, a straight forward non-equilibrium thermodynamic characterization is also possible using the recently developed fluctuation theorems. For example, to describe the interfacial enzyme kinetics of lipid metabolism, one needs to consider the mechanical motion of the enzyme on the fluid and product phases as well as the chemical reaction steps involved[1, 2]. For this kind of inhomogeneous situation analytical master equation is of no help and a kinetic Monte Carlo simulation technique is the only option[16]. Again for a single oligomeric enzyme with a few number of active sites, analytical model of master equation description of the kinetics provides immense qualitative understanding about the effect of external mechanical force on the reaction[12, 17]. Similar master equation can also explain the non-equilibrium cooperativity phenomena developed in single oligomeric enzyme at chemiostatic condition on the basis of different substrate binding mechanisms[18]. The kinetics and non-equilibrium thermodynamics of a voltage gated potassium ion channel in presence of constant as well as oscillating voltages can also be studied in terms of the master equation. The common underlying thread here is a master equation description of single molecule activity to understand the overall kinetics and nonequilibrium thermodynamics of various heterogeneous biochemical processes by which ultimately the reaction in bulk can be predicted. In the present thesis en-titled, "Stochastic approaches to heterogeneous and complex reaction kinetics" we have discussed the related issues with the emphasis on the following topics.

A. Interfacial enzyme kinetics

The study of interfacial enzymatic reaction is important in biological science as enzyme plays a crucial role as a catalyst of lipid metabolism. Berg *et al.*[3, 7, 19], Jain *et al.*[20] and Ghomashchi *et al.*[21, 22] carried out several experiments in bulk solution to understand the action of the interfacial enzyme, phospholipase, namely, PLA_1 and PLA_2, on the phospholipid vesicles, micelles or mono-layer. They observed that the interfacial enzymes hydrolyze the phospholipid molecules either in the scooting or hopping mechanism[3, 20]. They also found the lag-burst phe-nomenon which is characterized by initial slow hydrolysis in the lag phase, followed by a sudden increase in activity of the enzyme by two or three orders of magnitude, the burst phase[3]. Later, Honger *et al.*[23], Jorgensen *et al.* [24] and Mouritsen *et al.*[25] extensively studied the lag-burst phenomenon both experimentally and theo-retically. They observed that the formation of an appreciable size of product domain is responsible for the lag-burst kinetics. Recently, Gudmand *et al.* have studied the

action of PLA$_2$ on phospholipid monolayers by the wide-field fluorescence microscope with single molecule sensitivity[1]. From this experiment it is now possible to directly visualize the activity and diffusive behavior of single PLA$_2$ enzyme in a heterogeneous lipid environment during active hydrolysis. Although a lot of kinetic analysis had been performed[23, 25], it is pertinent here to develop a microscopic theory based on the single enzyme experimental data and the theory should meet the kinetic result in the limit of bulk interfacial catalysis.

B. Effect of external force on reaction kinetics

Recently, with the advent of atomic force microscope(AFM) or magnetic or optical tweezers, pulling experiments have been widely used to probe the subangstrom level changes[26, 27]. Single molecule force spectroscopy represents a novel experimental method to perform mechanochemistry, in which forces of the order of 10-100 pN applied in manipulating transition state structure even in the solution phase or in living cells to understand chemical reactivity[26, 27, 28, 29, 30]. Originally, Bell had shown that the rate of the chemical reaction in cell to cell adhesion process is influenced by the hydrodynamic forces[31]. Now this concept is extended to arbitrary chemical reactions in biosystem using external mechanical force. In a series of works, Szabo and others have established the concept of single molecule pulling experiment to get kinetics and non-equilibrium thermodynamics[32, 33]. Fernandez *et al.* have championed the idea of controlling chemical reaction kinetics by the mechanical force by first showing the reduction in disulphide bonds in a protein, a thiol/disulphide exchange reaction, as this reaction serves as the key step in the function of folding processes of proteins[28, 29, 30]. It is shown that ten fold increase in reduction rate is possible by applying force over 300 pN range through a force-clamp AFM on an engineered polyprotein. Recent experimental and theoretical analysis of Gumpp *et al.* on the single molecule level by the triggering of enzymatic activity through AFM opens the new avenue to study the direct influence of force to manipulate bio-catalytic reactions[6]. Although a great deal of theoretical effort has been utilized on the exploration of single molecule mechano-chemical systems, the attempt to find out the nonequilibrium dynamical properties as a consequence of the fluctuation theorem is not yet explored with its full potential. Here it is relevant to show how the trajectory based approach can provide the kinetic and thermodynamic effect of mechanical force in an oligomeric enzyme catalysis.

C. Cooperativity in oligomeric enzyme

Cooperativity phenomenon is mainly developed in the oligomeric proteins due to different binding affinity of ligands to the subunits of the protein or enzyme[34, 35]. The oligomeric proteins show either positive, negative or no cooperativity phenomenon. The common example of positive cooperativity is the binding of oxygen molecule to hemoglobin and the binding curve is sigmoidal in nature. However, binding curve of oxygen of closely related myoglobin becomes hyperbolic in nature

which is an example of no cooperativity phenomenon. In 1910, A.V. Hill made a first attempt to interpret the sigmoidal binding curve of oxygen of hemoglobin by assuming that all ligand molecules would have to bind to the oligomeric protein simultaneously and to characterize the nature of cooperativity he introduced the Hill coefficient[34, 35]. For positive and negative cooperative cases, the Hill coefficient, becomes greater than or less than one, respectively, whereas the non-cooperative case is characterized by Hill coefficient equal to one. By considering all individual binding steps, Adair first systematically described the sigmoidal binding curve of the oxygen of hemoglobin[36]. These types of cooperativity based on the affinity of the ligand binding belong to the class of allosteric cooperativity. In 1965, Monod, Wyman and Changeux presented the first comprehensive model for the description of allosteric enzyme which is sometimes referred to as the symmetrical model or MWC model[37]. It became a guideline for the improved understanding of regulatory mechanisms on enzymes. However, the drawback is that the negative cooperativity phenomenon can not be explained by this model. In 1976 Koshland, Nemethy and Filmer proposed an alternative model for allosteric enzymes, the concerted model which described the positive, negative as well as no cooperativity phenomenon[38]. These two models are widely used to describe the allosteric cooperativity. There is another type of cooperativity, termed as temporal cooperativity[39], reflected in the zero-order ultra sensitivity of the phosphorylation-dephosphorylation cycle which is shown to be mathematically equivalent to the allosteric cooperativity Beside allosterism, cooperativity has been studied in monomeric enzymes with only a single substrate binding site. This has led to the important concept of hysteretic[40, 41, 42] and mnemonic enzymes[43, 44]. These two types of enzymes show the cooperativity phenomena due to the slow conformational disorder of the active site. Clearly, a general classification of cooperativity based on the above substrate binding mechanisms for a single oligomeric enzyme is needed here which can provide a theoretical basis of kinetic and thermodynamic origin of cooperativity.

D. Ion channel kinetics and thermodynamics

Voltage-gated ion channel is a transmembrane protein which plays an important role in the propagation of nerve impulse[45, 46]. In 1952, Hodgkin and Huxley first proposed a mathematical model to explain the ionic mechanism underlying the initiation and propagation of nerve impulse in the squid giant axon[47]. They have calculated the potassium and sodium ion conductance by considering some phenomenological equations which are still valid now. By using the voltage clamp technique, they had experimentally determined the sodium and potassium channel conductance. In the voltage clamp technique, ion flow across a cell membrane is measured as electric current, while the membrane voltage is held under experimental control with a feedback circuit[47, 48]. Neher and Sakmann had advanced this research field by inventing the patch-clamp technique which permits the possibility

of measuring ionic current through the individual ion channels[5]. The experimental works by Skaugen *et al.*[49], Hille *et al.*[50] and Nossal *et al.*[51] demonstrated that the individual ion channels are essentially stochastic entities that open and close in a random way. The experimental and theoretical work by DeFelice and co-workers produced a computer model to describe the noise properties of clusters of ion channels in a small area of membrane[52]. Later Fox *et al.* had given a stochastic description of the kinetics of many ion channels by considering the master equation[53]. After isolation of individual sodium and potassium ion channels, several workers have studied the single ion channel kinetics experimentally to understand how the ion channel works. To describe the single sodium or potassium ion channel kinetics, several Markov models had been proposed. However, to select the appropriate Markov model from various possible schemes of ion channel kinetics, several experiments are carried out[4, 48]. For example, Zagotta*et al.* had performed an experiment for the selection of the best suited Markov model for the description of potassium ion channel kinetics[48, 54, 55]. In recent years, Millonas and co-workers have invented the non-equilibrium response spectroscopy for the selection of the best Markov models of sodium and potassium ion channel kinetics at non-equilibrium situation[56, 57]. In this technique they have used the oscillating voltage protocol which drive the ion channel out of equilibrium. Therefore, it is now possible to study the ion channel kinetics at the non-equilibrium condition which can provide the information about the thermodynamic response properties such as dynamical hysteresis at non-equilibrium steady state(NESS).

1.1   Scope of the thesis

The scope of studying the heterogeneous and complex reactions within the general purview of kinetics and non-equilibrium thermodynamics to interpret both for microscopic and macroscopic feature is vast. Therefore, in the present thesis we have worked on some specific aspects of this broad topic theoretically by considering some important biological systems using relevant experimental parameters for realistic applications. Consideration of stochastic approach becomes essential to describe the fluctuation in small system as the fluctuation carries the information about the structure and non-equilibrium behavior[58] and sometimes it becomes so large that it can affect the overall dynamics of the system in an irreproducible way [8, 9, 10, 59]. By incorporating the stochastic ideas, McQuarrie first systematically explained the kinetics of the small chemically reacting systems containing a finite number of molecules[8, 9, 10]. Based on some phenomenological assumptions, he constructed the differential-difference equation or chemical master equation to describe the time evolution of the various first order and second order reactions[10]. However, sometimes it becomes too difficult to obtain the analytical solution of the

master equation for complex reactions. To resolve this problem, in 1976 Gillespie had developed a time-dependent Monte-Carlo simulation technique[14], known as the stochastic simulation algorithm to obtain the information about the time evolution of any spatially homogeneous mixture of molecular species which interact through a specified set of coupled chemical reactions[14, 15]. The results obtained from the simulation is equivalent to the chemical master equation.

Nowadays the reaction kinetics can be studied at the single molecule level by using the single molecule spectroscopy[60, 61] and single molecule imaging technique[1]. From single molecule experiments, it is now possible to track the diffusive motion of an individual biological molecule[1, 2] and map out the probability distribution and correlation as a function of time[62]. The microscopic detailing of any reaction can also be obtained from the single molecule experiments. For example, by using the wide field fluorescence microscope, it becomes possible to visualize the activity and diffusion behavior of single interfacial enzyme, PLA_2 in a heterogeneous lipid environment during active hydrolysis[1]. Furthermore, these experiments help us to detect the molecular intermediates of a reaction and give the information about the thermodynamic and kinetic behavior of the reacting systems. Single molecule enzyme kinetics is widely studied both theoretically and experimentally due to its physiological importance in the regulation of the biological reactions[60, 61, 63, 64]. At the single molecule level, an enzymatic reaction becomes a stochastic event and in this experiment the waiting time for the completion of the enzymatic reaction is typically measured[60, 61]. The probability density of these waiting times, can be obtained by recording the histogram of many turnovers over a long period of time[61, 63]. Therefore, single-molecule kinetics cannot be formulated in terms of enzyme concentration, but must be formulated instead in terms of the probabilities for the enzyme to be in one of the possible states in the reaction pathway[63, 64]. By the single-molecule enzymatic experiment, it is now possible to distinguish the static and dynamic disorder of reaction rates, which are not possible in the ensemble-averaged experiments[60]. Usually the single molecule enzyme kinetics is studied at the chemiostatic condition where the concentrations of the substrate(s) and the product(s) remain approximately constant over the course of the entire experiment[64, 65]. From the thermodynamic analysis, it is observed that at the chemiostatic condition the reaction system goes to a non-equilibrium steady state(NESS) instead of equilibrium [12, 13, 64, 66, 67]. Ge *et al.*[68] and Qian *et al.*[39] also studied the non-equilibrium temporal cooperativity to describe the signal transduction module of phosphorylation-dephosphorylation cycle at NESS. Therefore, consideration of chemiostatic condition opens a new avenue to give the stochastic description of non-equilibrium cooperativity developed in a oligomeric protein due to different substrate binding mechanism. In recent years, single molecule force spectroscopy is used to manipulate the overall dynamics of the

reactions[27, 58]. Using this spectroscopic technique an external mechanical force is applied on a single molecule, which can change the thermodynamic stability of this molecule by increasing or decreasing the activation free energy of the reaction [27, 28, 29, 30, 58]. This external mechanical force can also drive the overall reaction far away from equilibrium. Recently Gumpp *et al.* have carried out an experiment at the single molecule level which demonstrated that the enzymatic activity can also be monitored by applying an external mechanical force through atomic force microscope(AFM)[6]. This experiment opens a new technique to study the direct influence of force to manipulate the bio-catalytic reactions. Dynamics of a protein molecule is usually studied at equilibrium but nowadays it becomes possible to study the protein dynamics at non-equilibrium condition by using some time-dependent external perturbation. For example, the kinetics of ion channel protein can be studied at non-equilibrium situation by applying an oscillating voltage protocol. This technique is used in non-equilibrium response spectroscopy developed by Millonas and co-workers[56, 57]. The oscillating voltage drives the ion channel out of equilibrium and resists the system to relax back to equilibrium [4, 56, 57, 69]. Using this technique it is now possible to select the appropriate Markov model from various possible schemes of ion channel kinetics. Therefore, this spectroscopic technique has added another exciting dimension in the field of ion channel experiments. Recently, Andersson *et al.*[70] have observed that using the oscillating voltage protocol, ion channel conductance shows the hysteretic behavior which makes a new area in the study of ion channel kinetics. With this background in mind we have made the following theoretical studies as our own contribution in the flow of the related research and development.

At first, we have described the interfacial enzyme kinetics by formulating a theory to explore the advancement of this reaction at the single enzyme level, which is ultimately utilized to obtain the ensemble average macroscopic feature, the lag-burst kinetics. We have provided a theory of the transition from the lag phase to the burst phase kinetics. The theory has been developed by considering the gradual development of electrostatic interaction among the positively charged enzyme and the negatively charged product molecules, deposited on the phospholipid surface. In the single trajectory analysis, it has been observed that the different diffusion time scales of the enzyme over the fluid and product regions, are responsible for the memory effect in the correlation of successive turnover events of the hopping mode. This memory effect is again reflected on the non-Gaussian distribution of turnover times on the macroscopic kinetics in the lag phase unlike the burst phase kinetics.

Next we have shown how an applied mechanical force affects an immobilized oligomeric enzyme kinetics in a chemiostatic condition. The statistical characteristics of random walk of the substrate molecules over a finite number of active sites of the enzyme plays an important contributing factor in governing the overall rate and

the non-equilibrium thermodynamic properties. The net rate of the reaction and the corresponding entropy production are determined through a chemical master equation and the analytical results are supported by the simulation, based on the single trajectory approach of Gillespie's stochastic algorithm. This microscopic numerical approach not only gives the macroscopic entropy production from the mean of the distribution of entropy production which depends on the force but also a broadening of the distribution by the applied mechanical force. In the non-equilibrium steady state(NESS), both the mean and the variance of the distribution increases and then saturates with the rise in applied force corresponding to the situation when the net rate of product formation reaches a limiting value with an activationless transition. It is also observed that at NESS, the net rate of the reaction is enhanced by more than two orders of magnitude with the application of an external mechanical force of the order of $10 - 100$ pN.

Then we have systematically studied the cooperative binding of substrate molecules on the active sites of a single oligomeric enzyme in a chemiostatic condition. The average number of bound substrate and the net velocity of the enzyme catalyzed reaction are studied by the formulation of master equation for the cooperative binding classified here as spatial and temporal. We have estimated the entropy production for the cooperative binding schemes based on single trajectory analysis using a kinetic Monte Carlo technique. It is found that the total as well as the medium entropy production show the same generic diagnostic signature for detecting the cooperativity, usually characterized in terms of the net velocity of the reaction. This feature is also found to be valid for the total entropy production rate at the non-equilibrium steady state(NESS). We have introduced an index of cooperativity defined in terms of the ratio of the surprisals or equivalently, the stochastic system entropy associated with the fully bound state of the cooperative and non-cooperative cases. The criteria of cooperativity in terms of the cooperativity index is compared with that of the Hill coefficient and gives a microscopic insight on the cooperative binding of substrate on a single oligomeric enzyme which is usually characterized by macroscopic reaction rate.

Finally, we have studied the non-equilibrium thermodynamic response of a voltage-gated *Shaker* potassium ion channel using master equation approach. For a constant external voltage, the system reaches equilibrium indicated by the vanishing total entropy production rate, whereas for oscillating voltage the current and entropy production rates show dynamic hysteretic behavior. Here we have shown quantitatively that although the hysteresis loop area vanishes in low and high frequency domains of the external voltage, they are thermodynamically distinguishable. At very low frequency domain, system remains close to equilibrium whereas at high frequency, it goes to a non-equilibrium steady state(NESS) associated with a finite value of dissipation function. At NESS, the efficiency of the ion-conduction can also

be related with the nonlinear dependence of the dissipation function on the power of the external field. Another intriguing aspect is that at the high frequency limit, the total entropy production rate oscillates at NESS with half of the time period of the external voltage.

1.2   Plan of the Thesis

We have presented the contents of the thesis in the following chapters.

In Chapter-II we have given a brief overview regarding the stochastic description of the kinetics as well as the thermodynamics of small chemical systems.

In Chapter-III the inhomogeneous interfacial enzyme kinetics is studied where mechanical and chemical processes of the enzyme are involved. We have provided a microscopic theory for single enzyme activity and consequently the ensemble average kinetics for the reaction in bulk surface.

In Chapter-IV we have constructed the master equation for an oligomeric enzyme and described how an applied mechanical force affects the enzyme kinetics in a chemiostatic condition.

Chapter-V is devoted to analyze the cooperative binding of substrate molecules on the active sites of a single oligomeric enzyme in a chemiostatic condition. Similar to that of Hill coefficient, we have introduced an index of cooperativity at non-equilibrium steady state.

In Chapter-VI we have studied the kinetic and non-equilibrium thermodynamic response of a voltage-gated *Shaker* Potassium ion channel for oscillating voltage protocol based on the master equation approach.

Chapter 2

Overview on the stochastic description of some small chemical systems

Chemical kinetics is generally described by the conventional deterministic rate equations where the concentrations of the reacting species are calculated as a function of time[8, 9]. However, the description of the kinetics by this approach needs serious modification to accommodate the fluctuation of the concentrations of the reactants of a small system containing a finite number of molecules[8, 9, 14, 15, 71, 72, 73]. In a small system, fluctuation carries the information about the structure and non-equilibrium dynamics[58] and sometimes it can overwhelmly affect the main course of the reaction[8, 59]. Stochastic approach provides an appropriate description of the inherent statistical nature as well as the fluctuating dynamics of the reaction system[8, 9, 13, 74]. An extreme limit of such consideration is the temporal fluctuation of catalytic rate of an enzyme observed in single-molecule fluorescence experiments[60, 61] which can not be described without consideration of probabilistic approach[63].

Incorporation of the stochastic ideas into chemical kinetics[59, 71, 75, 76, 77] was first successfully carried out by Kramers[75, 76], who treated a chemical reaction as a Brownian motion of particles, whose rate of passage over a potential barrier represents the rate of decomposition. After the work of Kramers, Delbruck[71] and Renyi[77] studied a stochastic model of the auto-catalytic reaction, A→B and showed that during the initial stages of reaction, the fluctuations in the number of reactant molecules was of the order of the square root of the number of reactant molecules. Singer discussed the application of a stochastic method to the study of *irreproducible reactions* such as the oxidation of formic acid by potassium nitrate and the slow or explosive decomposition of some solids and some initial stages of polymerization[59]. He concluded that in small system, large fluctuations in the number of reactant species could be responsible for irreproducible reactions to-

gether with the presence of impurities. In 1957, Bartholomay first explained the uni-molecular reaction, A→B by considering the Markovian approach[73] and then Ishida extended the Bartholomay's method to a more general stochastic process, having a time dependent rate constant[72]. However, McQuarrie championed the stochastic approaches[8, 9, 10], popularly known as the chemical master equation, to describe several first and second order reactions and also considered the effect of initial conditions on the expectation value and variance of product formation.

In the master equation, time and the reactant-populations appear as independent variables and it measures the probability of finding various molecular populations at each instant of time[15]. Gillespie gave a rigorous derivation of the chemical master equation for a chemically reacting gas-phase system which is kept well stirred and in thermal equilibrium[78]. Later it was shown that the stochastic simulation algorithm[14, 15] and the chemical master equation are equivalent[78, 79]. It is shown that this simulation algorithm can be applicable as realizations of jump Markov processes in arbitrary non-equilibrium situations[74]. For a closed system, reactions occur at equilibrium condition where the change in Gibbs free energy and the change of total entropy production becomes zero[66]. However, a chemical system can be driven out of equilibrium by some continuous in-letting of reactants and out-letting of products *i.e.*, the system acts as a flow reactor[66, 64, 74]. In this situation, the open chemically reacting system goes to the non-equilibrium steady state(NESS) indicated by the non-zero value of total entropy production rate[66, 74]. Due to the constancy of the concentration of the reactants and products, the reactant and product molecules behave like chemiostats and the differences of chemical potentials between the chemiostats generate the fluxes of matter across the system which mainly drive the system out of equilibrium[13].

Recent studies of non-equilibrium thermodynamics reveal that if a small chemical system remains in far from equilibrium, the thermodynamic quantities like entropy of the system becomes a fluctuating quantity and it follows some exact relations, called the fluctuation theorems [13, 80, 81, 82]. The non-equilibrium thermodynamic behavior of small chemical systems can be estimated by the use of such fluctuation theorems[13, 81, 82]. These theorems also provide the insight regarding how the macroscopic irreversibility appears in the system from the time-reversible microscopic dynamics[83, 84, 85]. In the past 15 years, several fluctuation theorems(FT) are proposed [83, 84, 85, 86, 87, 88] which changes our understanding about the global properties of a small system that are not amenable from conventional thermodynamics.

Lay out of this chapter is as follows. In section 2.1 we have first discussed on the McQuarrie's description of the kinetics of small chemically reacting system. In section 2.2, the birth-death master equations are introduced by considering some chemical and biological processes. In section 2.3, we have briefly explained the

single enzyme kinetics and single molecule diffusion in heterogeneous phases. Then we have discussed the cooperativity in oligomeric enzyme in section 2.4 and voltage-gated ion channel kinetics is introduced in section 2.5. In section 2.6 we have given a microscopic description of a small chemical system and constructed the chemical master equation from the basic probability theory. We have also briefly reported on the Gillespie's stochastic simulation algorithm in this section. Next in section 2.7, we have revised the non-equilibrium thermodynamics of small systems. We have thoroughly discussed the Crooks fluctuation theorem and then described the integral and detailed fluctuation theorems from it. We have extended this discussion to describe the non-equilibrium thermodynamics of small chemical systems.

2.1 Kinetics of small system: McQuarrie's description

Stochastic models for various types of first order and second order reaction kinetics was first systematically described by McQuarrie for the small chemically reacting systems containing a finite number of molecules[8, 9]. In these stochastic kinetic models, the number of reacting species is considered as a integer-valued random variable and the state of the system is described in terms of the population of reactant molecules at a particular instant of time. The time evolution of the system is described by a differential difference equation which is constructed on the basis of some phenomenological assumptions. From the solution of the master equation, the probability density function of the random variable is obtained from which various moments may be calculated. The first moment gives the mean of the probability density function which can also be obtained from the deterministic dynamics. However, the second central moment i.e, variance is a measure of the statistical fluctuations about the mean which is unobtainable from the conventional deterministic approach. For clear understanding about how a stochastic model is constructed for the chemical reactions, here we have considered three different uni-molecular reactions: (I) $A \xrightarrow{k_1} B$, (II)$A \underset{k_{-1}}{\overset{k_1}{\rightleftharpoons}} B$ (III) $A \xrightarrow{k_1} B$, $A \xrightarrow{k_2} C$.

To describe the uni-molecular reaction $A \xrightarrow{k_1} B$, it is considered that at time t, the number of A molecules present in the system is $n(t) = n$. The stochastic model of this reaction is described by considering the following assumptions[8]: (I) The probability of a transition, $n \rightarrow (n + 1)$ in the interval $(t, t + \Delta t)$ is $k_1 n \Delta t + o(\Delta t)$, where k_1 is the rate constant and $o(\Delta t)/\Delta t \rightarrow 0$ as $\Delta t \rightarrow 0$. (II) The probability of a transition, $n \rightarrow (n - j)$, $j > 1$, in the interval $(t, t + \Delta t)$ is $o(\Delta t)$ and the reverse reaction occurs with probability zero. Using the following assumptions one can write the differential-difference equation as

$$P_n(t + \Delta t) = k_1(n + 1)\Delta t P_{(n+1)}(t) + (1 - k_1 n \Delta t)P_n(t) + o(\Delta t), \qquad (2.1)$$

where $P_n(t)$ is the probability of having n number of A molecules at time t. By the standard procedure of expanding the probability $P_n(t + \Delta t)$, dividing by Δt and then taking the limit $\Delta t \rightarrow 0$, the master equation can be written as

$$\frac{dP_n(t)}{dt} = k_1(n+1)P_{(n+1)}(t) - k_1 n P_n(t). \tag{2.2}$$

Using the generating function $G(s, t) = \sum_{n=0}^{\infty} P_n(t)s^n$, the Eq.(2.2) becomes

$$\frac{\partial G(s, t)}{\partial t} = k_1(1 - s)(\partial G(s, t)/\partial s), \tag{2.3}$$

and considering the initial condition $G(s, 0) = s^{n_0}$, one obtains

$$G(s, t) = \left[1 + (s - 1)e^{-k_1 t}\right]^{n_0}. \tag{2.4}$$

Mean, $\langle n(t) \rangle$ and variance, $\langle n^2(t) \rangle - \langle n(t) \rangle^2$ of $n(t)$ can be calculated as

$$\langle n(t) \rangle = (\partial G/\partial s)_{s=1}$$

,

$$\langle n^2(t) \rangle - \langle n(t) \rangle^2 = (\partial^2 G/\partial s^2)_{s=1} + (\partial G/\partial s)_{s=1} - (\partial G/\partial s)_{s=1}^2. \tag{2.5}$$

Using the relations described in Eq.(2.5), one can calculate the mean and variance of the corresponding reaction as

$$\langle n(t) \rangle = n_0 e^{-k_1 t}$$

and

$$\langle n^2(t) \rangle - \langle n(t) \rangle^2 = n_0 e^{-k_1 t}(1 - e^{-k_1 t}), \tag{2.6}$$

respectively. From the above expression(Eq.(2.6)), it is observed that the mean value of the stochastic representation is consistent with the deterministic result. However, this is true only for the uni-molecular reactions.

For the second reaction, $A \underset{k_{-1}}{\overset{k_1}{\rightleftharpoons}} B$ which is a reversible first order reaction, consider again $n(t)$ be the number of A molecules present at the reacting system at time t and k_1 and k_{-1} are the forward and backward rate constants, respectively. The corresponding master equation for this reaction can be written as[8]

$$\frac{dP_n(t)}{dt} = k_{-1}(n_T - n + 1)P_{(n-1)}(t) + k_1(n + 1)P_{(n+1)}(t)$$

$$- [k_1 n + k_{-1}(n_T - n)]P_n(t), \tag{2.7}$$

where n_T is the total number of A and B molecules. Using the generating function, $G(s, t)$, Eq.(2.7) becomes,

$$\partial G(s, t)/\partial t = \left[k_1 + (k_{-1} - k_1)s - k_1 s^2\right](\partial G(s, t)/\partial s) + n_T k_{-1}(s - 1)G(s, t). \tag{2.8}$$

Solving the differential equation in Eq.(2.8) and using the relations described in Eq.(2.5), one can obtain

$$\langle n(t) \rangle = \frac{n_T[k_1 e^{-Kt} + k_{-1}]}{(k_1 + k_{-1})}$$

and

$$\langle n^2(t) \rangle - \langle n(t) \rangle^2 = [n_T \gamma/(1+\lambda)]\left(1 - [\gamma/(1+\lambda)]\right), \tag{2.9}$$

where $\lambda = k_1/k_{-1}$ and $\gamma = \left(\lambda e^{-Kt} + 1\right)$ with $K = (k_1 + k_{-1})$.

For the third reaction, $A \xrightarrow{k_1} B$, $A \xrightarrow{k_2} C$, which is mainly the parallel first-order reactions and it can be described by considering the two dimensional stochastic process. If the number of A and B molecules at time t be $n_1(t)$ and $n_2(t)$, respectively, then the master equation can be written as[8]

$$\frac{\partial P_{(n_1,n_2)}(t)}{\partial t} = k_1(n_1 + 1)P_{(n_1+1,n_2-1)}(t) + k_2(n_1 + 1)P_{(n_1+1,n_2)}(t)$$

$$+(1 - k_1 n_1 - k_2 n_1)P_{(n_1,n_2)}(t). \tag{2.10}$$

Now using the generating function, $G(s, r, t) = \sum_{n_1=0}^{\infty}\sum_{n_2=0}^{\infty} s^{n_1} r^{n_2} P_{(n_1,n_2)}(t)$, we obtain

$$\frac{\partial G(s, r, t)}{\partial t} = (k_1 r + k_2 - Ks)\left(\frac{\partial G(s, r, t)}{\partial s}\right), \tag{2.11}$$

where $K = k_1 + k_2$. Considering the initial condition $s^{n_1^0} r^{n_2^0}$, one obtains $F(s, r, t)$ from the above equation(Eq.(2.11))

$$F(s, r, t) = \left(\frac{[k_1 r + k_2 - (k_1 r + k_2 - Ks)e^{-Kt}]}{K}\right)^{n_1^0} r^{n_2^0}. \tag{2.12}$$

Using $F(s, r, t)$ one can obtain the value of mean and variance of $n_1(t)$ and $n_2(t)$ as

$$\langle n_1(t) \rangle = n_1^0 e^{-Kt},$$

$$\langle n_1^2(t) \rangle - \langle n_1(t) \rangle^2 = n_1^0 e^{-Kt}(1 - e^{-Kt}),$$

$$\langle n_2(t) \rangle = n_2^0 + (k_1 n_1^0/K)(1 - e^{-Kt}),$$

and

$$\langle n_2^2(t) \rangle - \langle n_2(t) \rangle^2 = (k_1 n_1^0/K)(1 - e^{-Kt})(1 - [k_1(1 - e^{-Kt})/K]). \tag{2.13}$$

Here n_1^0 and n_2^0 are the initial values of A and B, respectively. The stochastic models for second order reactions can not be solved exactly in many cases. For this reason, some approximate methods are used to determine the first and second moments without solving the probability generating function.

To describe such approximate method one can consider a second order reaction[9], $2A \xrightarrow{k} B$, whose probability rate equation is

$$\frac{dP_n(t)}{dt} = \frac{1}{2}k(n+2)(n+1)P_{(n+2)}(t) - \frac{1}{2}kn(n-1)P_n(t), \qquad (2.14)$$

where $P_n(t) = \text{Prob}\{n(t) = n, n = 0, 2, 4, ..., n_0\}$. Multiplication of Eq.(2.14) by n and n^2, respectively, and summing over n, gives

$$\frac{d\langle n \rangle}{dt} = -k\langle n^2 \rangle + k\langle n \rangle, \qquad (2.15)$$

and

$$\frac{d\langle n^2 \rangle}{dt} = -2k\langle n^3 \rangle + 4k\langle n^2 \rangle - 2k\langle n \rangle. \qquad (2.16)$$

Now taking the assumption that the higher moments as a product of the lower moments, $e.g.,$ $\langle n^3 \rangle = \langle n^2 \rangle \langle n \rangle$ and $\langle n^2 \rangle = \langle n \rangle^2$ we get

$$\langle n \rangle = \frac{n_0}{n_0 + (1 - n_0)\exp[-kt]}, \qquad (2.17)$$

where n_0 is the initial population of A molecules. The assumption, $\langle n^2 \rangle = \langle n \rangle^2$ is equivalent to reducing the stochastic model to deterministic model. Using $\langle n^3 \rangle = \langle n^2 \rangle \langle n \rangle$ and the value of $\langle n \rangle$ in Eq.(2.17), one obtains

$$\langle n^2 \rangle = \langle n \rangle^2 \left[\frac{2}{3}\{(n_0 - 1)/n_0\}(e^{2kt} - e^{-kt}) + 1 \right]. \qquad (2.18)$$

Therefore, the variance, $\langle n^2 \rangle - \langle n \rangle^2$ can be calculated as

$$\langle n^2 \rangle - \langle n \rangle^2 = \left[\frac{2}{3}\{(n_0 - 1)/n_0\}(e^{2kt} - e^{-kt}) \right]. \qquad (2.19)$$

2.2 Birth-death master equation

Here we have described the birth-death processes by stochastic master equation. The name birth-death comes from the modeling of the dynamics of animal or human populations in which individuals are born, or die. The birth-death processes are generally described by the master equation where it is considered that a finite number of reactant molecules are created (born) or destroyed (die) in a given event[89]. If a reacting species, say X has n in number at time t, the master equation can be written as

$$\frac{dP_n(t)}{dt} = w^+(n-1)P_{(n-1)}(t) + w^-(n+1)P_{(n+1)}(t) - [w^+(n) + w^-(n)]P_n(t), \quad (2.20)$$

where, $w^+(n)$ and $w^-(n)$ are the transition probabilities from state, $n \rightarrow n+1$ and $n \rightarrow n-1$, respectively. The stationary solution of the corresponding master

equation in Eq.(2.20) can be obtained by considering $\frac{dP_n(t)}{dt} = 0$. The stationary solution can be written as

$$P_n^{st} = P_{(0)}^{st} \prod_{z=1}^{z=n} \frac{w^+(z-1)}{w^-(z)},\qquad(2.21)$$

where P_0^{st} is the steady state probability distribution for $n = 0$. To discuss the birth-death process, here we have considered Lotka-Volterra process, Brusselator reaction and the Schlogl model of bistable chemical reaction.

2.2.1 Lotka-Volterra reaction:

. The Lotka-Volterra model is composed of a set of coupled, auto-catalytic processes which was first observed by Lotka in 1920. Several years later Volterra independently described this process by formulating a mathematical model. The reaction scheme of Lotka-Volterra model is proposed for the dynamical populations of prey and predator species. It can be written as[14]

$$X + Y_1 \xrightarrow{k_1} 2Y_1,\qquad(2.22)$$

$$Y_1 + Y_2 \xrightarrow{k_2} 2Y_2,\qquad(2.23)$$

$$Y_2 \xrightarrow{k_3} Z.\qquad(2.24)$$

The deterministic rate equations are

$$\frac{dY_1}{dt} = k_1 XY_1 - k_2 Y_1 Y_2,$$

and

$$\frac{dY_2}{dt} = k_2 Y_1 Y_2 - k_3 Y_2.\qquad(2.25)$$

The reaction in Eq.(2.23) describes how a certain predator species Y_2 reproduces by feeding on a certain prey species Y_1. However, from Eq.(2.22) it is observed that the prey species Y_1 reproduces by feeding on a certain foodstuff X, which is assumed here to be depleted insignificant amount. The isomerization in Eq.(2.24) describes the eventual death of predator species, Y_2 due to some natural causes.

The corresponding master equation of this reaction is

$$\frac{\partial P_{(Y_1,Y_2)}(t)}{\partial t} = k_1 X(Y_1 - 1)P_{(Y_1-1,Y_2)}(t) + k_2(Y_1 + 1)(Y_2 - 1)P_{(Y_1+1,Y_2-1)}(t)$$

$$+ k_3(Y_2 + 1)P_{(Y_1,Y_2+1)}(t) - [k_1 XY_1 + k_2 Y_1 Y_2 + k_3 Y_2]P_{(Y_1,Y_2)}(t)\qquad(2.26)$$

The solution of the master equation is not possible in analytical technique, however, from simulation we obtain the variation of Y_1 with Y_2 which is depicted in Fig.(2.1).
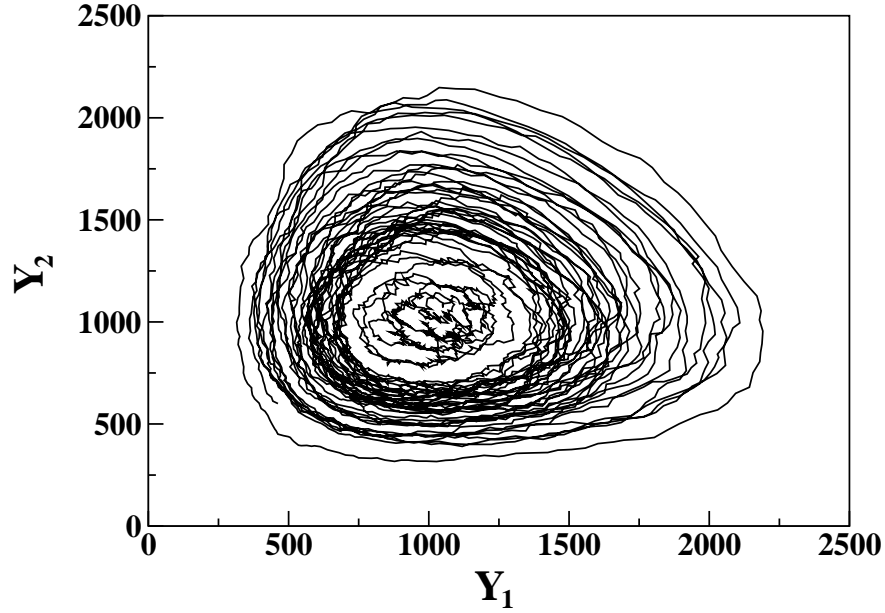
Figure 2.1: The intermediate species, Y_1 and Y_2 are oscillating in the Y_1Y_2 plane. Initial populations of Y_1 and Y_2 are 1000, 1000, respectively. The value of the rate constants are $k_1X = 10.0$, $k_2 = 0.01$ and $k_3 = 10.0$.

From Fig.(2.1), it is observed that the intermediate species Y_1 and Y_2 are oscillating in time. However, this oscillation is not stable and area depends on the initial condition.

2.2.2 Brusselator reaction

Brusselator is a type of auto-catalytic, oscillating chemical reaction which was proposed by Prigogine and Lefevre in 1967 at Brussels. The kinetic scheme of this reaction is[14]

$$X_1 \xrightarrow{k_1} Y_1, \tag{2.27}$$

$$X_2 + Y_1 \xrightarrow{k_2} Y_2 + Z_1, \tag{2.28}$$

$$2Y_1 + Y_2 \xrightarrow{k_3} 3Y_1, \tag{2.29}$$

$$Y_1 \xrightarrow{k_4} Z_2. \tag{2.30}$$

In this reaction, the population of the reactants, X_1 and X_2 are assumed to be depleted insignificant amount. The intermediate substances Y_1 and Y_2 are connected with one another via a trimolecular reaction (2.29), which ensures the existence of an oscillatory regime. The deterministic rate equations for this reaction can be written
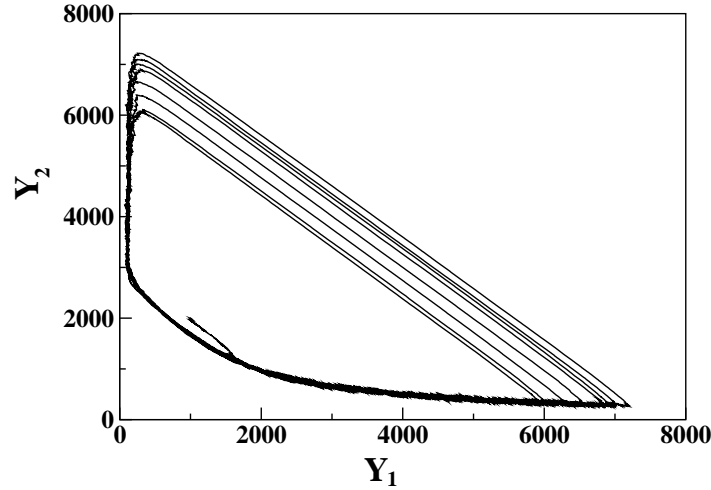
Figure 2.2: Y_1 and Y_2 oscillate around a well defined, closed, stable path in the Y_1Y_2 plane. Initial population of Y_1 and Y_2 are 1000, 2000, respectively. The value of the rate constants are $k_1X_1 = 5000.0$, $k_2X_2 = 50.0$, $k_3 = 0.00005$ and $k_4 = 5.0$

as

$$\frac{dY_1}{dt} = k_1X_1 - k_2X_2Y_1 + (k_3/2)Y_1^2Y_2 - k_4Y_1,$$

and

$$\frac{dY_2}{dt} = k_2X_2Y_1 - (k_3/2)Y_1^2Y_2. \tag{2.31}$$

The description of the time evolution of this reaction can be cast into a master equation which can be written as

$$\frac{\partial P_{(Y_1,Y_2)}(t)}{\partial t} = k_1X_1P_{(Y_1-1,Y_2)}(t) + k_2X_2(Y_1+1)P_{(Y_1+1,Y_2-1)}(t)$$

$$+k_3\left(\frac{1}{2}(Y_1-1)(Y_1-2)\right)(Y_2+1)P_{(Y_1-1,Y_2+1)}(t) + k_4(Y_1+1)P_{(Y_1+1,Y_2)}(t)$$

$$-\left[k_1X_1 + k_2X_2Y_1 + k_3\left(\frac{1}{2}Y_1(Y_1-1)\right)Y_2 + k_4Y_1\right]P_{(Y_1,Y_2)}. \tag{2.32}$$

The solution of the master equation in Eq.(2.32) is not possible analytically, however, the oscillation of the intermediate substances, Y_1 and Y_2 can be obtained from simulation which is depicted in Fig.(2.2). From Fig.(2.2), it is observed that the system will eventually wind up orbiting around a well defined, closed, stable path in the Y_1Y_2 plane which does not depend on the initial state of the system. So this reaction is considered as an example of the 'limit cycle' chemical oscillator.

2.2.3   Schlogl model of bistable chemical reaction

Schlogl model is an example of a chemical reaction system that exhibits bistability. The scheme of the reaction is[11]

$$A + 2\,X \underset{k_2}{\overset{k_1}{\rightleftharpoons}} 3\,X, \tag{2.33}$$

$$B \underset{k_4}{\overset{k_3}{\rightleftharpoons}} X, \tag{2.34}$$

where the concentration of the reactant A and B are held constant. The deterministic rate equation of this reaction is

$$\frac{dX}{dt} = k_1 A X^2 - k_2 X^3 + k_3 B - k_4 X, \tag{2.35}$$

which is a first order, nonlinear ordinary differential equation. The stochastic de-
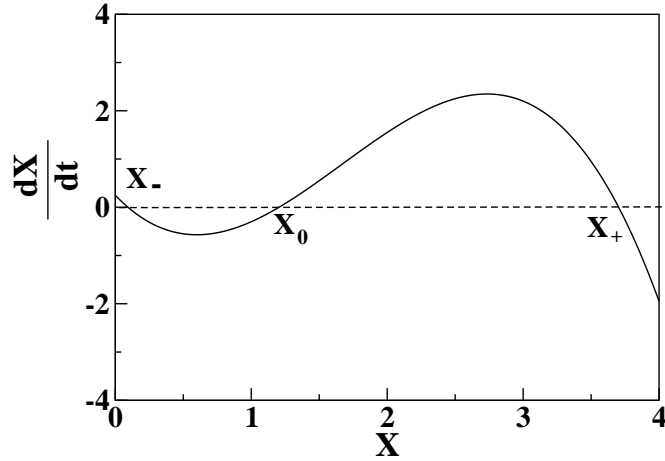
Figure 2.3: dX/dt is plotted as a function of X by taking the rate parameters, $k_1 = 3.0$, $k_2 = 0.6$, $k_3 = 0.25$ and $k_4 = 2.95$. The values of A and B are A = 1 and B = 1, respectively. The plot show the bistability of the system and generated by solving Eq.(2.35).

scription of this reaction can be given by constructing the master equation for this reaction and that can be written as

$$\frac{dP_x(t)}{dt} = k_1 A \left(\frac{1}{2}(x-1)(x-2) \right) P_{(x-1)}(t) + k_2 \left(\frac{1}{3}(x+1)x(x-1) \right) P_{(x+1)}(t) + k_3 B P_{(x-1)}(t) +$$

$$k_4(x+1)P_{(x+1)}(t) - \left[k_1 A \left(\frac{1}{2}x(x-1) \right) + k_2 \left(\frac{1}{3}x(x-1)(x-2) \right) + k_3 B + k_4 x \right] P_x(t), \tag{2.36}$$

where $P_x(t)$ is the probability of having x number of X molecules at time t.

We have numerically solved the Eq.(2.35) and plotted $\frac{dX}{dt}$ as a function of X in the Fig.(2.3). In this figure X_- and X_+ represent two stable steady states and X_0 is an unstable steady state. The system will always tend towards one of the two stable fixed points, X_- and X_+, depending on the initial condition of the reaction. The result of the simulation of master equation is not shown here.

2.3 Study of reaction kinetics at single molecule level

In the previous section, we have given the stochastic description of the reaction systems having finite number of reactant molecules by the master equation. Here we have discussed the reaction kinetics at the single molecule level which can be studied experimentally by single-molecule spectroscopy[60, 61] and single molecule imaging technique[1]. To understand how single molecule and ensemble kinetics are reconciled and what new informations are obtained from single molecule data, a stochastic description of the reaction kinetics is essential as the reactions become stochastic in nature[60, 61, 63]. Here we have discussed mainly the single enzyme kinetics and single molecule detection of translational diffusion.

2.3.1 Single enzyme kinetics: waiting time distribution

The kinetic scheme of a single enzyme molecule can be written as [60, 61, 63]

$$E + S \underset{k_{-1}}{\overset{k_1{}'}{\rightleftharpoons}} ES \overset{k_2}{\rightarrow} E^0 + P \quad E^0 \overset{\delta}{\rightarrow} E, \tag{2.37}$$
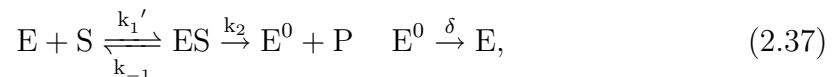
where a substrate, S binds reversibly with a conformation of an enzyme E to form an enzyme-substrate complex, ES which undergoes uni-molecular decomposition to form a product P and E^0. The intermediate conformation of enzyme, E^0 immediately goes to the original conformation of enzyme, E. The corresponding probabilistic rate equation can be written as

$$\frac{dP_E(t)}{dt} = -k_1 P_E(t) + k_{-1} P_{ES}(t), \tag{2.38}$$

$$\frac{dP_{ES}(t)}{dt} = k_1 P_E(t) - (k_{-1} + k_2) P_{ES}(t), \tag{2.39}$$

and

$$\frac{dP_{E^0}(t)}{dt} = k_2 P_{ES}(t), \tag{2.40}$$

where $k_1 = k_1'[S]$ is the pseudo first-order rate constant. Usually in the single molecule enzymatic experiments, the waiting time distribution, f(t) is measured for

one turnover and experimentally it is obtained by recording the histogram of many turnovers[63]. Theoretically f(t) is calculated as

$$f(t) = \frac{dP_{E^0}(t)}{dt} = k_2 P_{ES}(t). \tag{2.41}$$

From the solution of Eq.(2.38) to Eq.(2.40) and using the above relation for f(t) in Eq.(2.41), it can be easily shown that

$$f(t) = \frac{k_1 k_2}{2A} \left[e^{-(B-A)t} - e^{-(B+A)t} \right], \tag{2.42}$$

where $B = (k_1 + k_{-1} + k_2)/2$ and $A = \sqrt{(k_1 + k_{-1} + k_2)^2/4 - (k_1 k_2)}$. The mean waiting time for the reaction, $\langle t \rangle$ can be obtained from the waiting time distribution as, $\langle t \rangle = \int_0^\infty t f(t) dt$ and the inverse of $\langle t \rangle$ gives the traditional Michaelis-Menten equation

$$\frac{1}{\langle t \rangle} = \frac{k_2 [S]}{[S] + K_M}, \tag{2.43}$$

with the Michaelis-Menten constant, $K_M = \frac{k_{-1} + k_2}{k_1'}$. Therefore, the waiting time distribution, f(t) on the one hand gives the ensemble average kinetic result and on the other hand it provides the crucial information on dynamic disorder. In the presence of dynamic disorder, f(t) shows a highly stretched multi-exponential decay at high substrate concentrations and a mono-exponential decay at low substrate concentrations [63].

Sometimes the single molecule enzyme kinetic reaction is carried out at chemiostatic condition where the substrate and product concentrations are maintained at a constant value throughout the experiment[64, 65]. Therefore, the reaction scheme described in Eq.(2.37) can be written as

$$E + S \underset{k_{-1}}{\overset{k_1'}{\rightleftharpoons}} ES \underset{k_{-2}'}{\overset{k_2}{\rightleftharpoons}} E + P. \tag{2.44}$$
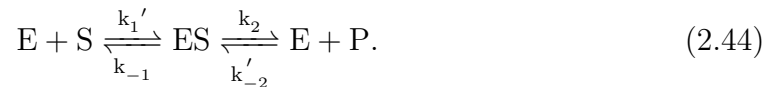
The above reaction scheme in Eq.(2.44) can be reduced to

$$E \underset{\mu}{\overset{\lambda}{\rightleftharpoons}} ES, \tag{2.45}$$

where $\lambda = (k_1 + k_{-2})$ and $\mu = (k_{-1} + k_2)$. The pseudo first order rate constants, k_1 and k_{-2} are $k_1 = k_1'[S])$ and $k_{-2} = k_{-2}'[P])$, respectively. The probabilistic rate equations can be written as

$$\frac{dP_E(t)}{dt} = -(k_1 + k_{-2})P_E + (k_{-1} + k_2)P_{ES}, \tag{2.46}$$

and

$$\frac{dP_{ES}(t)}{dt} = (k_1 + k_{-2})P_E - (k_{-1} + k_2)P_{ES}. \tag{2.47}$$

The steady state probabilities P_E and P_{ES} are obtained from the solution of the rate equations in Eq.(2.46) and Eq.(2.47) as

$$P_E = \frac{\lambda}{(\lambda + \mu)}, \quad P_{ES} = \frac{\mu}{(\lambda + \mu)}. \tag{2.48}$$

The net velocity of the reaction can be calculated as

$$v_{net} = k_2 P_{ES} - k_{-2} P_E = \frac{(k_2\lambda) - (k_{-2}\mu)}{\lambda + \mu}. \tag{2.49}$$

For $k_{-2} = 0$ then we obtain the Michaelis-Menten equation described in Eq.(2.43).

2.3.2 Tracking of heterogeneous diffusion: Single molecule study

Using single molecule imaging technique[1], one can follow the diffusive motion of individual Brownian particle and map out the probability distribution and correlation as a function of time. In the homogeneous environment, the diffusion of a Brownian particle follows Gaussian distribution. However, in the heterogeneous environments, a Brownian particle travels through distinct diffusion areas of various sizes and geometrical arrangements and the distribution becomes non-Gaussian[62].
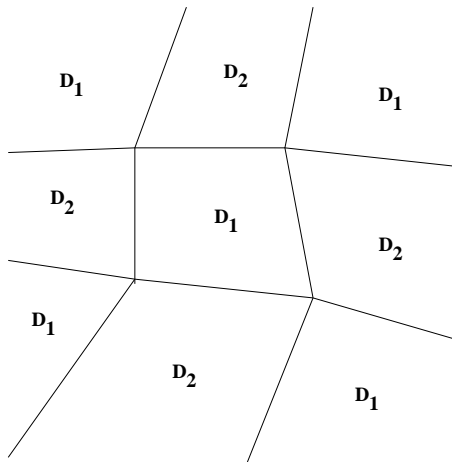
Figure 2.4: A schematic diagram of the two-state diffusive model for heterogeneous diffusion

To describe the heterogeneity developed in the system due to diffusion, we have considered here a model of diffusion of a Brownian particle in two different regions having diffusion constants D_1 and D_2. The rate from first to second region is η_1, and from D_2 to D_1 is η_2, where the the diffusion rate of the particle is Poissonian. The two state heterogeneous diffusion is described here by the reaction-diffusion equation in Fourier space,

$$\dot{P}_1(t,k) = -(\eta_1 + k^2 D_1)P_1(t,k) + \eta_2 P_2(t,k), \tag{2.50}$$

$$\dot{P}_2(t, k) = -(\eta_2 + k^2 D_2) P_2(t, k) + \eta_1 P_1(t, k). \tag{2.51}$$

Here $P_i(t, k)$ is the probability of remaining the particle with wave vector, k at time t in the region i where (i $= 1, 2$). Using the Laplace transformation, the above equations (2.50-2.51) can be written as

$$\begin{pmatrix} P_1(s, k) \\ P_2(s, k) \end{pmatrix} = \frac{1}{\text{Det}(s, k)} \begin{pmatrix} s + k^2 D_2 + \eta_2 & \eta_1 \\ \eta_2 & s + k^2 D_1 + \eta_1 \end{pmatrix} \times \begin{pmatrix} P_1(0, k) \\ P_2(0, k) \end{pmatrix}, \tag{2.52}$$

where the determinant is $\text{Det}(s, k) = (s + k^2 D_1 + \eta_1)(s + k^2 D_2 + \eta_2) - \eta_1 \eta_2$. The total probability distribution for the Brownian particle is $P(s, k) = P_1(s, k) + P_2(s, k)$ with the equilibrium distributions, $P_1(0) = \eta_2/(\eta_1 + \eta_2)$ and $P_2(0) = \eta_1/(\eta_1 + \eta_2)$. If $\eta_1 = \eta_2 = \eta$, the Fourier transform of the probability distribution becomes

$$P(t, k) = \exp\left[-\left(k^2 D_0 + \eta\right) t\right] \times \left[\cosh(\Delta t) + \frac{\eta}{\Delta} \sinh(\Delta t)\right] P(0, k). \tag{2.53}$$

Here $D_0 = (D_1 + D_2)/2$ and $\Delta^2 = k^4 \xi^2 + \eta^2$ where $\xi = (D_1 - D_2)/2$. The distribution in Eq.(2.53) tends to the usual diffusion equation $P(t, k) = e^{-k^2 D t} P(0, k)$ in the limit of $\xi \to 0$ or $\eta \to \infty$. To quantify the distribution, one can measure the time dependent spatial moment, $I_n(t) = \langle |r(t) - r(0)|^n \rangle$, where $r(t)$ and $r(0)$ is the position of the Brownian particle at initial time t $= 0$ and at time t[62, 90]. For a Gaussian distribution the higher order moments, say $I_4(t)$ is determined by the second moment $I_2(t)$, as $I_4(t) = 3 I_2^2(t)$. Therefore, the deviation from the Gaussian distribution can be measured as $J(t) = I_4(t) - 3 I_2(t)$. To scale $J(t)$, the non-Gaussian indicator is defined as[62]

$$\sigma(t) = \frac{J(t)}{3 I_2^2(t)}. \tag{2.54}$$

The mean square displacement of a diffusive Brownian particle in the heterogeneous environment obeys the Einstein relation. So the second moment can be written as $I_2(t) = 2\langle D \rangle t$, where D is the effective diffusion constant expressed as an inhomogeneous average. Consequently, in the short time limit $I_4(t)$ can be expressed as $3\langle (2Dt)^2 \rangle$, where $\langle D^2 \rangle$ denotes an inhomogeneous average. The initial value of $\sigma(t)$ is given explicitly as $\sigma(0) = \frac{\langle \delta D^2 \rangle}{\langle D \rangle^2}$, with $\langle \delta D^2 \rangle = \langle D^2 \rangle - \langle D \rangle^2$. Thus the non-Gaussian indicator[62] can be normalized as

$$g(t) = \frac{\sigma(t)}{\sigma(0)} = \frac{\langle D \rangle^2}{\langle \delta D^2 \rangle} \frac{J(t)}{3 I_2^2(t)}, \tag{2.55}$$

where $g(t)$ is independent of the diffusion constant. In the two-state Poisson kinetics, $g(t)$ can be calculated from the probability distribution, $P(t, k)$ in Eq.(2.53) as

$$g(t) = \frac{\eta t - e^{-\eta t} \sinh(\eta t)}{(\eta t)^2}. \tag{2.56}$$

To describe the diffusion process of a single Brownian particle it is essential to measure the square displacement of the particle at two different times which can be calculated in terms of the joint moment function[62]

$$I(t_1, \tau, t_2) = \langle |r(t_1) - r(0)|^2 |r(\tau + t_1 + t_2) - r(\tau + t_1)|^2 \rangle, \qquad (2.57)$$

where τ is the time separation of the two different measurements at t_1 and t_2. From this joint moment function, $I(t_1, \tau, t_2)$ the memory effect developed in the system can be described. Without the memory effect, the joint moment function becomes, $I(t_1, \tau, t_2) = I_2(t_1)I_2(t_2)$, with $I_2(t) = \langle |r(t) - r(0)|^2 \rangle$. Therefore, the memory effect can be quantified by the normalized correlation function of the square displacement[62] as

$$f(t, \tau) = \frac{I(t_1, \tau, t_2) - [I_2(t)]^2}{I(t, 0, t) - [I_2(t)]^2}. \qquad (2.58)$$

Using the above relation in Eq.(2.58), the normalized correlation function, $f(t, \tau)$ for the two state Poisson process, becomes

$$f(t, \tau) = e^{-2\tau\eta}. \qquad (2.59)$$

From the above discussion, one can get an idea about the nature of the diffusion process of a single Brownian particle, i.e, to know whether the diffusion is homogeneous or non-homogeneous. In the non-homogeneous diffusive process a memory effect is developed in the system which can be characterized by measuring the normalized non-Gaussian indicator, $g(t)$ and the correlation function $f(t, \tau)$. This memory effect is developed due to diffusion in the inhomogeneous environment with an effective fluctuating diffusion coefficient.

2.4   Cooperativity in enzyme kinetics

In enzymology, the cooperativity phenomenon is mainly displayed by the oligomeric enzymes consisting two or more sub-units usually linked to each other by non-covalent interactions. Possibility of interaction between the sub-units during the substrate binding process can give rise to different cooperative phenomena [34, 40, 91, 92]. Positive cooperativity is said to occur when the binding of one substrate molecule with a sub-unit increases the affinity of further attachment of the substrate to another subunit [34, 40, 93]. An example of positive cooperativity is the binding of oxygen to hemoglobin which has a characteristic of sigmoidal shape. From experiment it is observed that when an oxygen molecule binds to a sub-unit of hemoglobin, the oxygen affinity increases, allowing the second molecule to bind more easily, and the third and fourth even more easily *i.e.,* the oxygen affinity of 3-oxy-hemoglobin is 300 times greater than that of deoxy-hemoglobin. In the case of negative cooperativity, attachment of a substrate molecule to one subunit decreases the tendency

of further attachment of the substrate molecules to other subunits. For the non-cooperative case, substrate molecules independently bind to the sub-units of the oligomeric enzyme and the enzyme follows the Michaelis-Menten kinetics.

In 1910, A.V. Hill first described the sigmoidal binding curve of oxygen of hemoglobin by taking the assumption that all ligand molecules would have to bind to the oligomeric protein simultaneously and reach saturation in a single step. According to the Hill's description, if an oligomeric protein, E consists of n number of sub-units, the n number of ligands simultaneously bind with that oligomeric enzyme and form the complex, EL_n. The corresponding binding scheme can be written as
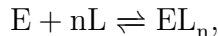
$$E + nL \rightleftharpoons EL_n,$$

where K_b is the equilibrium binding constant and can be defined as

$$K_b = \frac{[EL_n]}{[E][L]^n}. \tag{2.60}$$

Now taking the logarithm on both sides, we get

$$\ln K_b + n \ln [L] = \ln\frac{[EL_n]}{[E]} = \ln\left(\frac{[EL_n]}{[E_0] - [EL_n]}\right) = \ln\left(\frac{Y}{1-Y}\right), \tag{2.61}$$

where, Y is the fractional saturation of the oligomeric enzyme, i.e, $Y = \frac{[EL_n]}{[E_0]}$ with $[E_0] = [E] + [EL_n]$. The above relation described in Eq.(2.61) is known as Hill equation. The plot of $\ln\left(\frac{Y}{1-Y}\right)$ versus $\ln [L]$ be a straight line with slope n and intercept, $\ln K_b$. Such a graph is called a Hill plot, and its experimentally determined slope is known as the Hill coefficient, generally indicated by the symbol h. Experimentally the Hill coefficient is obtained by determining the fractional saturation, Y at various ligand concentrations [L], constructing the Hill plot ($\ln(\frac{Y}{1-Y})$ vs. $\ln[L]$) and then finding the slope at the half-saturation point, $Y = 0.5$ or at a point where the slope deviates maximum from unity. For positive and negative cooperative cases, the Hill coefficient, h becomes greater than or less than one, respectively, whereas the non-cooperative case is characterized with Hill coefficient equal to one.

G.S. Adair first developed an equation to describe the sigmoidal binding curve of the oxygen of hemoglobin by considering all individual binding steps[36]. The general binding scheme of Adair can be written as

$$E \underset{k_2^{(1)}}{\overset{k_1^{(0)}}{\rightleftharpoons}} ES_1 \underset{k_2^{(2)}}{\overset{k_1^{(1)}}{\rightleftharpoons}} \cdots\cdots \underset{k_2^{(j)}}{\overset{k_1^{(j-1)}}{\rightleftharpoons}} ES_j \underset{k_2^{(j+1)}}{\overset{k_1^{(j)}}{\rightleftharpoons}} \cdots\cdots \underset{k_2^{(n-1)}}{\overset{k_1^{(n-2)}}{\rightleftharpoons}} ES_{n-1} \underset{K_2^{(n)}}{\overset{k_1^{(n-1)}}{\rightleftharpoons}} ES_n. \tag{2.62}$$
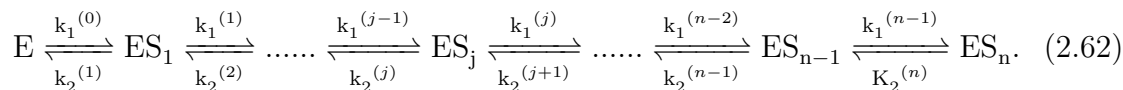
Here ES_j represents the conformational state of the oligomeric enzyme in which j number of subunits are occupied by the ligands. $k_1^{(j-1)}$ and $k_2^{(j)}$ are designated as the formation and dissociation rate constants in the j-th reaction step, respectively.

The fractional saturation, Y is simply expressed as

$$Y = \frac{\sum_{n=0}^{n_T} n \begin{pmatrix} n_T \\ n \end{pmatrix} \prod_{j=0}^{n-1} K^{(j)}}{\sum_{n=0}^{n_T} \begin{pmatrix} n_T \\ n \end{pmatrix} \prod_{j=0}^{n-1} K^{(j)}}, \tag{2.63}$$

where $K^{(j)} = k_1^{(j)}/k_2^{(j+1)}$, is the equilibrium constant for the j-th binding step.

By the Adair scheme, positive, negative and no cooperativity phenomenon can be described very nicely. If the step-wise equilibrium binding constant increases, positive cooperativity is observed, whereas, for the reverse case, an oligomeric protein shows the negative cooperativity. If the step-wise binding constants remain the same then no cooperativity phenomenon is developed. These types of cooperativity based on the affinity of the substrate binding belong to the class of allosteric cooperativity which is mainly described by the concerted or sequential models. The concerted model of allostery was proposed by Monod, Wyman and Changeux which is sometimes referred to as the symmetrical model or MWC model[37]. In this model each sub-unit or active site can exist in two conformational states, T and R states, where the R-state predominates in the protein-ligand complexes. The model is based on the assumption that in a particular protein molecule, all of the sub-units must remain either in the R or T conformational state. The two conformational states of the protein are in equilibrium in the absence of ligand but the equilibrium is disturbed when a ligand binds to a sub-unit of the protein. The sequential model was proposed by Koshland, Nemethy and Filmer(KNF) [38] which dictates that the ligands bind via an induced fit protocol. The basic assumptions of this model are: (a) the two conformational states T and R are available to each subunit, (b) only the subunit to which the ligand is bound changes its conformation and (c) the ligand-induced conformational change in one subunit alters its interactions with neighboring subunits[38, 91]. These two allosteric models are constructed by considering the equilibrium condition, however, in living cell most of the reactions occur in non-equilibrium condition which is developed due to the imbalanced chemical reactions and the presence of chemiostats. So to describe the non-equilibrium cooperativity phenomenon, it becomes essential to modify these two equilibrium allosteric models. In chapter five, we have thoroughly discussed the non-equilibrium cooperativity.

2.5 Voltage-gated ion channel kinetics:

In neuro-physiology, voltage-gated ion channels, mainly sodium and potassium channels play an important role in generation and propagation of action potential(nerve impulse) by controlling the voltage gradient across the plasma membrane of nerve

cells, by allowing the flow of ions down their electrochemical gradient[45, 46]. Hodgkin and Huxley made the first intracellular recording of an action potential and developed a voltage-clamp circuit to measure the ionic currents from squid axon. However, their most remarkable achievement was the proposition of a mathematical model to explain the ionic mechanisms underlying the initiation and propagation of action potentials in the squid giant axon [47]. The Hodgkin-Huxley theory of the action potential is still considered as the most significant conceptual breakthrough in neuro-science and they received the Nobel Prize in Physiology or Medicine in 1963. In this model the lipid bilayer is considered as a capacitor (C_m) and the current can be carried through the membrane either by charging the membrane capacity or by movement of ions through the ion channel[47]. Therefore, the total membrane current, I_{MI} can be written as the summation of capacity current, I_C and ionic current, I_i as

$$I_{MI} = I_C + I_i. \tag{2.64}$$

Here $I_C = C_m \frac{dV}{dt}$ where C_m is the specific membrane capacitance per unit area and V is the membrane potential. The ionic current is divided into components carried by sodium and potassium ions (I_{Na}) and (I_K), and a small 'leakage current', (I_l) made up by chloride and other ions. Therefore, the ionic current is calculated as

$$I_i = I_{Na} + I_K + I_l. \tag{2.65}$$

The individual ionic currents are calculated according to the relations

$$I_{Na} = g_{Na}(V - E_{Na}),$$

$$I_K = g_K(V - E_K),$$

and

$$I_l = g_l(V - E_l), \tag{2.66}$$

where E_{Na}, E_K and E_l are the sodium, potassium and leakage reversal potential, respectively[47, 53]. The sodium and potassium ion conductance are calculated as

$$g_{Na} = \bar{g}_{Na} N_{Na} h \, m^3$$

and

$$g_K = \bar{g}_K N_K n^4, \tag{2.67}$$

where $\bar{g}_{Na}$ and $\bar{g}_K$ are the sodium and potassium conductance per channel. N_{Na} and N_K are the sodium and potassium channel density per unit area. n,h and m are the gate parameters which satisfy the equation as [47],

$$\frac{dn}{dt} = \alpha_n(1 - n) - \beta_n n, \tag{2.68}$$

$$\frac{dm}{dt} = \alpha_m(1 - m) - \beta_m m, \tag{2.69}$$

and

$$\frac{dh}{dt} = \alpha_h(1 - h) - \beta_h h. \tag{2.70}$$

Here α_J and β_J with $J = n, h, m$ are gate opening and closing rates with dimension time^{-1} and depend on the membrane potential, V. Solving the Eq.(2.68), Eq.(2.69) and Eq.(2.70) we obtain

$$n = n_\infty - (n_\infty - n_0)\exp(-t/\tau_n), \tag{2.71}$$

$$m = m_\infty - (m_\infty - m_0)\exp(-t/\tau_m), \tag{2.72}$$

and

$$h = h_\infty - (h_\infty - h_0)\exp(-t/\tau_h), \tag{2.73}$$

where J_0 and J_∞ are the initial and final values of j where $j = n, m, h$. The values J_0 and J_∞ are determined as $J_0 = \alpha_{J_0}/(\alpha_{J_0} + \beta_{J_0})$. $J_\infty = \alpha_J/(\alpha_J + \beta_J)$ and $\tau_J = 1/(\alpha_J + \beta_J)$, where $J = n, h, m$. Here τ_J is the characteristic relaxation time. The time-dependence of potassium and sodium conductance can be calculated as[47]

$$g_K = (g_{K_\infty})^{1/4} - [(g_{K_\infty})^{1/4} - (g_{K_0})^{1/4}]\exp(-t/\tau_n)^4, \tag{2.74}$$

and

$$g_{Na} = g'_{Na}[1 - \exp(-t/\tau_m)]^3\exp(-t/\tau_h), \tag{2.75}$$

where $g'_{Na} = \bar{g}_{Na}m_\infty^3 h_0$. g_{K_0} and g_{K_∞} are the values of initial and final potassium conductance. The time-dependent values of g_K and g_{Na} obtained from Eq.(2.74) and Eq.(2.75) exactly match with the conductance values obtained from the Voltage-clamp experiment. However, the conductance g_l is considered as constant.

The propagation of action potential can be described by substituting the value of membrane current for unit length, $I_{MC} = \frac{a}{2r}\frac{\partial^2 V}{\partial x^2}$ in Eq.(2.64), where a is the radious of the nerve fibre, r is the specific resistance of the axoplasam, x is distance along the fibre and V is the membrane potential[47]. Thus one can write

$$\frac{a}{2r}\frac{\partial^2 V}{\partial x^2} = C_m\frac{dV}{dt} + g_{Na}(V - E_{Na}) + g_K(V - E_K) + g_l(V - E_l). \tag{2.76}$$

Eq.(2.76) is a partial differential equation, and it is not practicable to solve it as it stands. During steady propagation, the curve of V against time at any one position is similar in shape to that of V against distance at any one time, and it follows that

$$\frac{\partial^2 V}{\partial x^2} = \frac{1}{\theta^2}\frac{\partial^2 V}{\partial t^2},$$

where θ is the velocity of conduction. Therefore, Eq.(2.76) can be written as

$$\frac{a}{2r\theta^2}\frac{\partial^2 V}{\partial t^2} = C_m\frac{dV}{dt} + g_{Na}(V - E_{Na}) + g_K(V - E_K) + g_l(V - E_l). \tag{2.77}$$

This is an ordinary differential equation and can be solved numerically. This equation describes how the action potential wave propagates with time.

In 1976 Neher and Sakmann developed the patch clamp technique by which they have measured the ionic current through an individual ion channel[5]. This advancement has revolutionized both experimental and theoretical approaches and for this work they have received the Nobel Prize in Physiology or Medicine in 1991. From the study of single ion channel, it becomes clear that individual ion channels are essentially stochastic entities that open and close in a random fashion. From the single ion channel experiments, it is now possible to study the kinetics of individual ion channels and determine accurately the model parameters of a channel. MacKinnon and colleagues have determined the three-dimensional molecular structure of a potassium ion channel by utilizing the X-ray crystallography[94] and explained the exact mechanism of the selectivity of potassium ion channel. For this work he won the Nobel prize in chemistry in 2003. In chapter six, we have thoroughly discussed the kinetics as well as thermodynamics of a single potassium ion channel.

2.6 Microscopic description of small chemical systems: Chemical master equation

For the microscopic description, a chemical system is considered having m different types of chemical species $\{S_1, S_2, ..., S_m\}$, which interact through M chemical reactions $\{R_1, R_2, ..., R_M\}$. Each reaction, $R_\mu(\mu = 1, 2, ...M)$ describes a distinct physical event which happens instantaneously[14, 15, 78, 79]. The system is confined to a constant volume Ω and is in thermal (but not in chemical) equilibrium at some constant temperature T. The number of molecules of species S_i in the system at time t is $n_i(t)$ and the corresponding molecular populations state vector is $\bar{n}(t) = (n_1(t), n_2(t), ..., n_m(t))$, given that the system was in state $\bar{n}(t_0)$ at some initial time t_0.

The change in the population state vector is induced by a single occurrence of a particular reaction, R_μ. Mathematically the reaction, R_μ is characterized by two quantities. The first is the state change vector, $\boldsymbol{\nu}_\mu = (\nu_{1\mu}, ..., \nu_{m\mu})$ where $\nu_{i\mu}$ is the change in the S_i molecular population due to occurrence of the R_μ reaction. So if the system is in state, $\bar{n}(t) = \mathbf{n}$ at time t and one R_μ reaction occurs, the system immediately jumps to state $\mathbf{n} + \boldsymbol{\nu}_\mu$. The other quantity is the propensity function, a_μ where[14, 15, 78, 79] $a_\mu(\mathbf{n})dt \equiv c_\mu h_\mu(\mathbf{n})dt$ is the probability that a particular reaction R_μ will occur in $(t, t + dt)$ in Ω given that the system is in state $\mathbf{n}$ at time t. Here c_μ is the specific probability rate constant of the reaction R_μ and $h_\mu(\mathbf{n})$ indicates the number of distinct R_μ reactant combinations available in the state $\mathbf{n}$. Thus, if R_μ has the form $S_1 + S_2 \rightarrow$products, then we will have $h_\mu(\mathbf{n}) = n_1(t)n_2(t)$ and if R_μ is $2S_1 \rightarrow$products, the form of $h_\mu(\mathbf{n})$ will be $h_\mu(\mathbf{n}) = \frac{1}{2}n_1(t)(n_1(t)-1)$. The

specific probability rate constant, c_μ is related with the traditional deterministic rate constant, k_μ as $c_\mu = k_\mu/\Omega^{(j-1)}$, where j indicates the number of reactant molecules participating in the μ-th reaction. So for the reaction $2S_1 \rightarrow$ products, the propensity function a_μ will be $a_\mu(\mathbf{n}) = \frac{1}{2}[c_\mu n_1(t)(n_1(t) - 1)] = \frac{1}{2}[k_\mu n_1(t)(n_1(t) - 1)/\Omega]$. Usually the propensity function is independent of time, however, if the specific probability rate constant, c_μ is time-dependent then the propensity function also becomes a function of time.

2.6.1 Chemical master equation

In the master equation[11], time and the reactant-populations appear as independent variables and the function which satisfies the equation measures the probability of finding various molecular populations at each instant of time[15]. The chemical master equation can be constructed from the microscopic point of view as follows[15]. Let at time t system remains in the state $\mathbf{n} = (n_1(t), n_2(t), ..., n_m(t))$ and the corresponding probability of remaining in the state is $P_\mathbf{n}(t)$. We want to find out the probability, $P_\mathbf{n}(t + dt)$ *i.e.,* the probability of remaining the system in the state $\mathbf{n}$ at time $t + dt$. During this time interval dt, three events can occur which are independent and mutually exclusive to each others[78]. The first event is that one $R_\mu(\mu = 1, 2, ..., M)$ reaction occurs in the time interval dt and due to occurrence of the first event, the system goes from the state $\mathbf{n} - \boldsymbol{\nu}_\mu$ to $\mathbf{n}$ state at time t to $t + dt$ [78]. The second event is that no reaction occurs during this time interval and if no reaction occurs in dt, system remains in the state $\mathbf{n}$ from time t to $t + dt$ [78]. The last event can be about more than one reaction occur in this time interval[78]. First calculate the probability of occurring the first event, P(I). By applying the laws of probability to the fundamental premise [78], it can be easily calculated as[14, 15, 78],

$$P(I) = c_\mu h_\mu(\mathbf{n})dt + o(dt), \tag{2.78}$$

where o(dt) is the higher order terms. Similarly the probability of occurring the second reaction event, P(II) can be constructed as [14, 15, 78]

$$P(II) = 1 - \sum_{\mu=1}^{M} c_\mu h_\mu(\mathbf{n})dt + o(dt). \tag{2.79}$$

If dt is too small, then one can neglect the third event. Summing all the probabilities one obtains

$$P_\mathbf{n}(t + dt) = P_\mathbf{n}(t) \times \left(1 - \sum_{\mu=1}^{M} c_\mu h_\mu(\mathbf{n})dt + o(dt) \right)$$

$$+ \sum_{\mu=1}^{M} P_{(\mathbf{n}-\boldsymbol{\nu}_\mu)}(t) \times [c_\mu h_\mu(\mathbf{n})dt + o(dt)]. \tag{2.80}$$

Taking the limit, dt → 0 and neglect the higher order terms o(dt), one finally obtains the master equation as[78]

$$\frac{\partial P_{\mathbf{n}}(t)}{\partial t} = \sum_{\mu=1}^{M} \left[c_\mu h_\mu(\mathbf{n} - \boldsymbol{\nu}_\mu) P_{(\mathbf{n}-\boldsymbol{\nu}_\mu)}(t) - c_\mu h_\mu(\mathbf{n}) P_{\mathbf{n}}(t) \right]. \qquad (2.81)$$

The form of this master equation is familiar as Gillespie's chemical master equation which is constructed in terms of the propensity function by considering the individual reaction event. Usually master equation is formulated in terms of the transition probabilities which is equivalent to the propensity function. In terms of the transition probability, the Gillespie's chemical master equation (Eq.2.81) can be written as

$$\frac{\partial P_{\mathbf{n}}(t)}{\partial t} = \sum_{\mu=1}^{M} \left[w_\mu(\mathbf{n} - \boldsymbol{\nu}_\mu | \mathbf{n}) P_{(\mathbf{n}-\boldsymbol{\nu}_\mu)}(t) - w_\mu(\mathbf{n} | \mathbf{n} + \boldsymbol{\nu}_\mu) P_{\mathbf{n}}(t) \right], \qquad (2.82)$$

where $w_\mu(\mathbf{n}|\mathbf{n} - \boldsymbol{\nu}_\mu)$ is the transition probability from the population state, $\mathbf{n}$ to $(\mathbf{n} - \boldsymbol{\nu}_\mu)$. For M reversible reactions the Gillespie's chemical master equation can be written as[13]

$$\frac{\partial P_{\mathbf{n}}(t)}{\partial t} = \sum_{\mu=\pm1}^{\pm M} \left[w_\mu(\mathbf{n} - \boldsymbol{\nu}_\mu | \mathbf{n}) P_{(\mathbf{n}-\boldsymbol{\nu}_\mu)}(t) - w_{-\mu}(\mathbf{n} | \mathbf{n} - \boldsymbol{\nu}_\mu) P_{\mathbf{n}}(t) \right]. \qquad (2.83)$$

Solution of the master equation gives information about the time evolution of a chemically reacting system. However, as this equation is a set of coupled ordinary differential equations, the analytical solution is possible only for some simple cases. For complex systems when the non-chemical or non-linear rate processes are involved in the master equation, the analytical as well as the direct numerical solution becomes quite difficult. Gillespie's stochastic simulation technique gives the numerical realizations about how a chemically reacting system evolves stochastically with time.

2.6.2   Stochastic simulation of the chemical reactions

Here we have briefly discussed the stochastic simulation which was first developed by Gillespie to simulate the time evolution of the chemically reacting system [14, 15]. This is mainly a Monte-Carlo simulation where the trajectory of n̄(t) is generated with time following the probability function $P(\tau, \mu)$. The quantity $P(\tau, \mu)d\tau$ is defined as the probability that, given the state $\bar{n}(t) = \mathbf{n}$ at time t, the next reaction in Ω will occur in the infinitesimal time interval $(t + \tau, t + \tau + d\tau)$, and will be an R_μ reaction[14, 15, 78, 79]. The function is also called in the name of 'reaction probability density function' because in mathematical terminology it is a joint probability density function in the space of the continuous variable $\tau(0 \leq \tau < \infty)$ and the discrete variable $\mu(\mu = 1, 2, ..., M)$ [14, 15] and the exact formula of $P(\tau, \mu)$ is

$$P(\tau, \mu) = a_\mu(\mathbf{n}) \exp[-a_{\text{tot}}(\mathbf{n})\tau], \qquad (2.84)$$

where $a_{tot} = \sum_{\mu=1}^{M} a_\mu(\mathbf{n})$.

From this probability density function one can get the informations about when the next reaction will occur and what kind of reaction it will be. The next reaction time, τ gives the first information whereas the index of the next reaction, μ gives the second. To obtain the explicit expression of the random variable τ, the joint probability density function, $P(\tau, \mu)$ can be written as[14, 15]

$$P(\tau, \mu) = P_1(\tau)P_2(\mu \mid \tau), \tag{2.85}$$

where $P_1(\tau)$ indicates the probability of occurring any one reaction during the time interval $d\tau$ and the mathematical expression of $P_1(\tau)$ is,

$$P_1(\tau) = a_{tot}\exp(-a_{tot}\tau). \tag{2.86}$$

Another probability, $P_2(\mu \mid \tau)$ is designated as the probability of occurring the μ-th reaction, R_μ during this time interval, $d\tau$ and $P_2(\mu \mid \tau)$ can be written as

$$P_2(\mu \mid \tau) = a_\mu/a_{tot}. \tag{2.87}$$

Using the inverse generating function method [14, 113] we obtain the next reaction time τ from $P_1(\tau)$ as

$$\tau = \left(\frac{1}{a_{tot}}\right) \ln\left(\frac{1}{r_1}\right), \tag{2.88}$$

where r_1 is the the uniform random number. The condition of what reaction will occur during the time interval $d\tau$ can be calculated from the probability $P_2(\mu \mid \tau)$ and the condition can be written as[14, 15]

$$\sum_{\nu=1}^{\mu-1} a_\nu < r_2 a_{tot} \leq \sum_{\nu=1}^{\mu} a_\nu, \tag{2.89}$$

where r_2 is another uniform random number. In the simulation algorithm the successive values of $a_1, a_2, ...$ are cumulatively added until their sum is observed to equal or exceed $r_2 a_{tot}$, whereupon μ is then set equal to the index of the last a_ν, term added.

2.7 Non-equilibrium thermodynamic description of small systems

In the previous sections we have described the kinetics of small reacting systems, however, for complete understanding of these reacting systems, here we have provided a non-equilibrium thermodynamic description. In a closed system, reactions occur at equilibrium condition where the change of Gibbs free energy, ΔG and the change of total entropy production, ΔS_{tot} becomes zero[66]. However, an open chemical system goes arbitrarily far from equilibrium due to the presence of the chemiostats. For an example, the living cells behave like open system where the biochemical reactions occur in non-equilibrium condition.

2.7.1 Non-equilibrium thermodynamics: Fluctuation theorem

Before going to describe the non-equilibrium thermodynamic behavior of small chemical systems, here we have provided a brief discussion of the fluctuation theorems which describe the thermodynamics of finite, even small systems that are arbitrarily far away from equilibrium. These theorems also explain how macroscopic irreversibility appears in the system from the time-reversible microscopic dynamics. In the past 15 years, several fluctuation theorems(FT) are proposed [83, 84, 85, 86, 87, 88] which entends our understanding over the conventional thermodynamics. However, here we have provided a discussion on the Crooks FT.

Crooks Fluctuation Theorem(FT):

The Crooks FT provides a method of predicting equilibrium free-energy differences from non-equilibrium paths that connect two equilibrium states[83, 95, 96]. The fluctuation theorem is constructed by considering the two assumptions, (I) the system evolves with time by following the Markovian dynamics and (II) each single time step is microscopically reversible. To discuss the FT of Crooks, we consider a system which is in thermal equilibrium [83, 96] with a bath at temperature, T. The internal state of the system, x_t at time t depends on the externally controlled parameter, λ_t which determines the energy of the state, $E(x_t, \lambda_t)$. By moving the parameter λ_t through a fixed sequence $\{\lambda_0, \lambda_1, ..., \lambda_\tau\}$, the system evolves with time sequence $\{t_0, t_1, ..., t_\tau\}$ which generates a trajectory, $\chi(t)$ in the phase phase as

$$\chi(t) \equiv \left(x_0 \xrightarrow{\lambda_1} x_1 \xrightarrow{\lambda_2} x_2 \xrightarrow{\lambda_3} .... \xrightarrow{\lambda_\tau} x_\tau \right), \tag{2.90}$$

where the initial state x_0 is an equilibrium state at time t = 0 and the corresponding value of the controlled parameter at this time is λ_0.

In this fluctuation theorem it is assumed that after reaching the state x_τ, the system quickly relaxes to equilibrium. So the final state x_τ can also be considered as an equilibrium state. As the system is a canonical ensemble, the equilibrium probability of the states x_0 and x_τ can be written as

$$P(x_l, \lambda_l) = \frac{e^{-\beta E(x_l, \lambda_l)}}{\sum_i e^{-\beta E(x_i, \lambda_i)}} = \exp\left[\beta F(\beta, \lambda_l) - \beta E(x_l, \lambda_l)\right], \tag{2.91}$$

where $l = 0, \tau$ and $F(\beta, \lambda_l) = -\beta^{-1} \ln \sum_i e^{-\beta E(x_i, \lambda_i)}$ is the Helmholtz free energy of the system. Here $\beta = \frac{1}{k_B T}$, with β is the Boltzmann constant and T is the absolute value of temperature. To describe the time evolution of the system it is considered that until the value of λ_t is changed the system remains in the same state. Therefore, for changing the parameter value from λ_j to λ_{j+1}, system performs work, $E(x_j, \lambda_{j+1}) - E(x_j, \lambda_j)$. At constant λ_{j+1}, when the system goes from x_j state to

x_{j+1}, the system exchanges a quantity $E(x_{j+1}, \lambda_{j+1}) - E(x_j, \lambda_{j+1})$ of heat with the surroundings. This evolution of the system through phase space is repeated for τ time steps. Therefore, the total work performed on the system, W, the total heat exchanged with the reservoir, Q, and the total change in energy, ΔE are given by[83]

$$W = \sum_{t=0}^{\tau-1} \left[E(x_t, \lambda_{t+1}) - E(x_t, \lambda_t) \right], \tag{2.92}$$

$$Q = \sum_{t=1}^{\tau} \left[E(x_t, \lambda_t) - E(x_{t-1}, \lambda_t) \right] \tag{2.93}$$

and

$$\Delta E = Q + W = \left[E(x_\tau, \lambda_\tau) - E(x_0, \lambda_0) \right]. \tag{2.94}$$

The free energy difference between two equilibrium ensembles, $\Delta F = F(\beta, \lambda_\tau) - F(\beta, \lambda_0)$ is equal to the reversible work, W_{rev} and the dissipative work, W_d is the difference between the actual work and the reversible work *i.e.,*

$$W_d = W - W_{\text{rev}} = W - \Delta F. \tag{2.95}$$

Here the actual work and the dissipative work both depend on the path followed through phase space but the reversible work depends only on the initial and final ensembles.

Similar to the forward trajectory, a backward trajectory[83, 96], $\tilde{\chi}(t)$ can be generated by considering the reverse direction of time and that can be written as

$$\tilde{\chi}(t) \equiv \left(x_0 \xleftarrow{\lambda_1} x_1 \xleftarrow{\lambda_2} x_2 \xleftarrow{\lambda_3} \ldots\ldots\ldots \xleftarrow{\lambda_\tau} x_\tau \right). \tag{2.96}$$

It is important to note that the forward trajectory begins with a change in λ, whereas the reverse trajectory is started with a change in the internal state of the system[83, 96]. In the reverse time direction, the thermodynamic quantities like heat, work, change in energy and change in free energy would be negative that of the forward time value. Now if we consider that the evolution of the system is Markovian, the probability of the forward trajectory, $P[\chi(t)|x_0]$ can be written as

$$P[\chi(t)|x_0] = P\left(x_0 \xrightarrow{\lambda_1} x_1 \right) P\left(x_1 \xrightarrow{\lambda_2} x_2 \right) \ldots P\left(x_{\tau-1} \xrightarrow{\lambda_\tau} x_\tau \right), \tag{2.97}$$

where $P\left(x_{j-1} \xrightarrow{\lambda_j} x_j \right)$ is the probability of transition from x_{j-1} to x_j. If each single time step is microscopically reversible then the individual steps obey the detailed balance and we can write [83, 96]

$$\frac{P\left(x_{j-1} \xrightarrow{\lambda_j} x_j \right)}{P\left(x_{j-1} \xleftarrow{\lambda_j} x_j \right)} = \frac{P(x_j, \lambda_j)}{P(x_{j-1}, \lambda_j)} = \frac{e^{-\beta E(x_j, \lambda_j)}}{e^{-\beta E((x_{j-1}, \lambda_j))}}. \tag{2.98}$$

Similarly the probability of backward trajectory, $\tilde{P}[\tilde{\chi}(t)|\tilde{x}_0]$ can be written as

$$\tilde{P}[\tilde{\chi}(t)|\tilde{x}_0] = P\left(x_0 \xleftarrow{\lambda_1} x_1\right) P\left(x_1 \xleftarrow{\lambda_2} x_2\right).....P\left(x_{\tau-1} \xleftarrow{\lambda_\tau} x_\tau\right), \qquad (2.99)$$

where $\tilde{x}_t = x_{\tau-t}$ and the tilde symbol implies time reverse path. x_0 and $\tilde{x}_0$ are the initial points of forward and backward processes. Now using Eq.(2.97), Eq.(2.99) and Eq.(2.98), the ratio of the probability of the forward trajectory and the backward trajectory can be written as

$$\frac{P[\chi(t)|x_0]}{\tilde{P}[\tilde{\chi}(t)|\tilde{x}_0]} = \frac{P\left(x_0 \xrightarrow{\lambda_1} x_1\right) P\left(x_1 \xrightarrow{\lambda_2} x_2\right).....P\left(x_{\tau-1} \xrightarrow{\lambda_\tau} x_\tau\right)}{P\left(x_0 \xleftarrow{\lambda_1} x_1\right) P\left(x_1 \xleftarrow{\lambda_2} x_2\right).....P\left(x_{\tau-1} \xleftarrow{\lambda_\tau} x_\tau\right)}$$

$$= \frac{e^{-\beta E(s_1,\lambda_1)}e^{-\beta E(s_2,\lambda_2)}...e^{-\beta E(s_\tau,\lambda_\tau)}}{e^{-\beta E(s_0,\lambda_1)}e^{-\beta E(s_1,\lambda_2)}....e^{-\beta E(s_{\tau-1},\lambda_\tau)}} = e^{-\beta Q}, \qquad (2.100)$$

where Q is the heat exchange with the heat bath and $-\beta Q$ is the corresponding change in entropy of the bath in units of Boltzmann's constant. The relation described in Eq.(2.100) is known as the Crooks fluctuation theorem.

If we consider the initial equilibrium distribution of the forward and backward trajectories, we obtain[83]

$$\frac{P[\chi(t)|x_0]P(x_0)}{\tilde{P}[\tilde{\chi}(t)|\tilde{x}_0]P(\tilde{x}_0)} == e^{-\beta Q}.e^{\beta(\Delta E-\Delta F)} = e^{\beta(W-\Delta F)} = e^{\beta W_d}, \qquad (2.101)$$

as $W = \Delta E - Q$.

Now suppose we find other trajectories, $\chi'(t), \chi''(t), \chi'''(t), ...$ along which the same amount of work W has been done. Then Eq.(2.101) tells us

$$\frac{P[\chi(t)|x_0]P(x_0)}{\tilde{P}[\tilde{\chi}(t)|\tilde{x}_0]P(\tilde{x}_0)} = \frac{P[\chi'(t)|x_0']P(x_0')}{\tilde{P}[\tilde{\chi}'(t)|\tilde{x}_0']P(\tilde{x}_0')} = \frac{P[\chi''(t)|x_0'']P(x_0'')}{\tilde{P}[\tilde{\chi}''(t)|\tilde{x}_0'']P(\tilde{x}_0'')} = ... = e^{\beta(W-\Delta F)}. \quad (2.102)$$

Using the standard properties of ratios, we have

$$\frac{P[\chi(t)|x_0]P(x_0) + P[\chi'(t)|x_0']P(x_0') + P[\chi''(t)|x_0'']P(x_0'') + ...}{\tilde{P}[\tilde{\chi}(t)|\tilde{x}_0]P(\tilde{x}_0) + \tilde{P}[\tilde{\chi}'(t)|\tilde{x}_0']P(\tilde{x}_0') + \tilde{P}[\tilde{\chi}''(t)|\tilde{x}_0'']P(\tilde{x}_0'') + ...} = e^{\beta(W-\Delta F)}. \quad (2.103)$$

In Eq.(2.103), the numerator is the sum of probabilities of trajectories along with work W has been performed on the system, whereas the denominator consists of the corresponding reverse trajectories. Thus, the numerator is the ensemble average probability of work W being done on the system, and the denominator is that of work W done by the system along the reverse trajectory. Therefore, we can write the work fluctuation theorem as[83, 95]

$$\frac{P(W)}{P(-W)} = e^{(W-\Delta F)}. \qquad (2.104)$$

Now we can write

$$\langle e^{-\beta W} \rangle = \sum_{\chi(t),x_0} P(x_0)P[\chi(t)|x_0]e^{-\beta W}$$

$$= \sum_{\tilde{\chi}(t),\tilde{x}_0} \tilde{P}(\tilde{x}_0)\tilde{P}[\tilde{\chi}(t)|\tilde{x}_0]e^{-\beta(W-W_d)} = e^{-\beta \Delta F}, \tag{2.105}$$

where we have considered Eq.(2.101) in the second step.

The above relation is called the Jarzynski equality[88]

$$\langle e^{-\beta W} \rangle = e^{-\beta \Delta F}, \tag{2.106}$$

which relates the free energy difference between two equilibrium states and an ensemble average of the work required to switch between these two configurations.

Integral Fluctuation Theorem:

Here we have briefly described the integral fluctuation theorem [80, 97, 98]. To describe the fluctuation theorem a quantity $r[\chi(t)]$ is defined which can be written as

$$r[\chi(t)] \equiv \ln \left\{ \frac{P[\chi(t)|x_0]P(x_0)}{\tilde{P}[\tilde{\chi}(t)|\tilde{x}_0]\tilde{P}(\tilde{x}_0)} \right\}, \tag{2.107}$$

where $P[\chi(t)|x_0]P(x_0)$ is the probability of forward trajectory and $\tilde{P}[\tilde{\chi}(t)|\tilde{x}_0]P(\tilde{x}_0)$ is the probability of the reverse trajectory. Normalization in forward and reverse path ensemble implies that $\sum_{\chi(t),x_0} P[\chi(t)|x_0]P(x_0) = \sum_{\tilde{\chi}(t),\tilde{x}_0} \tilde{P}[\tilde{\chi}(t)|\tilde{x}_0]\tilde{P}(\tilde{x}_0) = 1$. From the Crooks fluctuation theorem described in Eq.(2.100) we obtain

$$\frac{P[\chi(t)|x_0]}{\tilde{P}[\tilde{\chi}(t)|\tilde{x}_0]} = e^{\Delta s_m},$$

where Δs_m is the change of medium entropy production along a trajectory with $\Delta s_m = -\beta Q$. Therefore, Eq.(2.107) can be written as

$$r[\chi(t)] \equiv \Delta s_m + \ln \frac{P(x_0)}{\tilde{P}(\tilde{x}_0)}. \tag{2.108}$$

According to Seifert, the system entropy along a trajectory is $s(t) = -\ln P(x_t)$[80], where $P(x_t)$ is the probability of remaining the system in the state x_t at time t. Using this definition we can obtain the change of system entropy production, $\Delta s_{sys} = s(\tau) - s(0) = -\ln P(x_\tau) + \ln P(x_0) = -\ln \ln P(\tilde{x}_0) + \ln P(x_0)$, along a trajectory as

$$\Delta s_{sys} = \ln \frac{P(x_0)}{\tilde{P}(\tilde{x}_0)}. \tag{2.109}$$

Therefore, $r[\chi(t)]$ is equivalent to the change of total entropy production along a trajectory i.e.,

$$r[\chi(t)] = \Delta s_m + \Delta s_{sys} = \Delta s_{tot}. \tag{2.110}$$

The following general identity can easily obtain as

$$\langle e^{-\Delta s_{tot}} \rangle = \langle e^{-r[\chi(t)]} \rangle = \sum_{\chi(t),x_0} P[\chi(t)|x_0]P(x_0)e^{-r[\chi(t)]} = \sum_{\tilde{\chi}(t),\tilde{x}_0} \tilde{P}[\tilde{\chi}(t)|\tilde{x}_0]P(\tilde{x}_0) = 1,$$

(2.111)

which is the integral fluctuation theorem. This is supported by the Jarzynski relation, $\langle e^{-\beta W} \rangle e^{\beta \Delta F} = 1$ or $\langle e^{-\beta(W-\Delta F)} \rangle = \langle e^{-\beta W_d} \rangle = 1$. The dissipation function related to the βW_d or Δs_{tot} is the measure of non-equilibriumness.

Detailed Fluctuation Theorem

To prove the detailed fluctuation theorem, another quantity, $\tilde{r}[\tilde{\chi}(t)]$ is defined for the backward trajectory dynamics by keeping the analogy with Eq.(2.107),

$$\tilde{r}[\tilde{\chi}(t)] = \ln \left\{ \frac{\tilde{P}[\tilde{\chi}(t)|\tilde{x}_0]\tilde{P}(\tilde{x}_0)}{P[\chi(t)|x_0]P(x_0)} \right\},$$

(2.112)

where $r[\chi(t)] = -\tilde{r}[\tilde{\chi}(t)]$[99]. Now if the probability $P(R)$ to observe a trajectory with $r[\chi(t)] = R$ during the forward dynamics is related to the probability $P(-R)$ to observe a trajectory with $\tilde{r}[\tilde{\chi}(t)] = -R$ during the backward dynamics, we can write

$$P(R) \equiv \sum_{\chi(t),x_0} P(x_0)P[\chi(t)|x_0]\delta(R-r[\chi(t)]) = \sum_{\chi(t),x_0} \tilde{P}(\tilde{x}_0)\tilde{P}[\tilde{\chi}(t)|\tilde{x}_0]e^{r[\chi(t)]}\delta(R-r[\chi(t)])$$

$$= e^R \sum_{\tilde{\chi}(t),\tilde{x}_0} \tilde{P}(\tilde{x}_0)\tilde{P}[\tilde{\chi}(t)|\tilde{x}_0]\delta(R + r[\tilde{\chi}(t)])$$

$$\text{or} \quad P(R) = e^R P(-R),$$

(2.113)

where we have used Eq.(2.107) and Eq.(2.112). As $R = r[\chi(t)] = \Delta s_{tot}$ from Eq.(2.110), so the detailed fluctuation theorem can be written as

$$\frac{P(\Delta s_{tot})}{P(-\Delta s_{tot})} = e^{\Delta s_{tot}}.$$

(2.114)

This is useful for the entropy production for single trajectory in non-equilibrium dynamics which is proved here for both initial and final conditions at equilibrium.

Other Fluctuation Theorems

Here we have just mentioned FT of Evans-Searles[84] and Gallavotti-Cohen[87] which are not explicitly used in this thesis. The Evans-Searles' FT explains how irreversibility is developed naturally in the system whose dynamics are deterministic and microscopically reversible[84, 95]. This FT bridges the microscopic and macroscopic descriptions, relating the time-reversible equations of motion of a system to the second law and provides a resolution to the long- standing irreversibility paradox[95]. The FT relates the relative probabilities, P of observing forward

and backward trajectories of duration t characterized by the dissipation function, $\Omega_d = A$, taking on arbitrary values A and $-A$, respectively. So the FT can be written as[84, 95]

$$\frac{p(\Omega_d = A)}{p(\Omega_d = -A)} = \exp[A], \qquad (2.115)$$

which holds for arbitrary initial distribution. The dissipation function, Ω_d is a dimensionless dissipative energy expressed in units of $k_B T$, accumulated along the system's trajectory. From the Eq.(2.115) it can be realized that as the system size gets larger or the observation time gets longer, anti-trajectories become rare and it becomes overwhelmingly likely that the system appears time-irreversible according to the second law of thermodynamics. Gallavotti and Cohen also derived a steady state FT which is defined at asymptotic limit but its applicability is very rare.

2.7.2 Chemiostatic condition: Non-equilibrium steady state

For a closed system, reactions occur at equilibrium condition where the change of Gibbs free energy, ΔG and the change of total entropy production, ΔS_{tot} becomes zero[66]. However, a chemical system can be driven out of equilibrium due to continuous in-letting of reactants and out-letting of products *i.e.*, the system acts as a flow reactor. In this situation, this open chemically reacting system goes to the non-equilibrium steady state(NESS) indicated by the non-zero value of ΔS_{tot}. Due to constancy of the concentration of the reactants and products at constant value, the reactant and product molecules behave like chemiostats and the differences of chemical potentials between the chemiostats generate the fluxes of matter across the system which mainly drive the system out of equilibrium[13].

To investigate the role of chemiostats to drive the system away from equilibrium, we have considered the single molecule enzyme kinetics where the substrate and product molecules remain constant. The chemical potential difference between the substrate and the product molecules, $\Delta\mu_{S,P}$ is the summation of the chemical potential differences $\Delta\mu_I$ and $\Delta\mu_{II}$ corresponding to the reactions

$$\text{E} + \text{S} \underset{k_{-1}}{\overset{k_1'}{\rightleftharpoons}} \text{ES}, \qquad (2.116)$$

and

$$\text{ES} \underset{k_{-2}'}{\overset{k_2}{\rightleftharpoons}} \text{E} + \text{P}, \qquad (2.117)$$

respectively. The value of $\Delta\mu_i$ (i = I, II) for these two reactions can be calculated as[11, 64]

$$\Delta\mu_i = k_B T \ln\left(\frac{\text{backward reaction flux}}{\text{forward reaction flux}}\right). \qquad (2.118)$$

For the reaction in Eq.(2.116), $\Delta\mu_I$ is calculated as

$$\Delta\mu_I = k_B T \ln\left(\frac{J_{-1}}{J_1}\right),\qquad (2.119)$$

where the forward and backward reaction flux of corresponding reaction are, $J_1 = k_1'[S]P_E$ and $J_{-1} = k_{-1}P_{ES}$, respectively. Similarly, the value of $\Delta\mu_{II}$ is

$$\Delta\mu_{II} = k_B T \ln\left(\frac{J_{-2}}{J_2}\right),\qquad (2.120)$$

where the forward and backward reaction flux of reaction in Eq.(2.117) are, $J_2 = k_2 P_{ES}$ and $J_{-2} = k_{-2}'[P]P_E$, respectively. Therefore, for the overall reaction process, the change in the chemical potential between the substrate and the product molecules is

$$\Delta\mu_{S,P} = k_B T \ln\left(\frac{J_{-1}J_{-2}}{J_1 J_2}\right) = k_B T \ln\left(\frac{k_{-1}k_{-2}'[P]}{k_1'[S]k_2}\right).\qquad (2.121)$$

At equilibrium, $\Delta\mu_{S,P} = 0$ gives

$$\left(\frac{k_{-1}k_{-2}'[P]}{k_1'[S]k_2}\right) = 1.\qquad (2.122)$$

If the ratio of the substrate and product concentration, $\frac{[S]}{[P]}$ are maintained at the value of $\left(\frac{k_{-1}k_{-2}'}{k_1'k_2}\right)$, the system remains in equilibrium. Otherwise, it goes out of equilibrium $i.e.,$the non-equilibrium steady state(NESS).

To describe the non-equilibrium chemical systems, estimation of the thermodynamic quantities like ΔS_{tot} is essential and for the reacting system the thermodynamic quantities are generally calculated from the master equation. In the next sub-section we have discussed about how the thermodynamic quantities can be calculated from the master equation.

2.7.3 Fluctuation Theorem for chemical systems

Recent studies of non-equilibrium thermodynamics reveal that if a small chemical system remains in far from equilibrium, the thermodynamic quantities like ΔS_{tot} becomes a fluctuating quantity and it follows the fluctuation theorem [13, 80, 81, 82, 85]. The theorem generally relates the probability of entropy generating trajectories in the system to those of entropy consuming ones. So to describe the fluctuation theorem it is necessary to define the entropy on the level of a single trajectory [85, 81, 82].

To describe the fluctuation theorem for a chemical system we have considered a system having m different types of chemical species $\{S_1, S_2, ..., S_m\}$, which interact

through M chemical reactions $\{R_1, R_2, ..., R_M\}$. The system is confined to a constant volume Ω and is in thermal (but not in chemical) equilibrium at some constant temperature T. The number of molecules of species S_i in the system at time t is $n_i(t)$ and the corresponding molecular populations state vector is $\mathbf{n}(t) = (n_1(t), n_2(t), ..., n_m(t))$, given that the system was in state $\mathbf{n_0}$ at some initial time $t_0 = 0$. For this system a stochastic trajectory, $\chi(t)$ can be considered which is depicted in Fig(2.5), generated due to evolution of the population state vector, $\mathbf{n}(t)$ [81, 82, 85, 99] with time which starts from $\mathbf{n_0}$ at time $t_0 = 0$ and jumping at time t_j from $\mathbf{n_{j-1}}$ to $\mathbf{n_j}$ ending up at $\mathbf{n_N}$ with $t_{N+1} = T$ [99]. During jump from the state
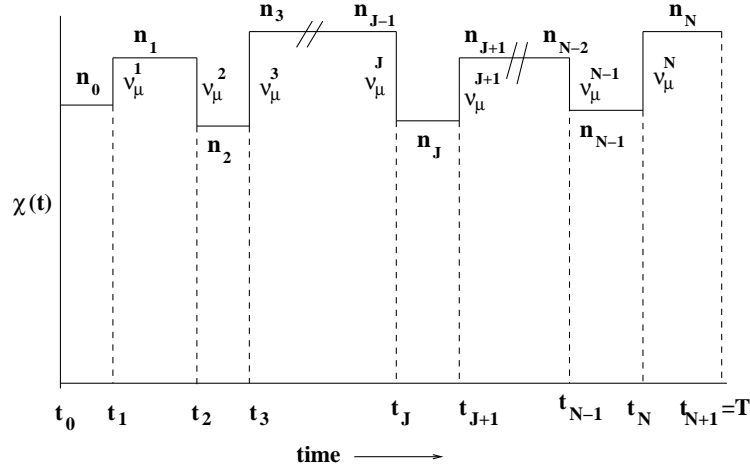
Figure 2.5: A schematic representation of a forward trajectory, $\chi(t)$.

$\mathbf{n_{j-1}}$ to $\mathbf{n_j}$, any one of the M reactions will occur and the time interval τ_j between the two jumps is a random variable following the exponential distribution which is described in Eq.(2.86). Here $w(\mathbf{n_{j-1}}, t_j | \mathbf{n_j})$ is the transition probability from the state $\mathbf{n_{j-1}}$ to $\mathbf{n_j}$ through a reaction R_μ with the stoitiometric vector $\boldsymbol{\nu}_\mu^j$ along a single trajectory. A time reverse trajectory, $\tilde{\chi}(t)$ shown in Fig.(2.6), is generated due to the occurrence of a reaction whose state changing vector $-\boldsymbol{\nu}_\mu^j$ is exactly opposite to the state changing vector, $\boldsymbol{\nu}_\mu^j$ of the forward reaction. Now the probability of occurring the forward trajectory can be calculated as

$$P[\chi(t)|\mathbf{n_0}] = P_{\mathbf{n_0}}(0) \left[\prod_{j=0}^{N-1} \left(\int_{t_j}^{t_{j+1}} P_{\mathbf{n_j}}(t')dt' \right) \times w(\mathbf{n_j}, t_{j+1}|\mathbf{n_{j+1}}) \right] \times \int_{t_N}^{t_{N+1}} P_{\mathbf{n_N}}(t')dt'.$$

(2.123)

Here $\int_{t_j}^{t_{j+1}} P_{\mathbf{n_j}}(t')dt'$ is the probability of occurring no reaction in the n_j state during the time interval t_j to t_{j+1} and normalization in the trajectory-space implies that $\sum_{\chi(t)} P[\chi(t)|\mathbf{n_0}] = 1$. Now using the relation of the probability of occurring no
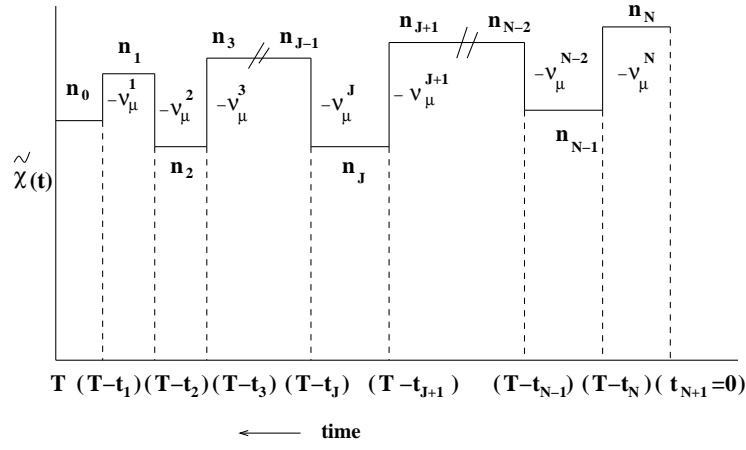
Figure 2.6: A schematic representation of a backward trajectory, $\tilde{\chi}(t)$.

reaction described in Eq.(2.79), we obtain

$$P_{\mathbf{n}_j}(t' + dt') = P_{\mathbf{n}_j}(t') \left[1 - \sum_{\mu=1}^{M} a_\mu(\mathbf{n}_j) dt' \right]. \tag{2.124}$$

Expanding the probability, $P_{\mathbf{n}_j}(t' + dt')$ by Taylor expansion method and neglecting the higher order terms we get[15]

$$\int_{t_j}^{t_{j+1}} P_{\mathbf{n}_j}(t') dt' = \int_0^{\tau_j} P_{\mathbf{n}_j}(\tau') d\tau' = \exp \left[-\sum_{\mu=1}^{M} a_\mu(\mathbf{n}_j) \tau_j \right], \tag{2.125}$$

where $\tau_j = (t_{j+1} - t_j)$ and $P_{\mathbf{n}_j}(0) = 1$. Similarly the probability of occurring the backward trajectory can be written as[99]

$$\tilde{P}[\tilde{\chi}(t)|\tilde{\mathbf{n}}_0] = \tilde{P}_{\mathbf{n}_{N+1}}(0) \left[\prod_{j=1}^{N} \left(\int_{T-t_{j+1}}^{T-t_j} \tilde{P}_{\mathbf{n}_j}(t') dt' \right) \times \tilde{w}(\mathbf{n}_j, T - t_j | \mathbf{n}_{j-1}) \right]$$

$$\times \int_{T-t_1}^{T} \tilde{P}_{\mathbf{n}_0}(t') dt', \tag{2.126}$$

where $\tilde{\mathbf{n}}_0 = \mathbf{n}_{N+1}$ and $P_{n_{(N+1)}}(T) = \tilde{P}_{n_{(N+1)}}(0)$. The normalization in the reverse path ensemble implies $\sum_{\tilde{\chi}(t)} \tilde{P}[\tilde{\chi}(t)|\tilde{\mathbf{n}}_0] = 1$. For the backward trajectory, Eq.(2.125) can be written as

$$\int_{T-t_{j+1}}^{T-t_j} \tilde{P}_{\mathbf{n}_j}(t') dt' = \int_0^{\tilde{\tau}_j} P_{\mathbf{n}_j}(\tilde{\tau}') d\tilde{\tau}' = \exp \left[-\sum_{\mu=1}^{M} a_\mu(\mathbf{n}_j) \tilde{\tau} \right], \tag{2.127}$$

where $\tilde{\tau} = [(T - t_j) - (T - t_{j+1})] = (t_{j+1} - t_j) = \tau$. From Eq.(2.125) and Eq.(2.127) it is observed that the probability of occurring no reaction in the $\mathbf{n}_j$ state for the

forward and backward trajectories is same. Therefore, the ratio of the probability of forward and backward trajectories can be written as

$$\frac{P[\chi(t)|\mathbf{n}_0]}{\tilde{P}[\tilde{\chi}(t)|\tilde{\mathbf{n}}_0]} = \frac{P_{\mathbf{n}_0}(0) \times w(\mathbf{n}_0, t_1|\mathbf{n}_1) \times w(\mathbf{n}_1, t_2|\mathbf{n}_2) \times \ldots\ldots \times w(\mathbf{n}_{N-1}, t_N|\mathbf{n}_N)}{\tilde{P}_{\mathbf{n}_{N+1}}(0) \times \tilde{w}(\mathbf{n}_N, T - t_n|\mathbf{n}_{N-1}) \times \ldots\ldots \times \tilde{w}(\mathbf{n}_1, T - t_1|\mathbf{n}_0)}. \tag{2.128}$$

Taking the logarithm on both sides we get

$$r[\chi(t)] = \ln\left\{\frac{P[\chi(t)]|\mathbf{n}_0]}{\tilde{P}[\tilde{\chi}(t)|\tilde{\mathbf{n}}_0]}\right\} = \ln\frac{P_{\mathbf{n}_0}(0)}{\tilde{P}_{\mathbf{n}_{(N+1)}}(0)} + \prod_{j=1}^{N}\ln\frac{w(\mathbf{n}_{j-1}, t_j|\mathbf{n}_j)}{\tilde{w}(\mathbf{n}_j, T - t_j|\mathbf{n}_{j-1})}, \tag{2.129}$$

where $r[\chi(t)]$ is the logarithmic ratio of the forward and backward trajectory probabilities. Now according to Seifert, the entropy production along a single stochastic trajectory can be defined as [81, 99]

$$\mathbf{s}(t) = -\ln P_{\mathbf{n}}(t), \tag{2.130}$$

where $P_{\mathbf{n}}(t)$ is the solution of the stochastic master equation for a given initial condition, $P_{\mathbf{no}}(t_0)$, taken along the specific trajectory $\chi(t)$. Therefore, the system entropy along a trajectory can be written as

$$\Delta\mathbf{s}_{\text{sys}} = \ln\frac{P_{\mathbf{n}_0}(0)}{P_{\mathbf{n}_{N+1}}(T)}, \tag{2.131}$$

and the medium entropy production is expressed as

$$\Delta s_m = \sum_j \ln\frac{w(\mathbf{n}_{j-1}, t_j|\mathbf{n}_j)}{w(\mathbf{n}_j, t_j|\mathbf{n}_{j-1})}. \tag{2.132}$$

Here $w(\mathbf{n}_{j-1}, t_j|\mathbf{n}_j)$ is the transition probability from the state $\mathbf{n}_{j-1}$ to $\mathbf{n}_j$. So the first term of the right hand side in Eq.(2.129), $\ln\left(\frac{P_{\mathbf{n}_0}(0)}{P_{\mathbf{n}_{(N+1)}}(T)}\right) = \Delta S_{\text{sys}}$ and the second term is equal to the medium entropy production along a single trajectory, ΔS_m. Therefore, Eq.(2.129) can be written as

$$\ln\left\{\frac{P[\chi(t)|\mathbf{n}_0]}{\tilde{P}[\tilde{\chi}(t)|\tilde{\mathbf{n}}_0]}\right\} = \Delta S_{\text{sys}} + \Delta S_m = \Delta S_{\text{tot}}. \tag{2.133}$$

Similar to the Eq.(2.129), we can write

$$\tilde{r}[\tilde{\chi}(t)] = \ln\left\{\frac{P[\tilde{\chi}(t)|\tilde{\mathbf{n}}_0]}{P[\chi(t)|\mathbf{n}_0]}\right\}, \tag{2.134}$$

where $r[\chi(t)] = -\tilde{r}[\tilde{\chi}(t)]$[99]. Now the probability $P(R)$ to observe a trajectory such that $r[\chi(t)] = R$ during the forward dynamics is related to the probability $P(-R)$ to observe a trajectory such that $\tilde{r}[\tilde{\chi}(t)] = -R$ during the backward dynamics

$$P(R) \equiv \sum_{[\chi(t)]} P[\chi(t)|\mathbf{n}_0]\delta(R - r[\chi(t)]) = \sum_{[\chi(t)]} \tilde{P}[\tilde{\chi}(t)|\tilde{\mathbf{n}}_0]e^{r[\chi(t)]}\delta(R - r[\chi(t)])$$

$$= e^R \sum_{[\tilde{\chi}(t)]} \tilde{P}[\chi^R(t)]\delta(r[\tilde{\chi}(t)] - (-R))$$

$$\text{or} \quad P(R) = e^R P(-R), \tag{2.135}$$

which is the detailed fluctuation theorem. By integrating over $e^{-R}P(R) = \tilde{P}(-R)$ over R, we obtain the integral fluctuation theorem

$$\langle e^{-r[\chi(t)]} \rangle = 1. \tag{2.136}$$

Therefore, if the system is in far from equilibrium, the fluctuating thermodynamic quantities like change in the total entropy production, ΔS_{tot} follows the integral as well as the detailed fluctuation theorem.

2.7.4   Estimation of thermodynamic quantities from the master equation

Here we have estimated the thermodynamic quantities, mainly the entropy production rates from the master equation. The system entropy is defined in terms of the Shannon entropy as [13, 74, 100, 101, 102, 103, 104],

$$S_{sys}(t) = -k_B \sum_{\mathbf{n}} P_{\mathbf{n}}(t)\ln P_{\mathbf{n}}(t), \tag{2.137}$$

where we set the Boltzmann constant, $k_B = 1$. Using the master equation described in Eq.(2.83), we get the system entropy production rate [13, 74, 100, 101] as

$$\dot{S}_{sys}(t) = \frac{1}{2}\sum_{\mathbf{n},\mu}[w_\mu(\mathbf{n} - \boldsymbol{\nu}_\mu|\mathbf{n})P_{(\mathbf{n}-\boldsymbol{\nu}_\mu)}(t) - w_{-\mu}(\mathbf{n}|\mathbf{n} - \boldsymbol{\nu}_\mu)P_{\mathbf{n}}(t)]$$

$$\times \ln \frac{P_{(\mathbf{n}-\boldsymbol{\nu}_\mu)}(t)}{P_{\mathbf{n}}(t)}. \tag{2.138}$$

We have assumed ideal reservoir(surroundings) with no inherent entropy production except through the boundaries of the system. The system entropy production(ep) rate can be split as[100, 101, 102, 103, 104]

$$\dot{S}_{sys}(t) = \dot{S}_{tot}(t) - \dot{S}_m(t). \tag{2.139}$$

Here the first term in the r.h.s. of equation(2.139) gives the total entropy production rate and the second term denotes the medium entropy production rate due to the entropy flux into the surroundings. Therefore the total and medium entropy production rates [13, 74, 100, 101] are defined as

$$\dot{S}_{tot}(t) = \frac{1}{2}\sum_{\mathbf{n},\mu}[w_\mu(\mathbf{n} - \boldsymbol{\nu}_\mu|\mathbf{n})P_{(\mathbf{n}-\boldsymbol{\nu}_\mu)}(t) - w_{-\mu}(\mathbf{n}|\mathbf{n} - \boldsymbol{\nu}_\mu)P_{\mathbf{n}}(t)]$$

$$\times \ln \frac{w_\mu(\mathbf{n} - \boldsymbol{\nu}_\mu|\mathbf{n})P_{(\mathbf{n}-\boldsymbol{\nu}_\mu)}(t)}{w_{-\mu}(\mathbf{n}|\mathbf{n} - \boldsymbol{\nu}_\mu)P_{\mathbf{n}}(t)} \tag{2.140}$$

and

$$\dot{S}_m(t) = \frac{1}{2}\sum_{\mathbf{n},\mu}[w_\mu(\mathbf{n} - \boldsymbol{\nu}_\mu|\mathbf{n})P_{(\mathbf{n}-\boldsymbol{\nu}_\mu)}(t) - w_{-\mu}(\mathbf{n}|\mathbf{n} - \boldsymbol{\nu}_\mu)P_\mathbf{n}(t)]$$

$$\times \ln\frac{w_\mu(\mathbf{n} - \boldsymbol{\nu}_\mu|\mathbf{n})}{w_{-\mu}(\mathbf{n}|\mathbf{n} - \boldsymbol{\nu}_\mu)}. \tag{2.141}$$

$\dot{S}_m(t)$ is equal to the heat dissipation rate $h_d(t)$. From the master equation we can also calculate the free energy dissipation rate as

$$\dot{F}(t) = \frac{T}{2}\sum_{\mathbf{n},\mu}[w_\mu(\mathbf{n} - \boldsymbol{\nu}_\mu|\mathbf{n})P_{(\mathbf{n}-\boldsymbol{\nu}_\mu)}(t) - w_{-\mu}(\mathbf{n}|\mathbf{n} - \boldsymbol{\nu}_\mu)P_\mathbf{n}(t)]$$

$$\times\ln\frac{P_{(\mathbf{n}-\boldsymbol{\nu}_\mu)}(t)P_\mathbf{n}^{ss}}{P_\mathbf{n}(t)P_{(\mathbf{n}-\boldsymbol{\nu}_\mu)}^{ss}}, \tag{2.142}$$

where $P_\mathbf{n}^{ss}$ is the steady state probability distribution of the $\mathbf{n}$ state.

At equilibrium, $\dot{S}_{tot}(t)$ becomes zero and the master equation satisfies the detailed balanced condition whereas, for non-equilibrium situation, the value of $\dot{S}_{tot}(t)$ becomes a non-zero quantity and at NESS the master equation follows the circular balance condition. Integrating $\dot{S}_{tot}(t)$ between the initial time, $t_0 = 0$ to final time, $t_f = t$, we get the total entropy production, ΔS_{tot}.

Chapter 3

A stochastic theory of interfacial enzyme kinetics: kinetic Monte Carlo study

In this chapter, we have formulated a theory to explore the advancement of the interfacial enzyme kinetics at the single enzyme level, which is ultimately utilized to obtain the ensemble average macroscopic feature, the lag-burst kinetics. After a brief introduction about the goal of our study in Section 3.1, we have introduced a model in section 3.2 to describe the hopping and scooting mode of motion of the interfacial enzyme kinetics. A stochastic formulation and simulation technique is provided in section 3.3. Numerical results are discussed in section 3.4 by first providing single enzyme activity for some experimental parameters and then the ensemble average kinetics in the bulk. Finally, the chapter is concluded in section 3.5.

3.1 Introduction

The study of interfacial enzymatic reaction is gaining increasing importance in biological science as enzyme plays a crucial role as catalyst of lipid metabolism on the membrane and as mediator of cell signaling processes[105]. It is a heterogeneous enzymatic reaction where the rate of the reaction depends on both the mechanical and chemical steps involved. From the experimental observation, it is well known that the activity of an interfacial enzyme is maximum where both the fluid and gel state phospholipid molecules coexist[1, 3]. Due to different packing pattern, gel state phospholipid molecules are tightly packed than the fluid state molecules. So an enzyme adsorbs exclusively in the fluid region and gradually diffuses to the fluid-gel boundary[1, 2]. With the progress of the reaction, the product molecules i.e, lyso-phospholipids and fatty acids are accumulated in the surface and forms a product domain in between the gel and fluid domain [3, 7, 19, 20, 21, 22, 106]. Usually the

product molecules i.e, fatty acids are negatively charged and with increase in size of the product domain, the electrostatic interaction between the positively charged enzyme and the negatively charged surface also increases. It is observed that the formation of an appreciable size of product domain is responsible for the lag-burst kinetics. This phenomenon is characterized by initial slow hydrolysis in the lag phase, followed by a sudden increase in activity of the enzyme by two or three orders of magnitude, the burst phase [23, 25, 107, 108, 109, 110]. Lag-burst kinetics is the most important macroscopic feature of interfacial enzyme kinetics. Previously, various kinetic analysis had been performed by considering the interactions among the enzyme-phospholipid molecules[23, 25]. However, no microscopic theoretical study is found in terms of the dynamical processes by considering the single molecule activity on the phospholipid monolayer.

Here we have studied the macroscopic feature of interfacial enzyme kinetics starting from the single enzyme activity. At the single molecule level, this reaction kinetics becomes a stochastic process and the analysis involves single molecule trajectory[60, 61, 111]. It is well known that due to thermal hopping, an enzyme can come out from the gel domain, or due to electrostatic binding of the enzyme on the gel surface, it can keep on doing hydrolysis of successive phospholipid molecules in the scooting mode. We have simulated the stochastic processes for the hopping and scooting mode of motion, as both the modes can be operated probabilistically at the same time and it depends on the amount of product formed in the trajectory of a single enzyme. The ensemble averaging of single trajectory events gives the macroscopic rate of the reaction, by which the lag-burst kinetics can be described. In the spirit of Gillespie's method [14, 15], we have studied the stochastic turnover events due to mechanical and chemical steps of the single enzyme activity. Finally, we have searched for any dynamic correlation which can be developed due to the motion of enzyme over various time scales of motion in the different heterogeneous phases.

3.2 Movement of the enzyme on the interface: hopping and scooting motion

In this section, we have given a probabilistic description of two familiar interfacial enzymatic reaction schemes, namely hopping and scooting mode of motion in terms of the desorption and adsorption probability of a surface bound enzyme as shown in Fig.(3.1) . The significant difference between these two mechanisms is that in the hopping mechanism, an enzyme moves out from the gel state after completing a Michaelis-Menten cycle along with the diffusion in fluid and product region. However, in the scooting mode, an enzyme is strictly attached with the phospholipid monolayer and gradually hydrolyzes the phospholipid molecules. Therefore,
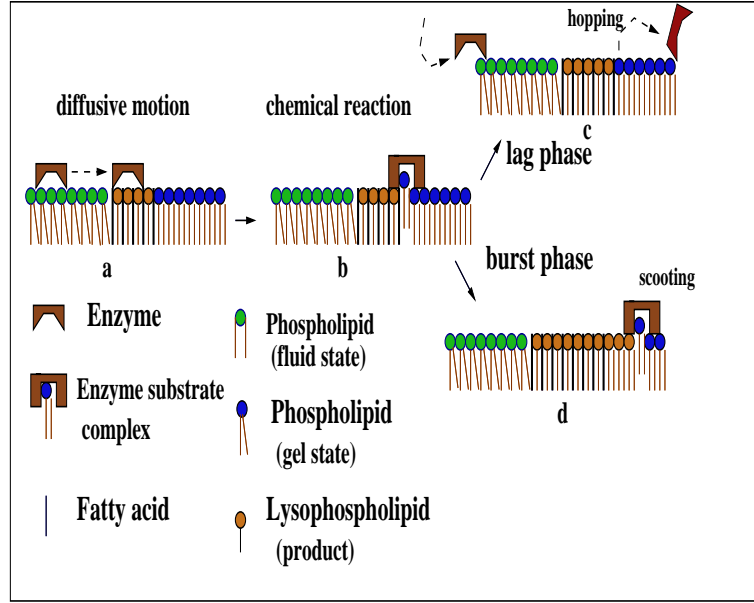
Figure 3.1: (a) An enzyme is attached with the fluid state phospholipid molecules on the Langmuir monolayer. (b) Through the diffusion, the enzyme molecule reaches the gel-fluid interface. (c) After hydrolysing a phospholipid molecule, it predominantly leaves the surface in the lag phase. (d) The enzyme is strictly attached to the surface with scooting mode of motion and the burst phase appears.

the reaction scheme of the hopping mode for one turnover can be written as

$$E_f^* \xrightarrow{K_{d_1}} E_P^* \xrightarrow{K_{d_2}} E_g^* + S \underset{k_{-1}}{\overset{k_1}{\rightleftharpoons}} E_g^*S \xrightarrow{k_2} E_g^*P \xrightarrow{k_3} E_g^{*0} + P \rightarrow E(\text{bulk}). \qquad (3.1)$$

Here, E_f^* and E_P^* are designated as the conformations of an interfacial enzyme in the fluid and the product region, respectively. Actually these two conformations are mainly responsible for the diffusive motion of the enzyme along the fluid and the product regions. To hydrolyze a gel state phospholipid molecule, an enzyme is first converted into the conformation E_g^* from the conformation E_P^* so that a phospholipid molecule binds to the interfacial enzyme. The other conformations, like E_g^*S, E_g^*P, and E_g^{*0} are designated as the substrate-bound enzyme, the product-bound enzyme, and the enzyme after just releasing a product molecule, respectively. In the hopping mode, an enzyme leaves the surface of the monolayer and goes to the bulk. The conformation E represents the free enzyme in the bulk. Similarly the reaction scheme for the scooting mode can be written as

$$E_g^* + S \underset{k_{-1}}{\overset{k_1}{\rightleftharpoons}} E_g^*S \xrightarrow{k_2} E_g^*P \xrightarrow{k_3} E_g^{*0} + P \qquad (3.2)$$

$$E_g^{*0} \xrightarrow{\delta} E_g^*.$$
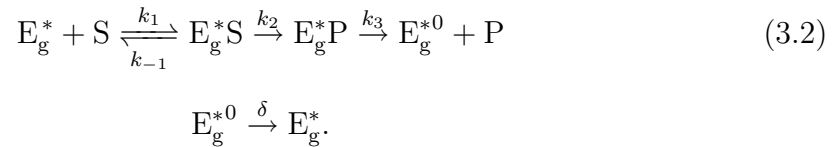
The terms, E_g^*, E_g^*S, E_g^*P and E_g^{*0} carry the similar meaning as described in the above case. In this mechanism, the conformation E_g^{*0} changes quickly to the conformation E_g^* and the enzyme starts another turnover cycle.

From the above two mechanisms, it is observed that a surface bound enzyme may desorb or reside at the monolayer after completion of a Michaelis-Menten turnover cycle. Therefore, at any instant these two modes compete each other and this competition strictly depends on the electrostatic interaction between the positively charged enzyme and the negatively charged surface. Here, the desorption probability of an enzyme is designated as p_d and the adsorption probability is p_a, where $p_d = (1 - p_a)$. With increase in the fraction of negatively charged product molecules, θ, the electrostatic energy as well as the adsorption probability, p_a of an enzyme increases with time. If we consider that $\Delta(\theta)$ is the electrostatic binding energy developed due to the fraction of product formed, θ at time t, then one can find

$$\mathrm{d}\Delta(\theta) = \mathrm{k}\Delta(\theta)\mathrm{d}\theta,$$

where k is the proportionality constant and it is unitless. It depends on the polarity of the substrate molecules. Integrating up to $\theta = \theta_{\mathrm{burst}}$, at which the interaction energy, $\Delta(\theta)$ reaches a saturation value, $\Delta(\theta)_{\mathrm{burst}}$, we get

$$\Delta(\theta) = \Delta(\theta)_{\mathrm{burst}}[\exp(-\mathrm{k}(\theta_{\mathrm{burst}} - \theta))]. \tag{3.3}$$

Here θ_{burst} is designated as the fraction of product molecules responsible for the burst kinetics. Actually beyond the value of θ_{burst}, enzyme is strictly attached to the gel surface and gradually hydrolyzes the gel state phospholipid molecules in the so called 'scooting mode'.

Furthermore, the above Eq.(3.3) can be written in terms of the adsorption probability as

$$p_a = \frac{\Delta(\theta)}{\Delta(\theta)_{\mathrm{burst}}} = [\exp(-\mathrm{k}(\theta_{\mathrm{burst}} - \theta))]. \tag{3.4}$$

In the initial stage, when θ is very small, p_d dominates over p_a and the enzyme follows the hopping mode motion. But when $\theta \gg \theta_{\mathrm{burst}}$, enzyme strictly follows the scooting mode motion as p_a dominates over p_d. However, at any intermediate time both the hopping and scooting mode mechanism will be operative with the respective probabilities, p_d and p_a. Basically, it is observed that $p_d \gg p_a$ during the lag period, whereas the reverse phenomenon is occurred after the burst. Therefore, the magnitude of the probabilities p_d and p_a determine the different enzymatic motion which ultimately dictates the macroscopic lag-burst kinetics.

3.3 Stochastic formulation of interfacial enzyme kinetics and simulation technique

In this section, we have provided a stochastic simulation kinetics following the approach of Gillespie for the chemical and mechanical steps of single enzyme activity, which upon ensemble averaging will give the macroscopic rate. To simulate the stochastic turnover time of a single enzyme, we have considered the kinetics along

its own trajectory. The movement of an enzyme along the fluid region is modelled by a two dimensional Brownian motion. The Monte-Carlo method has been used for simulating two-dimensional Brownian motion in a square plane of side L as a random walk model, in which each displacement is of equal length, say l, but in random direction[112]. By this technique, the mean square displacement, $\langle r^2 \rangle$ is calculated by the following relation

$$\langle r^2 \rangle = 4DMt_c = Ml^2, \tag{3.5}$$

where D is the diffusion coefficient of the particle, M is the sufficiently large Monte-Carlo (MC) steps, l is the length covered by the particle per MC step and t_c is the time interval between two successive MC steps. The total diffusion time, t can be calculated by the relation $t = Mt_c$, where $t_c = \frac{l^2}{4D}$.

Here our main interest is to calculate the time, τ_{fluid}, required to cross the fluid region of an arbitrary finite area by an enzyme *i.e.,* the residence time of the enzyme in that region. For this purpose, we have considered that n_f number of phospholipid molecules are present in the fluid region. If the area of the head group of a phospholipid molecule be a, then the total area of the fluid region is $(a \times n_f)$. Here we assume that the distance between two adjacent molecules is negligible compared to the dimension of the enzyme. The number of fluid state phospholipid molecules covered by an enzyme along its trajectory in a turnover is say, n, where n is an integer random number and that ranges from 1 to n_f. Here n is equivalent to the number of MC steps in the Eq.(3.5). However, to calculate the $\langle r^2 \rangle$, the Monte-Carlo steps, M should be large enough but in our case n can be small. Therefore, the above relation in Eq.(3.5) can not be directly useful in this context. So to calculate the residence time in the fluid region, τ_{fluid}, we have first calculated the area covered by an enzyme, $(n \times a)$ and then divided it by the diffusion coefficient of the enzyme in the fluid region, D_{fluid}. Hence τ_{fluid} can be written as

$$\tau_{fluid} = \frac{(n \times a)}{D_{fluid}}. \tag{3.6}$$

Similarly, if we consider that at any time t, m number of product molecules be present in the product region and the area of the head group of a product molecule, lyso-phospholipid, be b, then the residence time of the enzyme in the product region can be expressed as

$$\tau_{prod} = \frac{(m \times b)}{D_{prod}}, \tag{3.7}$$

where D_{prod} is the diffusion coefficient of the enzyme in the product region. The above two steps are mechanical in nature. When the enzyme molecule reaches the gel-fluid boundary, it starts performing chemical reaction which is modelled here as Michaelis-Menten steps. During a turnover cycle, a surface bound enzyme can hydrolyze only one substrate molecule among all the substrate molecules that E_g^*

"sees" on the surface, which are closer to its path. If at time t, S(t) number of substrate molecules are closer to the path of an enzyme, then the rate of the reaction, $E + S \xrightarrow{k_1'} ES$ will be $k_1 = k_1' \times S(t)$. Therefore, the rate constant of the reaction becomes second order as the the value of S(t) can vary with time. However, change in this number is very small compared to the total substrate molecules present in the surface. So, we have taken this number S(t) as a constant value. consequently, k_1 becomes the pseudo first order rate constant. Except at the very end of the reaction, when the accumulation of the product molecule is very high and well dispersed, this approximation can be physically tenable. To calculate the residence time in the gel state, τ_{gel}, for a single enzyme molecule, we have considered the following probabilistic rate equations[60, 111]:

$$\frac{dP_{E_g^*}(\tau)}{d\tau} = -k_1 P_{E_g^*}(\tau) + k_{-1} P_{E_g^*S}(\tau), \tag{3.8}$$

$$\frac{dP_{E_g^*S}(\tau)}{d\tau} = k_1 P_{E_g^*}(\tau) - (k_{-1} + k_2) P_{E_g^*S}(\tau), \tag{3.9}$$

and

$$\frac{dP_{E_g^*P}(\tau)}{d\tau} = k_2 P_{E_g^*S}(\tau). \tag{3.10}$$

The residence time distribution of an enzyme in the gel state, $f_{gel}(\tau)$ can be calculated as

$$f_{gel}(\tau) = \frac{dP_{E^*P}(\tau)}{d\tau} = k_2 P_{E^*S}(\tau). \tag{3.11}$$

Calculating the value of $P_{E^*S}(\tau)$ from the Eq.(3.8)- Eq.(3.10) and substituting this value in Eq.(3.11), we obtain

$$f_{gel}(\tau) = \frac{k_1 k_2}{2A} \left[e^{-(B-A)\tau} - e^{-(B+A)\tau} \right], \tag{3.12}$$

where $B = (k_1 + k_{-1} + k_2)/2$ and $A = \sqrt{(k_1 + k_{-1} + k_2)^2/4 - (k_1 k_2)}$. The average value of τ_{gel} is,

$$\langle \tau_{gel} \rangle = \frac{k_1 + k_{-1} + k_2}{k_1 k_2} = \frac{1 + K_M}{k_2}, \tag{3.13}$$

where K_M is the Michaelis-Menten constant of the corresponding enzyme.

In the next reaction step, $E_g^*P \xrightarrow{k_3} E_g^{*0}$, a gel state phospholipid molecule is converted into a product molecule, which is valid both for the hopping and the scooting modes of motion. The time taken to complete the reaction is designated here as $\tau_{convert}$, which is a random quantity at the single enzyme level. As the reaction is uni-molecular, its probability density function must be an exponential distribution which can be written as

$$f_{convert}(\tau) = k_3 e^{-(k_3\tau)}. \tag{3.14}$$

The average time required for an enzyme to complete the reaction step is

$$\langle \tau_{\text{convert}} \rangle = \frac{1}{k_3}. \tag{3.15}$$

To get the random time, τ_{gel} from the corresponding residence time distribution, f_{gel}, we use the inversion generating method and calculate the corresponding time in terms of the uniform random number[113]. In the inversion generating method, the random numbers from the uniform distribution in the unit interval is used to construct random numbers, distributed according to any desired probability density function. For generating a random number x, according to a prescribed density function P(x), a uniform random number 'r' is constructed and then the value of x is chosen so that it satisfies $F(x) = r$, where $F(x) = \int_{-\infty}^{x} P(x')dx'$. In other words, we take $x = F^{-1}(r)$, where F(x) is the cumulative distribution function of the given probability density function. For calculating the reaction time τ_{gel}, we consider the probability density function is, $f_{\text{gel}}(\tau)$. Hence the cumulative distribution function, $F_{\text{gel}}(\tau)$ corresponding to the residence time distribution function $f_{\text{gel}}(\tau)$ is,

$$F_{\text{gel}}(\tau) = -\frac{K}{B-A}\left[e^{-(B-A)\tau_{\text{gel}}} - 1\right] + \frac{K}{B+A}\left[e^{-(B+A)\tau_{\text{gel}}} - 1\right], \tag{3.16}$$

where $K = \frac{k_1 k_2}{2A}$. Now according to the inversion method, one can write $F_{\text{gel}}(\tau) = r$, where r is a uniform random number. Substituting the value of r instead of the term $F_{\text{gel}}(\tau)$ in the above equation and after simplifying we get,

$$\frac{r}{K} - \frac{2A}{(B^2 - A^2)} = -\frac{e^{-(B-A)\tau_{\text{gel}}}}{(B-A)}\left[1 - \frac{B-A}{B+A}e^{-2A\tau_{\text{gel}}}\right]. \tag{3.17}$$

As the value of 'A' is large, $e^{-2A\tau_{\text{gel}}} \to 0$ and we obtain the value of τ_{gel} as

$$\tau_{\text{gel}} = \frac{1}{(B-A)}\ln\left[\frac{k_1 k_2}{2A(B-A)r}\right], \tag{3.18}$$

where r is a uniform random number. Similarly the random time, τ_{convert} can be calculated from the probability density function $f_{\text{convert}}(\tau)$. The residence time distribution, $f_{\text{convert}}(\tau) = k_3 e^{-(k_3 \tau_{\text{convert}})}$ of this event gives the cumulative distribution function,

$$F_{\text{convert}} = 1 - \exp[-k_3 \tau_{\text{convert}}]. \tag{3.19}$$

According to the inversion method, we can write $F_{\text{convert}} = r$, where 'r' is a uniform random number. Hence $r = 1 - \exp(-k_3 \tau_{\text{convert}})$ gives,

$$\tau_{\text{convert}} = \frac{1}{k_3}\ln\left(\frac{1}{r}\right), \tag{3.20}$$

where r is a uniform random number.

From the above discussion, now we can calculate the corresponding turnover time *i.e,* total time required to hydrolyze a gel state phospholipid molecule during

the hopping or scooting mode which will obviously be stochastic in nature. The turnover time in the hopping mode is

$$\tau_{\text{hop}} = \tau_{\text{fluid}} + \tau_{\text{prod}} + \tau_{\text{gel}} + \tau_{\text{convert}}. \tag{3.21}$$

Similarly, for the scooting mode the turnover time can be written as

$$\tau_{\text{scot}} = \tau_{\text{gel}} + \tau_{\text{convert}}. \tag{3.22}$$

As the time required to hydrolyze a phospholipid molecule is greater in the hopping mode, the product formation rate must be higher in the scooting mode. After obtaining the corresponding turnover times for the hopping and scooting modes with their probabilistic occurrence with p_d and p_a, respectively, one can get the average turnover time of a trajectory for a single enzyme. Then we can easily calculate the ensemble average rate of product formation corresponding to the bulk kinetics. If X be the number of enzymes present in the monolayer and in a particular time interval, τ_{int} the number of product molecules formed by these enzymes are Q_1, Q_2,....,Q_X, respectively, then the average macroscopic rate of the reaction per unit enzyme is

$$v_{\text{net}} = \frac{\langle Q \rangle}{\tau_{\text{int}}}, \tag{3.23}$$

where $\langle Q \rangle = \frac{\sum_i Q_i}{X}$, is the average number of product molecules formed per unit enzyme over the monolayer.

From the earlier theoretical and experimental[60, 61, 62, 90, 63, 114, 115] studies on the kinetics of single enzyme molecule due to conformational fluctuation, the memory effect is explored through auto-correlation function among the random turnover times,

$$C(m) = \frac{\langle \Delta\tau(0)\Delta\tau(m) \rangle}{\langle \Delta\tau^2 \rangle}. \tag{3.24}$$

If $C(m) = 0$ for $(m > 0)$, it is considered that the dynamic correlation is absent in the reaction system and in the presence of dynamic correlation, $C(m)$ decays from the initial $(m = 1)$ value. The stochastic analysis of the turnover time can be performed from the detailed calculation of the correlation function of the turnover time for the hopping and scooting modes by using the formula[116],

$$C(m) = \frac{\frac{n^2}{n-m} \sum_{i=1}^{n-m} \tau_i \tau_{i+m} - \left(\sum_{i=1}^{n} \tau_i\right)^2}{n \sum_{i=1}^{n} \tau_i^2 - \left(\sum_{i=1}^{n} \tau_i\right)^2}, \tag{3.25}$$

where n is the total number of turnovers, τ_i is the time of the i-th turnover and m is the number of turnovers separating τ_i and τ_{i+m} in the time sequence.

3.4 Numerical result: from single enzyme stochastic turnover time to the bulk interfacial kinetics

In this section we have applied the simulation approach to obtain the stochastic
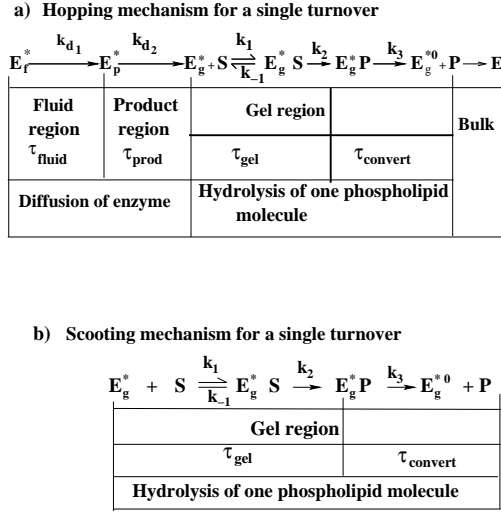
Figure 3.2: Schematic representation of the interfacial enzyme kinetics reaction in the (a) hopping and (b) scooting mode mechanism for a single turnover. Here k_{d_1} and k_{d_2} are the inverse of τ_{fluid} and τ_{prod} which represent the diffusion rates in the fluid and product regions, respectively.

turnover time of a single enzyme activity for PLA_2 enzyme. We have calculated the ensemble average rate profile for the description of the bulk kinetics of lag burst phenomenon. We have considered the diffusion parameters of the system for the stochastic features of the single trajectory of PLA_2 enzyme which is studied recently through wide-field fluorescence microscopy [1], whereas the chemical rate parameters are taken from the experimental papers of Berg *et al.* [3]. An arbitrary set of reaction rate parameters of single enzyme activity[60] are also taken to show the general validity of our theory.

3.4.1 Description of the single enzyme kinetics

To describe the kinetic schemes in the hopping and scooting modes, we have shown the various mechanical and chemical reaction steps which is shown in Fig.(3.2). According to the reaction scheme in the hopping mode, the steps $E_f^* \rightarrow E_p^*$, and $E_p^* \rightarrow E_g^*$, are occurred in the fluid and product region. These two reaction steps are completely mechanical in nature because in these steps only the diffusive movement of the enzyme is occurred. The other conformational states e.g, E_g^*, E_g^*S and E_g^*P must be in the gel region. Therefore, the reaction steps $E_g^* \rightarrow E_g^*S$, $E_g^*S \rightarrow E_g^*$, and $E_g^*S \rightarrow E_g^*P$ are occurred in the gel region. The other more nontrivial reaction step is, $E_g^*P \rightarrow E_g^{*0}$ because in this chemical step, a phospholipid molecule is totally converted into the product molecules, lyso-phospholipid and fatty acid. Therefore, a turnover time can be written as,

$$\tau_{\text{hop}} = \tau_{\text{mech}} + \tau_{\text{chem}}, \tag{3.26}$$
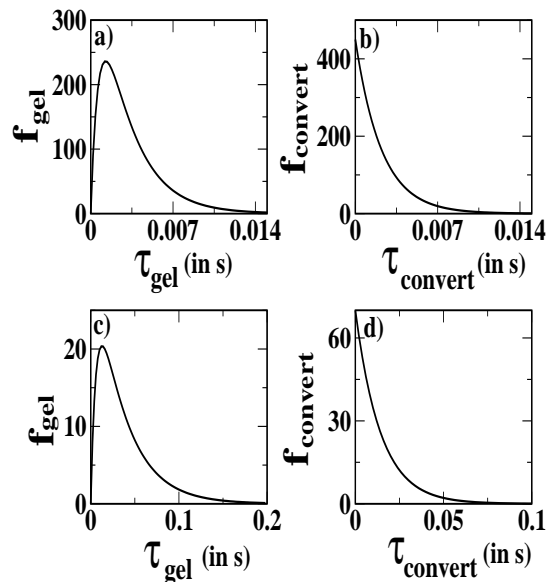
Figure 3.3: (a) Plot of f_{gel} versus τ_{gel} is displayed with the rate parameters, $k_1=1350.0$ sec^{-1}, $k_{-1}=35.0$ sec^{-1}, $k_2=400.0$ sec^{-1} and $k_3=450.0$ sec^{-1}. (b) $f_{convert}$ is plotted with $\tau_{convert}$ for the same rate parameters. Here $f_{convert}$ is an exponential distribution where k_3 is average rate constant of the product formaion step. Same plots, f_{gel} versus τ_{gel} and $f_{convert}$ versus $\tau_{convert}$ are plotted in (c) and (d) by considering the rate parameters, $k_1=120.0$ sec^{-1}, $k_{-1}=30.0$ sec^{-1}, $k_2=40.0$ sec^{-1} and $k_3=50.0$ sec^{-1}, respectively.

where τ_{mech} and τ_{chem} are designated as the time required to complete the mechanical and the chemical steps, respectively.

In the scooting mode, the turnover time can be written as,

$$\tau_{scoot} = \tau_{chem}, \tag{3.27}$$

thereby the time required to hydrolyze a phospholipid molecule is greater for the hopping mode than the scooting mode. We have considered the diffusion coefficient values along the fluid region and product region are $3\mu m^2/sec$ and $0.2\mu m^2/sec$, respectively. The experimental values of the average residence time along the fluid and product region is 30 and 220 msec, respectively. For simulation, we have taken the value of k in Eq. (3.4) is 300, which is unit less. We have suitably chosen the distribution of phospholipid molecules in the fluid region to obtain such average residence times in the fluid and product regions.

When a PLA$_2$ enzyme molecule starts hydrolyzing a substrate molecule, it first forms an intermediate complex, E$_g^*$S followed by another intermediate complex, E$_g^*$P which finally gives a product molecule. Fig.(3.3)(a) and (b) are displayed by taking the first set of parameters values, $k_1=1350.0$ sec^{-1}, $k_{-1}=35.0$ sec^{-1}, $k_2=400.0$ sec^{-1} and $k_3=450.0$ sec^{-1} [7], whereas Fig.(3.3)(c) and (d) are drawn by considering the second set of rate parameter values, $k_1=120.0$ sec^{-1}, $k_{-1}=30.0$ sec^{-1},
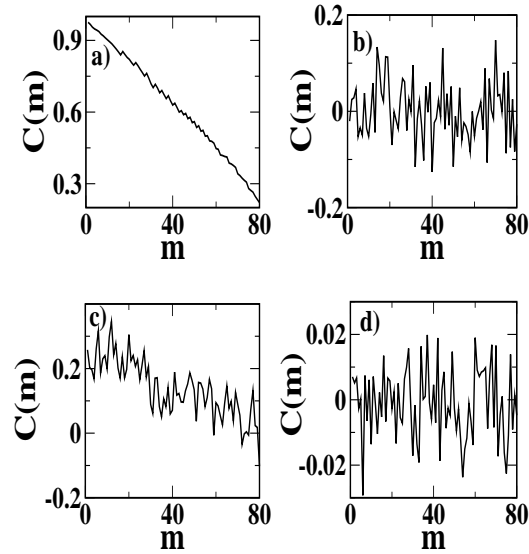
Figure 3.4: Plot of autocorrelation function, C(m) versus m is given for the turnover times, τ_i in hopping mode of motion in (a) and scooting mode of motion in (b). Here m is the number of turnovers separating τ_i and τ_{i+m} in the successive turnover sequence and the rate parameters, k_1=1350.0 sec^{-1}, k_{-1}=35.0 sec^{-1}, k_2= 400.0 sec^{-1} and k_3= 450.0 sec^{-1}, respectively. Same plots are given in (c) and (d) for hopping and scooting mode of motion by considering the rate parameters k_1=120.0 sec^{-1}, k_{-1}=30.0 sec^{-1}, k_2= 40.0 sec^{-1} and k_3= 50.0 sec^{-1}, respectively.

k_2= 40.0 sec^{-1} and k_3= 50.0 sec^{-1}. The first set of parameters values are considered experimentally[7], whereas the second set of parameters are arbitrarily considered which corresponds to single enzyme processes[60]. From Fig.(3.3)(a) and Fig.(3.3)(c), we observe that the probability of remaining in the gel phase, $i.e,$ $f_{gel}(\tau)$ first increases then after a certain time interval it decreases, which indicates that first an intermediate complex, E_g^*S is formed and then it starts to convert into another intermediate complex, E_g^*P. If the association rate constant, k_1 is large, then E_g^*S complex is formed quickly and it is converted into E_g^*P complex very soon, which is shown in the Fig.(3.3)(a) and Fig.(3.3)(c). As $f_{convert}(\tau)$ is an exponential distribution so it decreases with $\tau_{convert}$ exponentially, which indicates that the intermediate state, E_g^*P is converted into E_g^{*0} state exponentially according to the value of k_3.

In what follows, we have calculated the correlation coefficient, C(m) among the turnover times, τ_i and τ_{i+m}, where m is the number of turnovers separating τ_i and τ_{i+m} in the time sequence. Fig.(3.4)(a) and Fig.(3.4)(b) are displayed by taking the first set of parameter values, whereas Fig.(3.4)(c) and Fig.(3.4)(d) are plotted by considering the second set of parameter values. From Fig.(3.4)(b) and Fig.(3.4)(d), we have observed that the correlation coefficient, C(m) among the turnover times in the scooting mode, τ_{scoot} fluctuates around zero. Therefore, one can conclude

that through this mechanism no memory effect is developed in the system. In the scooting mode only chemical reaction steps are involved. The chemical reactions are simple Michaelis-Menten types in which no conformational fluctuation of the enzyme is considered. Such reactions are simply a renewal type of processes in which no memory effect is observed[90, 117]. However, turnover times in hopping mode, τ_{hop}, are strongly correlated which is observed in Fig.(3.4)(a) and Fig.(3.4)(c). The correlation indicates that during the hopping mode mechanism a memory effect is developed in the system. In the hopping mode both the mechanical and chemical steps are involved. As we have observed that no memory effect is developed due to the chemical reactions, we can conclude that the mechanical movements *i.e,* variable diffusion coefficients of the enzyme along the fluid and product regions create this memory effect. Recently, Cao *et al.* had shown that if a Brownian particle travels through two distinct diffusive areas of various sizes and geometrical arrangements *i.e,* diffusion along the heterogeneous environments, then a memory effect is developed for such processes[62]. A similar quantitative model can be built up here to understand the more detailed statistics of the memory effect which can in principle be observed on the single enzyme trajectory.

3.4.2 Description of bulk properties of interfacial kinetics

Here we have calculated the rate of product formation, v_{net} and observe a certain enhancement of product formation rate after the burst which is shown in the Fig. 3.5(a) and Fig. 3.5(b). As the time required to hydrolyze a phospholipid molecule is greater during the lag phase, the product formation rate must be higher at the burst phase. If the lag phase is absent then the curve of product formation rate versus time be a traditional hyperbolic one and that is usually observed from the ensemble average kinetics experiments carried out by Berg *et al.*[3].

As the turnover time is random in nature, the statistical features can be understood from its distribution. Here we have calculated the probability distribution function of such random quantity, $P(\tau_{turnover})$ and this distribution is non-Gaussian in nature which is expected for general non-Markovian process. From Fig.(3.6)(a) and Fig.(3.6)(b), we see that with increase in the value of θ_{burst}, the maximum height of the distribution curve decreases which indicates that more substrate molecules are hydrolyzed by the hopping mode of motion.

From the correlation of successive turnover times in single trajectory analysis in Fig.(3.4), it is found that the correlation arises in the hopping mode which again is predominantly present in the lag phase in macroscopic reactions. In the lag phase turnover times are larger and the values of the turnover times are sparsely distributed over a large range and thereby the distribution becomes skewed towards the higher values of turnover times. However, in absence of various diffusion time scales of enzymatic motion over the fluid and product phase the distribution would tend to
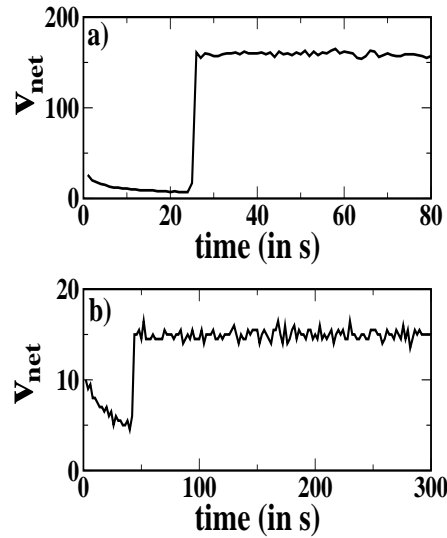
Figure 3.5: (a) Plot of rate of product formation versus time (in sec) is given with the rate parameters,k_1=1350.0 sec^{-1}, k_{-1}=35.0 sec^{-1}, k_2= 400.0 sec^{-1} and k_3= 450.0 sec^{-1}. These rate parameters are taken from the experimental paper of Berg et.al [3]. (b) Same as (a) by considering the rate parameters, k_1=120.0 sec^{-1}, k_{-1}=30.0 sec^{-1}, k_2= 40.0 sec^{-1} and k_3= 50.0 sec^{-1}. The value of $\theta_{\mathrm{burst}} = 0.05$. and its value is taken same in both the curves. We observe that the rate of product formation is increased suddenly after the burst.
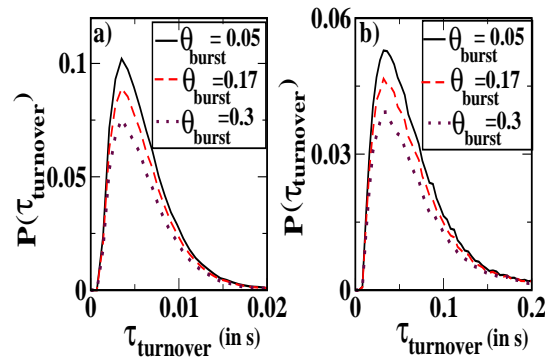
Figure 3.6: Probability distribution of τ_{turnover} is plotted in (a) for three different values of θ_{burst} with the rate parameters k_1=1350.0 sec^{-1}, k_{-1}=35.0 sec^{-1}, k_2= 400.0 sec^{-1} and k_3= 450.0 sec^{-1}, respectively. Same plot is provided by taking the rate parameters k_1=120.0 sec^{-1}, k_{-1}=30.0 sec^{-1}, k_2= 40.0 sec^{-1} and k_3= 50.0 sec^{-1}, respectively. The memory effect is reflected on the skewed non-Gaussian distribution towords the range of larger values of turn-over characteristic of the lag-phase.

be a Gaussian one.

3.5   Conclusion

In the spirit of Gillespie's stochastic approach, we have provided a kinetic Monte Carlo simulation technique for the study of interfacial enzyme kinetics which interpolates between the single enzyme trajectory to that of bulk surface. This trajectory based analysis is essential to describe the microscopic details and the statistical features at the single enzyme level which can in principle be observed by the single molecule fluorescence techniques. By averaging over many trajectories we can get the ensemble average properties like the lag-burst phenomenon for bulk interfacial enzyme kinetics.

Our model is based on the experimental observation that the presence of negatively charged hydrolysis product makes the electrostatic binding between the enzyme and the product molecules. We have defined the probabilities of occurrence of both the competing processes, namely the thermal hopping and scooting mode of motion which ultimately dictates the preference of an enzyme to choose one of them at a time. We have observed that after the formation of some critical number of product molecules, the enzyme gets strictly attached to the surface of the phospholipid and follows the scooting mode of motion. We have also applied the simulation to get the macroscopic results on the overall kinetic rate to show the burst followed by a lag period.

From the single trajectory analysis, it is found that the various time scales of diffusion of the enzyme over the fluid and product regions develop a dynamic correlation among the turnover times. The source of this correlation is very different from the dynamic correlation usually observed in single molecule enzymology due to the conformational fluctuations[90, 117, 118]. However, it corroborates the fact that if a Brownian particle travels through two distinct diffusive areas of various sizes *i.e,* diffusion along the heterogeneous environments, then a memory effect is developed[118]. This memory effect is also studied in terms of the distribution of turn-over times over the average of many trajectories to obtain a macroscopic impact of this correlation. The memory effect is identified with the range of the lag-phase in the overall rate profile which can again be characterized by the non-Gaussian distribution of random time steps in the hopping mode motion. In the lag phase turnover times are larger than in the burst phase and the values of the turnover times are distributed over a larger range and thereby the distribution becomes skewed towards the higher values of turnover times. However, in the absence of various diffusion time scales of enzymatic motion over the fluid and product phase the the distribution would tend to be a Gaussian one characteristic of chemical steps of the process.

This simulation technique can also be applicable to many complex biological

processes where various mechanical steps are involved along with the chemical steps in the overall rate process, *e.g.,* kinetics of the restriction enzyme on a DNA molecule[119, 120, 121]. By generalizing the model of thermal hopping one can also obtain the effect of temperature and pressure on the turnover rate and lag-burst feature of interfacial enzyme kinetics.

Chapter 4

On the mechanically controlled oligomeric enzyme catalysis

In this chapter, we have shown how an applied mechanical force affects the kinetics as well as the thermodynamics of an immobilized oligomeric enzyme in a chemiostatic condition where the statistical characteristics of random walk of the substrate molecules over a finite number of active sites of the enzyme plays important contributing factors in governing the overall rate and the non-equilibrium thermodynamic properties. After the introduction in Section 4.2, we have provided the scheme of the reaction and the master equation suitable for the calculation of net velocity of the reaction and shown its relation with the isolated turn over rate at steady state. In section 4.3, we have calculated the various entropy production rates and explain the simulation procedure to calculate the entropy production along the single trajectory. The numerical results about the effect of force on the kinetics and non-equilibrium thermodynamic properties of the reaction system are discussed in Section 4.4. Finally, The chapter is concluded in Section 4.5.

4.1 Introduction

With the advent of single molecule force spectroscopy and single molecule manipulation techniques, now it is possible to measure directly the forces generated in chemical reactions and even to exert external forces to alter the extent and fate of these reactions[26, 27]. This single molecule force spectroscopy represents a novel experimental method to perform mechanochemistry, in which forces of the order of $10 - 100$ pN applied in manipulating transition state structure even in the solution phase or in living cells to understand chemical reactivity[27, 28, 29, 30]. Originally, Bell had shown that the rate of the chemical reaction in cell to cell adhesion process is influenced by the hydrodynamic forces[31]. Now this concept is extended to arbitrary chemical reactions in biosystem using external mechanical force. For example, by using the single molecule manipulation technique, one can

investigate the folding kinetics of proteins and RNA[122, 123, 124, 125], the separation of DNA strands[126, 127] and the mechanical properties of various motor-like proteins[128, 129, 130]. In a series of works, Szabo and others have established the concept of single molecule pulling experiment to get kinetics and non-equilibrium thermodynamics[32, 33]. Fernandez *et al.* have championed the idea of controlling chemical reaction kinetics by the mechanical force by first showing the reduction in disulphide bonds in a protein, a thiol/disulphide exchange reaction, as this reaction serves as the key step in the function of folding processes of proteins[28, 29, 30]. It is shown that ten fold increase in reduction rate is possible by applying force over 300 pN range through a force-clamp AFM on an engineered polyprotein. Recent experimental and theoretical analysis of Gumpp *et al.* on the single molecular level by the triggering of enzymatic activity through AFM opens the new way to study the direct influence of force to manipulate bio-catalytic reactions[6].

Application of the external mechanical force through the atomic force microscope on a single molecule can drive the whole system far away from equilibrium. Very often this force can change the thermodynamic stability of a molecule and can modify the reaction rates [26, 27]. To describe the effect of force and to give the thermodynamic description of such non-equilibrium single molecule processes, trajectory analysis is the standard tool already developed in stochastic non-equilibrium thermodynamics[58, 131, 132]. Trajectory analysis gives fundamental relations known as the fluctuation theorems describing the statistical fluctuations in time-averaged properties of many-particle systems in far away from equilibrium states [83, 84, 85, 86, 87, 88, 97, 99, 133]. Using these relations one can understand how macroscopic irreversibility emerges from microscopically reversible dynamics[83, 95]. Stochastic trajectory approach has been successfully applied to various systems, e.g, single bio-molecular reactions[80], chemical reaction networks[134], driven colloidal particles [135] and also single two level systems[136].

Here we have studied the effect of external mechanical force on the kinetic and thermodynamic properties of an oligomeric enzyme catalysis. The statistical characteristics of binding of substrate molecules over a finite number of active sites on a single enzyme is formulated through a master equation which is used to calculate the entropy production. We have calculated the statistical average property over the finite number of active sites. In the limit of large number of active sites and with very low rate of association of substrates with the enzymatic active sites, the master equation gives a Poisson distribution in the steady state. Our approach is a generalization of single to oligomeric molecule enzymology containing many active sites, which is also an alternative approach of the mean waiting time distribution. We have also numerically obtained the microscopic picture of the entropy production through the single stochastic trajectory analysis [13, 80, 85] using the Gillespie's stochastic simulation approach. Although in the recent literature a great

deal of effort has been utilized on the exploration of the validity of the fluctuation theorem in various mechanical and chemical systems, the attempt to find out the non-equilibrium dynamical properties as a consequence of the fluctuation theorem is not yet explored with its full potential. Here it is shown how the trajectory based approach can provide the effect of mechanical force in terms of the distribution of the entropy production which can not be obtained from the analytical method of calculation of entropy production specially for the small system.

4.2 Kinetic description of the oligomeric enzyme

In this section we have first described the kinetic scheme of an oligomeric enzyme at chemiostatic condition and then constructed a master equation for it. We have also explained the effect of force on the enzyme kinetics reaction and calculated the the isolated turnover time at NESS.

4.2.1 Scheme of the reaction and the master equation

Single molecule enzyme kinetics are usually studied at the chemiostatic condition where the concentrations of substrate, [S] and product, [P] are maintained at constant values. In chemiostatic condition, the traditional bulk enzyme kinetics reaction scheme (see Fig.4.1 (a)) can be reformulated in a simplified manner which is shown in Fig.4.1(b). In our case, the oligomeric enzyme consists of n_T number of identical subunits and each subunit has one active site. The subunits are linked through extra covalent bonding by using some cross linking reagents[137]. As each active site can form one ES-complex, so the reaction scheme can be viewed in terms of the number of total active sites present at a particular time in the oligomeric enzyme. Here the active sites which have already formed ES-complex are referred to as occupied sites and those lying vacant at that moment are called the vacant sites. The scheme of the oligomeric enzyme catalyzed reaction in bulk and in chemiostatic condition are depicted in Fig.4.1(c) and Fig.4.1(d). The rate constants, $K_1 = (k_1 + k_2)$ and $K_2 = (k_{-1} + k_{-2})$ are designated as the total formation and dissociation rate constants. The pseudo first order rate constants, k_1 and k_2 are given by $k_1 = k_1^{'}[S]$ and $k_2 = k_2^{'}[P]$.

The oligomeric enzyme kinetics reaction consists of four reaction channels or sub-reactions (see Fig.4.1 (c)). Due to the random occurrence of various reaction channels, the number of occupied sites becomes a fluctuating quantity. If at time t, n number of occupied sites are present in the system, $i.e$, the system is in the n-th occupied state, then after a small time dt, the system goes to a new state, $(n + \nu_\mu)$ through any one of the four possible sub-reactions. Here ν_μ is designated as the stoichiometric coefficient of the μ-th reaction with rate constant k_μ. Now among the n_T number of total active sites, if n number of sites form ES-complex at time
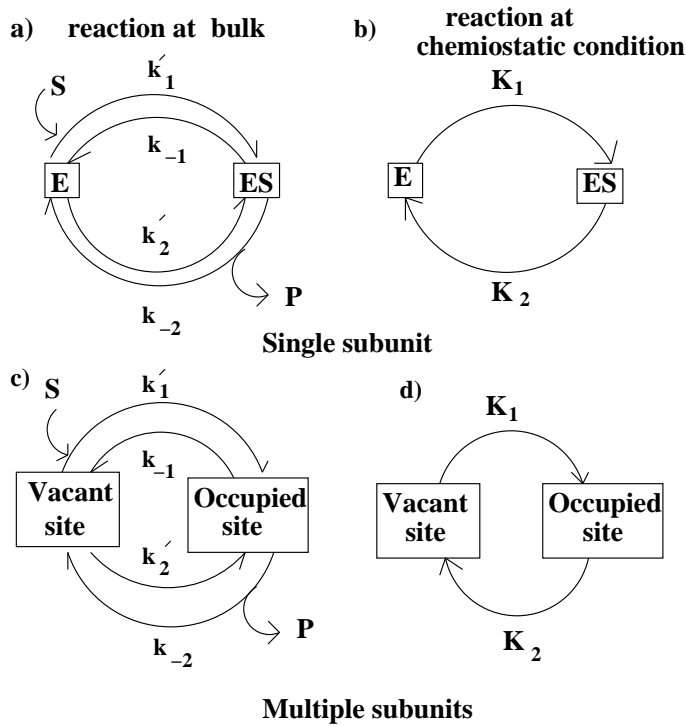
Figure 4.1: Kinetic scheme of an enzyme having only one subunit is shown in bulk in (a) and in chemiostatic condition (b). Similar types of reaction schemes are represented for oligomeric enzyme having more than one subunit in (c) and (d), respectively. The rate constants $K_1 = (k_1 + k_2)$ and $K_2 = (k_{-1} + k_{-2})$ are designated as the total forward and backward rate constants. The pseudo first order rate constants k_1 and k_2 are given by $k_1 = k_1'[S]$ and $k_2 = k_2'[P]$.

t and $(n_T - n)$ number of sites remain vacant, then the stochastic master equation can be written as

$$\frac{dP_n(t)}{dt} = \sum_{\mu=\pm 1}^{\pm 2} [w_\mu(n - \nu_\mu|n)P_{(n-\nu_\mu)}(t) - w_{-\mu}(n|n - \nu_\mu)P_{(n)}(t)], \qquad (4.1)$$

where $\nu_\mu = 1$ with $\mu > 0$ and $-\nu_\mu = 1$ with $\mu < 0$. $P(n, t)$ is the probability of having n number of occupied states at time t. The transition probabilities are defined as follows,

$$w_\mu(n - \nu_\mu|n) = k_\mu(n_T - (n - \nu_\mu)), \mu > 0$$

and

$$w_\mu(n - \nu_\mu|n) = k_\mu(n - \nu_\mu), \mu < 0. \qquad (4.2)$$

Substituting the values of transition probabilities from Eq.(4.2) into Eq.(4.1), we can obtain the simplified form of the master equation as

$$\frac{dP_n(t)}{dt} = K_1(n_T - n + 1)P_{(n-1)}(t) + K_2(n + 1)P_{(n+1)}(t)$$

$$-K_1(n_T - n)P_{(n)}(t) - K_2 n P_{(n)}(t). \tag{4.3}$$

Solving the master equation by the standard approach of generating function method[12, 89, 138], we get the probability distribution function as

$$P_{(n)}(t) = \frac{n_T!}{n!(n_T - n)!}[X(t)]^n[Y(t)]^{n_T - n}, \tag{4.4}$$

where, $X(t) = \frac{K_1(1 - \exp(-(K_1 + K_2)t))}{K_1 + K_2}$, $Y(t) = \frac{K_2 + K_1 \exp(-(K_1 + K_2)t)}{K_1 + K_2}$, assuming that initially all the active sites are unoccupied. With this initial condition, the time-dependent average number of occupied sites is given by $\langle n(t) \rangle = n_T X(t)$ and the average number of vacant sites is $\langle n_T - n(t) \rangle = n_T Y(t)$. The time dependent variance can be written as $\sigma^2(t) = n_T X(t) Y(t)$.

At NESS, the average number of occupied sites, $\langle n \rangle$ and the average number of unoccupied sites, $\langle n_T - n \rangle$ becomes, $\langle n \rangle = n_T X^{(ss)}$ and $\langle n_T - n \rangle = n_T Y^{(ss)}$, respectively, where $X^{(ss)} = \left(\frac{K_1}{K_1 + K_2}\right)$ and $Y^{(ss)} = \left(\frac{K_2}{K_1 + K_2}\right)$ with $K_1 = (k_1 + k_2)$ and $K_2 = (k_{-1} + k_{-2})$. Now at NESS, the probability distribution described in Eq.(4.4) can be written as

$$P_{(n)}^{(ss)} = \frac{n_T!}{n!(n_T - n)!}[X^{(ss)}]^n[1 - X^{(ss)}]^{n_T - n}, \tag{4.5}$$

which is independent of initial condition. If n_T is very large and $X^{(ss)}$ is very small, $\frac{n_T!}{(n_T - n)!}$ becomes $(n_T)^n$ and $(1 - X^{(ss)})^{(n_T - n)} \approx \exp[-n_T X^{(ss)}]$. Then the probability distribution becomes Poissonian,

$$P_{(n)}^{(ss)} = \frac{\left[n_T X^{(ss)}\right]^n}{n!}\exp\left[-n_T X^{(ss)}\right] = \frac{\left[\langle n \rangle^{(ss)}\right]^n}{n!}\exp\left[-\langle n \rangle^{(ss)}\right]. \tag{4.6}$$

If $X^{(ss)}$ is small, then the Michaelis-Menten constant, $K_M = \frac{(k_{-1} + k_{-2})}{k_1}$ becomes large. So the Poisson distribution is a natural candidate for the enzymes which have large Michaelis-Menten constants. In contrast to the equilibrium solution of the chemical master equation for bulk reaction, which is a Poisson distribution with respect to the number of molecules of each reactant, here also we obtain Poisson distribution with respect to the number of active sites of the oligomeric enzyme in chemiostatic condition but in a non-equilibrium steady state. So in the spirit of single molecule enzymology, single oligomeric enzyme with large Michaelis-Menten constant gives a bulk-like situation in NESS.

4.2.2 Effect of force on enzyme kinetics reaction:

To manipulate enzymatic activity, a force can be applied to separate the substrate or product from enzyme molecule. If one begins to separate the molecules along some direction of minimum work, then according to Bell[31], the free energy must vary with separation and it passes through a minimum at the equilibrium bonding

position and work must be done to further separate the molecules. Here we have considered an event where an external mechanical force is used to lower the activation barrier of breaking the ES complex, so the kinetics of the reaction can be understood in terms of the formation or dissociation of ES complex. Now the ES complex dissociates into either (E+S) or (E+P) and the formation of ES complex depends on the substrate and product population level. But the dissociation of ES complex is dependent on applied external mechanical force because if a constant external pulling force, F is applied on the oligomeric enzyme, then the bonds between the identical active sites of the enzyme and the substrates feel the force as F cosθ as shown in Fig.4.2. Here we have considered that each identical bond feels the same
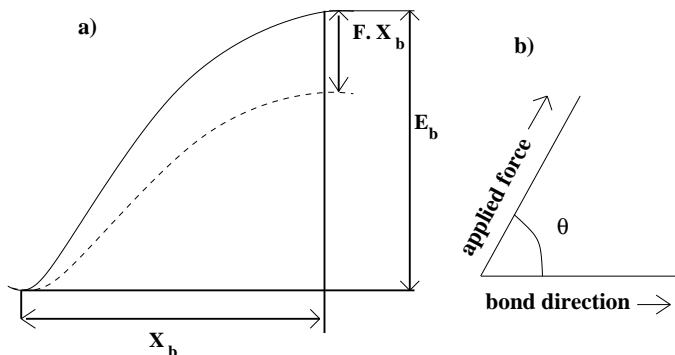
Figure 4.2: (a) The plot depicts the activation energy, E_b as a function of the extension of bond along which the bond is ruptured. Here F is the externally applied mechanical force and X_b is the minimum elongation of the bond for dissociation. The force reduces the activation energy for the ES-complex dissociation and for large enough force, the dissociation becomes almost activationless. (b) The direction of the externally applied mechanical force makes an angle θ with the ES bond direction, so each bond between an active site of the enzyme and a substrate experience the force, Fcosθ

magnitude of force F cosθ, so the energy required to break a bond which is between one active site of the enzyme and a substrate is FX$_b$cosθ, where X_b is the minimum elongation of a bond for dissociation. Here a typical magnitude of X_b of 0.5 A^0 is sufficient for bond rupture. The total dissociation rate constants should be modified as[31, 139],

$$K_2' = K_2 \exp\left[\frac{FX_b\cos\theta}{k_B T}\right], \tag{4.7}$$

where $K_2 = (k_{-1} + k_{-2})$ and K_2' is the total dissociation rate constant which is modified by the applied force. X_b is the minimum elongation of a bond for dissociation and θ is the angle between the force direction and the 'ES' bond direction with k_B is the Boltzmann constant and T is the absolute temperature.

4.2.3 Net velocity of the reaction and isolated turn over rate:

As we are interested to explain the force induced oligomeric enzyme kinetics in terms of the average number of occupied and unoccupied sites, which are usually the ensemble average properties, so we designate the rate of the overall reaction as 'net velocity of the reaction'. According to the above reaction scheme, at steady state the rate of product formation is, $k_{-2}\langle n \rangle$ and the rate of product dissociation is $k_2 \langle n_T - n \rangle$, so net product formation rate, v_{net} is given by

$$v_{net} = k_{-2}\langle n \rangle - k_2\langle n_T - n \rangle = n_T \left[\frac{k_{-2}(K_1) - k_2(K_2)}{K_1 + K_2} \right], \qquad (4.8)$$

where $K_1 = (k_1 + k_2)$ and $K_2 = (k_{-1} + k_{-2})$. Now if the third step of the reaction is irreversible, *i.e.*, if k_2 is zero, then v_{net} follows the traditional Michaelis-Menten equation

$$v_{net} = n_T \frac{v_{max}[S]}{K_M + [S]}, \qquad (4.9)$$

where K_M is the Michaelis-Menten constant with $v_{max} = k_{-2}$ and $K_M = \dfrac{k_{-1} + k_{-2}}{k_1}$.

A hypothetical isolated turnover reaction can be defined as a turnover initially with all the active sites of the enzyme are in vacant state and advancing with the first passage through the product release step, which subsequently means that all the occupied sites are converted to vacant sites [140]. Here among the n_T number of active sites present in the oligomeric enzyme, each active site completes only one enzymatic cycle. For one enzymatic cycle the reaction scheme can be written as, vacant site $\xrightarrow{K_1}$ occupied site $\xrightarrow{K_2}$.

During a time interval at normal reaction condition more than one enzymatic cycle may be performed by an active site and this cycle number are varied from active site to active site. Now in the hypothetical isolated turnover case, consider that the probability distribution $P^{iso}_{(m,n)}(t)$ as the probability of having 'm' number of vacant sites and 'n' number of occupied sites are present at time t. As the reaction scheme for an isolated turn over is similar to the concerted reaction of McQuarrie [9], the master equation can be written as

$$\frac{dP^{iso}_{(m,n)}(t)}{dt} = K_1(m+1)P^{iso}_{(m+1,n-1)}(t) + K_2(n+1)P^{iso}_{(m,n+1)}(t)$$

$$-K_1 m P^{iso}_{(m,n)}(t) - K_2 n P^{iso}_{(m,n)}(t). \qquad (4.10)$$

Solution of this master equation gives the average number of vacant sites, $\langle m(t) \rangle_{iso}$ and average number of occupied sites $\langle n(t) \rangle_{iso}$ at time t in a single isolated turnover. The expression of time dependent average $\langle m(t) \rangle_{iso}$ and $\langle n(t) \rangle_{iso}$ are

$$\langle m(t) \rangle_{iso} = n_T e^{-K_1 t}, \qquad (4.11)$$

and

$$\langle n(t) \rangle_{iso} = \frac{n_T K_1}{(K_2 - K_1)} \left[e^{-K_1 t} - e^{-K_2 t} \right]. \tag{4.12}$$

As the total number of active sites is constant, so $\langle m(t) \rangle_{iso}$ can be written as $\langle n_T - n(t) \rangle_{iso}$. Now integration of these expressions with respect to t by considering the limit from zero to infinity gives the residence time of vacant sites r_{vac} and residence time of occupied sites r_{occu}. Therefore, the total residence time is , $r_{total} = r_{vac} + r_{occu}$. The expressions of the r_{vac} and r_{occu} are

$$r_{vac} = \int_0^\infty \langle m(t) \rangle_{iso} dt = \frac{n_T}{K_1}, \tag{4.13}$$

$$r_{occu} = \int_0^\infty \langle n(t) \rangle_{iso} dt = \frac{n_T}{K_2}, \tag{4.14}$$

and

$$r_{total} = n_T \left[\frac{(K_1 + K_2)}{K_1 K_2} \right]. \tag{4.15}$$

The total residence time for one subunit r_{total} is given by, $r_{total} = \frac{(K_1+K_2)}{K_1 K_2}$. If $k_2 = 0$, the net rate becomes $v_{net} = \frac{v_{max}[S]}{K_M+[S]}$ where K_M is the Michaelis Menten constant with $v_{max} = k_{-2}$ and $K_M = \frac{k_{-1} + k_{-2}}{k_1}$. Hence $1/r_{total}$ is equal to the v_{net} for one subunit. As there is no interaction present among the subunits of the oligomeric enzyme, each sub-unit can be assumed as an enzyme having one active site and n_T/r_{total} gives the net velocity of the oligomeric enzyme having n_T number of subunits. Without going through the probability distribution function, the average value of occupied sites and vacant sites in non-equilibrium steady state can be easily calculated in terms of the residence time of vacant sites and the residence time of occupied sites in a isolated turnover as

$$\langle n \rangle = \frac{r_{occu}}{r_{total}} n_T = \frac{K_1}{(K_1 + K_2)} n_T, \tag{4.16}$$

and

$$\langle n_T - n \rangle = \frac{r_{vac}}{r_{total}} n_T = \frac{K_2}{(K_1 + K_2)} n_T. \tag{4.17}$$

So the net velocity of the reaction, v_{net} at non-equilibrium steady state in terms of mean residence time can be given by

$$v_{net} = n_T \left[k_{-2} \left(\frac{r_{occu}}{r_{total}} \right) - k_2 \left(\frac{r_{vac}}{r_{total}} \right) \right], \tag{4.18}$$

which are already derived through the master equation. From the expression of the net velocity of the reaction, it is found that the net rate of the product formation is directly proportional to the total number of active sites in the oligomeric enzyme. However, the force and other parameters of the reactions, *i.e*, substrate and product concentrations and various rate constants have subtle effect on the net rate of the product formation.

4.3 Non-equilibrium thermodynamic characterization of oligomeric enzyme kinetics

Here we have given a non-equilibrium thermodynamic description of the single oligomeric enzyme kinetics. It is observed that due to the chemiostatic condition, an oligomeric enzyme reaction occurs at the non-equilibrium condition. Here we have first calculated the various entropy production rates from the master equation and then describe the entropy production along a trajectory.

4.3.1 Entropy production rates from the master equation

To calculate the various entropy production rates, here we have assumed that the surroundings behaves like an ideal reservoir with no inherent entropy production except through the boundaries of the system. Usually the system entropy is defined in terms of the Shannon entropy as

$$S_{sys}(t) = -k_B \sum_n P_n(t) \ln P_n(t). \tag{4.19}$$

We set the Boltzmann constant, $k_B = 1$. Using the above master equation, we get the system entropy production rate [13, 74, 100, 101] as

$$\dot{S}_{sys}(t) = \frac{1}{2} \sum_{n,\mu} [w_\mu(n - \nu_\mu|n) P_{(n-\nu_\mu)}(t) - w_{-\mu}(n|n - \nu_\mu) P_n(t)]$$

$$\times \ln \frac{P_{(n-\nu_\mu)}(t)}{P_n(t)}. \tag{4.20}$$

The system entropy production(ep) rate can be split as[100]

$$\dot{S}_{sys}(t) = \dot{S}_{tot}(t) - \dot{S}_m(t). \tag{4.21}$$

Here the first term in the r.h.s. of Eq.(4.21) gives the total entropy production rate and the second term denotes the medium entropy production rate due to the entropy flux into the surroundings. Therefore, the total and medium entropy production rates are defined as

$$\dot{S}_{tot}(t) = \frac{1}{2} \sum_{n,\mu} [w_\mu(n - \nu_\mu|n) P_{(n-\nu_\mu)}(t) - w_{-\mu}(n|n - \nu_\mu) P_n(t)]$$

$$\times \ln \frac{w_\mu(n - \nu_\mu|n) P_{(n-\nu_\mu)}(t)}{w_{-\mu}(n|n - \nu_\mu) P_n(t)}, \tag{4.22}$$

and

$$\dot{S}_m(t) = \frac{1}{2} \sum_{n,\mu} [w_\mu(n - \nu_\mu|n) P_{(n-\nu_\mu)}(t) - w_{-\mu}(n|n - \nu_\mu) P_n(t)]$$

$$\times \ln \frac{w_\mu(n - \nu_\mu|n)}{w_{-\mu}(n|n - \nu_\mu)}. \tag{4.23}$$

Using the expressions of the corresponding transition probabilities from Eq.(4.2) and the time dependent solution of the master equation, we finally obtain

$$\dot{S}_{tot}(t) = \langle n(t) \rangle \left[k_{-1}\ln\left(\frac{k_{-1}X}{k_1 Y}\right) + k_{-2}\ln\left(\frac{k_{-2}X}{k_2 Y}\right) \right]$$

$$- \langle n_T - n(t) \rangle \left[k_1\ln\left(\frac{k_{-1}X}{k_1 Y}\right) + k_2\ln\left(\frac{k_{-2}X}{k_2 Y}\right) \right]. \tag{4.24}$$

Now at the NESS, we use the condition of equality of forward and backward cycle flux instead of detailed balance condition[11]. Therefore, from Eq.(4.1), we obtain

$$w_1(n - 1|n)P_{(n-1)} - w_{-1}(n|n - 1)P_n = w_{-2}(n|n - 1)P_n - w_2(n - 1|n)P_{(n-1)}. \tag{4.25}$$

By using equation (4.25) in equation (4.22), we obtain the total entropy production rate at the steady state as

$$\dot{S}_{tot}^{(ss)} = \sum_n \left[w_1(n - 1|n)P_{(n-1)} - w_{-1}(n|n - 1)P_n \right]$$

$$\times \ln\left(\frac{w_1(n - 1|n)P_{(n-1)} \times w_{-2}(n|n - 1)P_n}{w_{-1}(n|n - 1)P_n \times w_2(n - 1|n)P_{(n-1)}} \right). \tag{4.26}$$

After putting the values of the transition probabilities, $\langle n \rangle$ and $\langle (n_T - n) \rangle$ at the steady state, we obtain

$$\dot{S}_{tot}^{(ss)} = n_T \ln\left(\frac{k_{-1}k_2}{k_1 k_{-2}}\right) \left[\left(\frac{k_2 k_{-1} - k_1 k_{-2}}{k_1 + k_{-1} + k_2 + k_{-2}}\right) \right]. \tag{4.27}$$

At $\left(\frac{k_{-1}k_2}{k_1 k_{-2}}\right) = 1$, $\dot{S}_{tot}^{(ss)}$ becomes zero and the steady state corresponds to the detailed balance condition that holds in equilibrium. However, we are in general interested in the entropy production in the non-equilibrium steady state where $\left(\frac{k_{-1}k_2}{k_1 k_{-2}}\right) \neq 1$. Integrating $\dot{S}_{tot}$ between the time interval $t_0 = 0$ to t, we get the total entropy production, ΔS_{tot}. As we have considered that initially (time $t_0 = 0$) all the sub-units are vacant, i.e, n=0 with $P_n(0) = 1$, therefore, from equation 4.19, $S_{sys} = 0$ in the beginning.

4.3.2 Single trajectory analysis of entropy production and fluctuation theorem

In the previous subsection, the calculated total entropy production from the master equation is actually an average property. However, for a small system the fluctuation

is as important as the average and to get an idea about the distribution we have calculated the total entropy production of an ensemble of trajectories. For a single trajectory, the system can be quantified in terms of the time series of the number of occupied sites of the oligomeric enzyme which is a fluctuating quantity due to the random occurrence of the reaction events within a short time interval. The time series of the number of occupied sites is calculated by using the stochastic simulation approach [14, 15]. The simulated single trajectory of forward and backward path is used to calculate the total entropy production which varies from trajectory to trajectory as it is a fluctuating quantity.

Let us consider a stochastic trajectory of the number of occupied sites, $n(t)$ which starts at n_0 and jumping at times t_j from n_{j-1} to n_j ending up at n_l with $t = t_l$,

$$n(t) \equiv (n_0, t_0) \xrightarrow{\nu_\mu^1} (n_1, t_1) \xrightarrow{\nu_\mu^2} ..... \rightarrow (n_{j-1}, t_{j-1})$$

$$\xrightarrow{\nu_\mu^j} (n_j, t_j) \rightarrow ... \rightarrow (n_{l-1}, t_{l-1}) \xrightarrow{\nu_\mu^l} (n_l, t_l). \tag{4.28}$$

Here $n_j = n_{j-1} + \nu_\mu^j$ and $t_j = t_{j-1} + \tau_j$ where τ_j is the time interval between two successive jumps and j is the population state at time t. During the jump from the $(n_j - 1)$ state to the n_j state, any one of the four sub-reactions will occur and the time interval τ_j between the two jumps is a random variable following the exponential distribution

$$p(\tau_j) = a \ \exp(-a\tau_j) \tag{4.29}$$

with $a = \sum_{\mu=\pm1}^{\pm2} w(n_j - 1; \nu_\mu^j)$ and $w(n_{j-1}; \nu_\mu^j)$ denotes the transition probability from the state $(n_j - 1)$ to the n_j state through a reaction channel μ with the stoichiometric coefficient ν_μ^j along a single trajectory.

Now a time reversed trajectory can be defined as,

$$n^R(t) \equiv (n_l, t_l) \xrightarrow{-\nu_\mu^l} (n_{l-1}, t_{l-1}) \xrightarrow{-\nu_\mu^{l-1}} ... \rightarrow (n_j, t_j)$$

$$\xrightarrow{-\nu_\mu^j} (n_{j-1}, t_{j-1})... \rightarrow (n_1, t_1) \xrightarrow{-\nu_\mu^1} (n_0, t_0). \tag{4.30}$$

This time reversed trajectory is generated due to the occurrence of a reaction channel whose state changing vector $-\nu_\mu^j$ is exactly opposite to the state changing vector ν_μ^j of the forward reaction channel.

The entropy production along a single stochastic trajectory can be defined as[85]

$$s(t) = -\ln P_n(t) \tag{4.31}$$

where $P_n(t)$ is the solution of the stochastic master equation for a given initial condition, $P_{n_0}(t_0)$, taken along the specific trajectory $n(t)$. Note that, the single trajectory entropy is denoted by s whereas the average entropy production, whether being an ensemble average obtained from the master equation or averaged over many

trajectories generated in the simulation, is denoted by S. Now the time dependent total entropy production, Δs_{tot} can be split into a system part, Δs_{sys} and a medium contribution, Δs_m. Hence the change in total entropy along a trajectory can be written as[81, 82, 85]

$$\Delta s_{tot} = \Delta s_m + \Delta s_{sys} \tag{4.32}$$

where

$$\Delta s_{sys} = \ln \frac{P_{(n_0)}(t_0)}{P_{(n)}(t)} \tag{4.33}$$

and

$$\Delta s_m = \sum_j \ln \frac{w(n_{j-1}; \nu_\mu^j)}{w(n_j; -\nu_\mu^j)}. \tag{4.34}$$

The ratio of probabilities of the forward trajectory path, $p(n(t)|n(t_0))$ and that of the backward trajectory path, $p(n^R(t)|n_l)$ of the reaction system is given by the quantity $e^{\Delta s_{tot}}$, obtained by applying the stochastic simulation approach. For different trajectories we get different total entropy production values and among them some values may be negative, but the average total entropy production value must be positive. As the total entropy production values differ from trajectory to trajectory, so we get a distribution, $p(\Delta s_{tot})$. When the system reaches a steady state, the detailed fluctuation theorem is satisfied as

$$\frac{p(\Delta s_{tot})}{p(-\Delta s_{tot})} = e^{\Delta s_{tot}}. \tag{4.35}$$

Here we have studied the probability distribution function of entropy production in terms of the mean and variance of the distribution in the transient and steady state regime. We have numerically investigated how the negative values of total entropy appears in a single trajectory due to the applied force and the total number of active sites of the oligomeric enzyme or the system-size of the problem.

4.4   Results and Discussion:

In this section, we have discussed how an external mechanical force affects the overall kinetics as well as thermodynamics of an oligomeric enzyme catalysis. For the kinetic description, we have calculated the variation of average value of occupied sites as a function of time as well as a function of force and substrate at NESS. Similarly, the net velocity of the reaction is also studied as a function of force and substrate at NESS. We have also discussed the variation of average values of occupied and unoccupied sites with time and force for an isolated turnover. To discuss the non-equilibrium thermodynamic behavior of the system, we have calculated the system, medium and total entropy productions in the dynamic regime and at non-equilibrium steady state for different applied forces. To obtain the medium entropy production

as well as the distribution of the total entropy production, we have constructed the time series of the number of occupied sites on the basis of single trajectory concept and it is adapted with the Gillespie's stochastic simulation approach. The simulation studies help us to find out the change of the distribution of the total entropy production by the externally applied force and on the system size. We have also studied the variation of mean, variance and the relative variance of the distribution with function of force at NESS. The studies at NESS give an important correspondence between the total entropy production rate and the net velocity of the reaction. To calculate the average substrate binding, $\langle n(t) \rangle$, the net velocity of the reaction and the various entropy production rates, we have taken the rate parameters as $k_1 = 15.0$, $k_{-1} = 7.0$, $k_{-2} = 2.0$ and $k_2 = 1.0$, all in s^{-1}, for both analytical and numerical studies. The total number of subunits of the single oligomeric enzyme is taken as $n_T = 20$.

4.4.1   Kinetic descriptions of an oligomeric enzyme
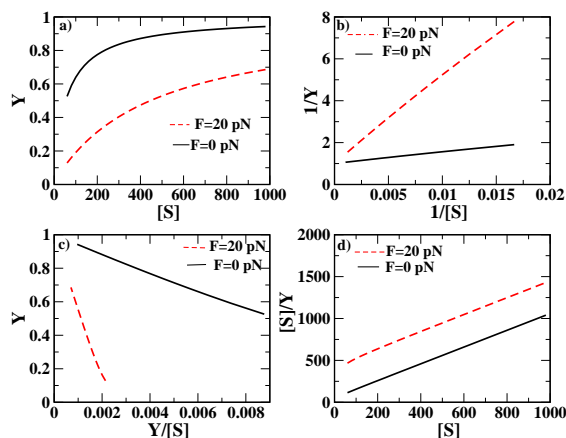
Figure 4.3: (a) Plot of fraction of occupied sites, Y versus substrate concentration, [S] is hyperbolic. (b) Plot of inverse of occupied sites, $(1/Y)$ versus inverse of population of substrate, $(1/[S])$ gives a straight line that is analogous to Lineweaver-Burk plot. (c) This plot is fraction of occupied sites, Y versus fraction of occupied sites/substrates, $(Y/[S])$ is Eadie-Hofstee type plot, which gives a straight line. (d) Substrate concentration/fraction of occupied sites, $([S]/Y)$ versus substrates, [S] plot is Hanes type plot that gives a straight line. All of these plots are done at F=0 pN and F=5 pN. The nature of the plots remain the same when F=0 pN and F=5 pN with $k_1'=0.15$.

An oligomeric enzyme shows either positive, negative or no cooperativity effect depending on the nature of the interactions present among the subunits of the enzyme. The nature of the cooperativity can be understood by the plot of fractional saturation of the oligomeric enzyme, Y versus substrate concentration, [S]. Usually fractional saturation of the oligomeric enzyme is expressed as $(\langle n \rangle / n_T)$, where $\langle n \rangle$ is

the average number of substrate-bound subunits present in the oligomeric enzyme at steady state and n_T is the total number of sub-units of the oligomeric enzyme. From the Fig.(4.3)(a), it is observed that Y versus [S] plot is hyperbolic and from the other plots such as Lineweaver-Burk (Fig.4.3(b)), Eadie-Hofstee (Fig.4.3(c)) and Hanes (Fig.4.3(d)), the curves are straight lines with positive and negative slopes. It can be said that the cooperativity is absent in this stabilized oligomeric enzyme for which the various conditions of cooperativity are extensively discussed[35, 34]. With the present kind of application of an external mechanical force, the nature of the curves remain the same, so it can be concluded that the application of force cannot change the nature of the cooperativity present in the enzyme.
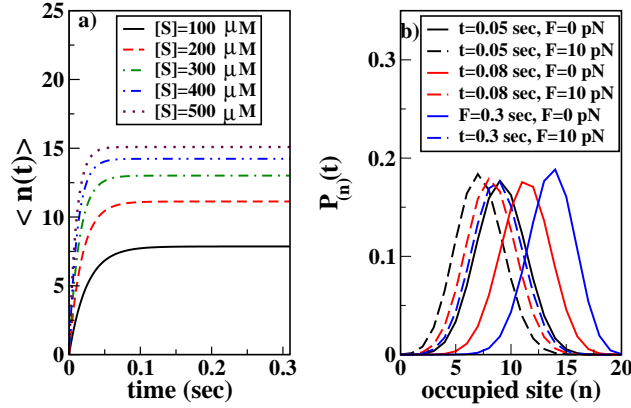
Figure 4.4: (a) Plot of average value of occupied sites $\langle n \rangle (t)$ versus time with $k_1^{'}$=0.15, k_{-1}= 7.0, k_{-2}=2.0, and k_2=1.0, in sec^{-1} at several substrate values. Time required to reach a NESS is dependent on the substrate concentration. (b) Probability distribution function $P_n(t)$ versus number of occupied sites, n gives the binomial distribution at different time with the values of force, F=0 and F=10 pN.

The rate of ES complex formation depends on the substrate concentration because it is maintained at a constant level in chemiostatic condition. From Fig.4.4(a), it is observed that at first the average value of occupied sites, $\langle n(t) \rangle$ increases with increase in time, but after a certain time, it reaches a non-equilibrium steady state(NESS). How fast the system reaches a steady state that depends on the concentration of the substrate. With increase in time, $\langle n(t) \rangle$ increases until a steady state is achieved but the distribution remains binomial because the total number of active sites is constant. When an extra mechanical force is applied on the enzyme, the rate of dissociation is enhanced, as a result $\langle n(t) \rangle$ becomes lower which is in conformity with Fig.4.4(b).

The effect of force on enzyme kinetics can be clearly understood from the consideration of the case of a hypothetical isolated turnover. In an isolated turnover, it

is observed that with increase in the magnitude of force, the dissociation rate constants are increased and consequently the residence time of the occupied sites, r_{occu} is decreased, but as the ES complex formation rate is force independent, so residence time of vacant site remains constant at a particular substrate concentration which is shown in Fig.4.5(a). As the residence time of occupied sites, r_{occu} is decreased
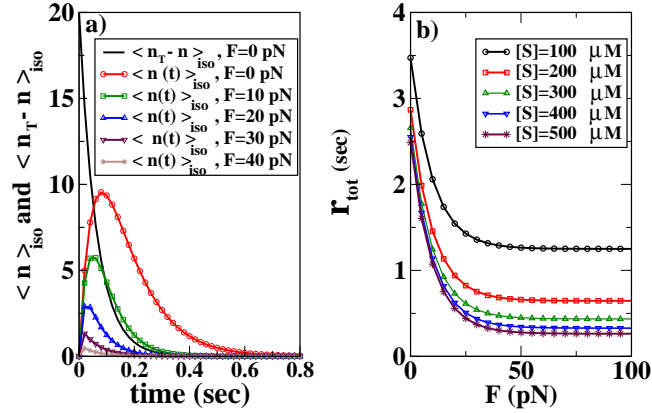
Figure 4.5: (a) Plot of average values of occupied sites for isolated turn over, $\langle n \rangle_{iso}$ and average value of unoccupied sites $\langle n_T - n \rangle_{iso}$ for isolated turnover versus time for different values of forces with substrate population S=100 μM and the rate parameters are k_1'=0.15, k_{-1}= 7.0, k_{-2}=2.0, and k_2=1.0 sec^{-1}. (b) Plot of the total residence time r_{total} versus Force in pN at different substrate population values with the same set of rate constants.

by the application of a mechanical force, so it is expected that the net velocity of the reaction, v_{net} must be increased. The residence time of vacant sites, r_{vac} is independent of force and the residence time of occupied sites, r_{occu} is decreased with increase in force. As the total residence time, $r_{total} = r_{vac} + r_{occu}$, so r_{total} decreases with time but when r_{occu} becomes zero at a critical value of force, the reaction of ES dissociation becomes barrierless and r_{total} reaches a steady value. The critical value at which r_{total} becomes constant that depends on the chemiostatic conditions which is shown in Fig.4.5(b). Dissociation rate constants are increased with increase in force which gives a lowering of the average value of occupied sites, $\langle n \rangle$ at NESS. But at a particular value of force, $\langle n \rangle$ becomes zero. Above this critical value of force, the ES complex dissociates instantly. The critical value of force is dependent on the chemiostatic condition which is shown in Fig.4.6(a). From Fig.4.6(b), it is observed that at NESS, $\langle n \rangle$ becomes saturated with increase in substrate concentration at lower value of external force, but at higher value of force it increases linearly with increase in concentration of substrate although $\langle n \rangle$ never exceeds n_T. This is due to the fact that at lower value of force the rate of ES complex formation is greater than the rate of dissociation, so $\langle n \rangle$ reaches a steady value but at higher value of
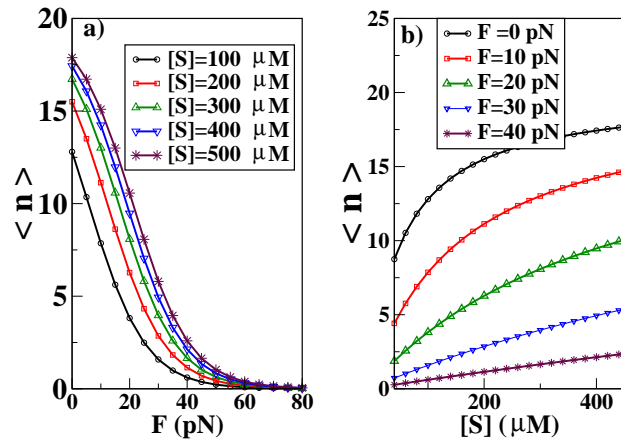
Figure 4.6: (a) Plot of average value of occupied sites $\langle n \rangle$ versus force, F in pN with substrate concentration, [S] in μM at NESS. The rate constants are $k_1'= 0.15$, $k_{-1}= 7.0$, $k_{-2}= 2.0$, and $k_2= 1.0 \text{ sec}^{-1}$. (b) $\langle n \rangle$ versus [S] is plotted at different values of force at NESS with the same set of rate parameters.

force, the rate of dissociation become greater than the rate of association. Consequently the reaction becomes a barrierless. From the mathematical point of view we give a possible explanation by which we can explain why $\langle n \rangle$ increases linearly with substrate concentration.
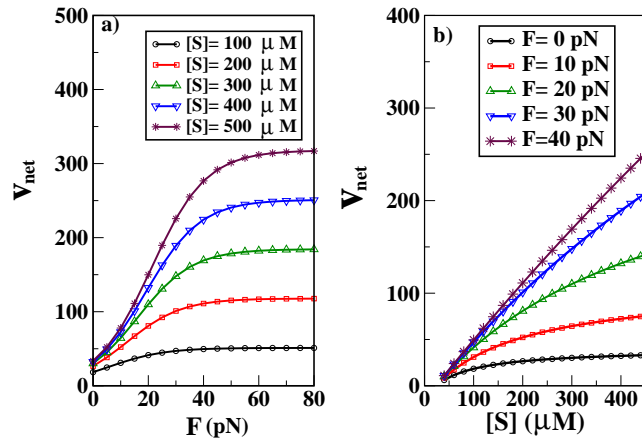
Figure 4.7: (a) The net velocity of the reaction, v_{net} versus force, F is plotted for different substrate concentration at NESS with the rate parameters $k_1'= 0.15$, $k_{-1}= 7.0$, $k_{-2}= 2.0$, and $k_2= 1.0 \text{ sec}^{-1}$. (b) Plot of the net velocity of the reaction, v_{net} versus [S] at different values of force at NESS with the same set of rate parameters. In the above two figures, minimum substrate concentration is considered as 60 μM.

The net velocity v_{net} increases with external force when the magnitude of force is comparatively small. But at a particular value of force v_{net} reaches a steady value.

This critical value of force is important because above this value, v_{net} does not increase with further application of force. The reason is that above this force value the ES complex dissociates instantly, so it can be said that above this critical value of force the enzyme kinetics reaction becomes a barrierless reaction. The critical value of force is dependent on the parametric values of substrate and product concentration in chemiostatic condition which can be seen in Fig.4.7(a). v_{net} increases with increase in concentration of substrate and becomes a steady value at lower values of force. But at a higher value of force, v_{net} increases linearly with the [S] as shown in Fig.4.7(b). The possible explanation is that at higher value force ES complex dissociates instantly.

4.4.2 Non-equilibrium thermodynamic analysis
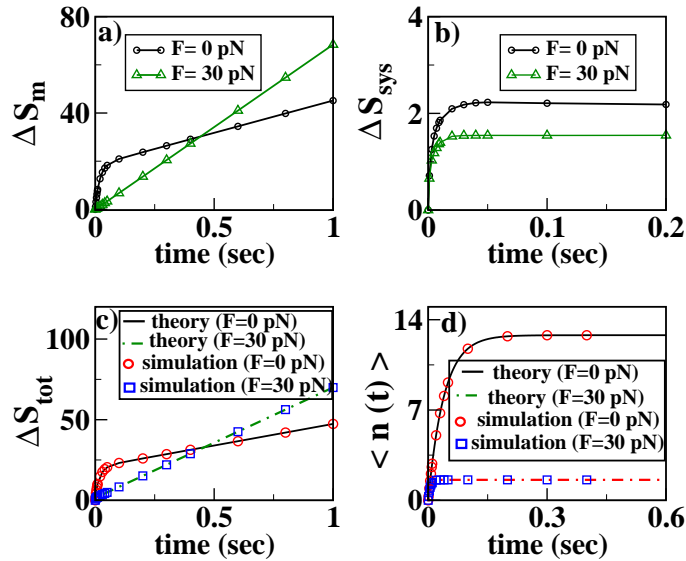
Figure 4.8: Plot of (a) ΔS_m, (b) ΔS_{sys}, (c) ΔS_{tot} and (d) $\langle n(t) \rangle$ versus time for force parameters, F=0 pN and F=30 pN.

Here we have determined the system, medium and total entropy productions, for a single trajectory using the Gillespie's stochastic simulation approach. The corresponding macroscopic (ensemble average) quantities are then calculated from the averaging over the trajectories (2×10^5 in number) obtained from the simulation. We have plotted ΔS_m, ΔS_{sys} and ΔS_{tot} in Fig.4.8 as a function of time determined at different forces. The time evolution of average number of occupied sites, $\langle n(t) \rangle$ at different forces are also shown. ΔS_{tot} and $\langle n(t) \rangle$ are determined from the simulation as well as from the analytical expression to provide a check of the simulation results. Now the determination of ΔS_{sys} from Eq.(4.33) uses the analytical solution of the master equation, $P_{(n)}(t)$ at various points of time. The plot of ΔS_m, as shown in Fig.4.8(a), increases with time, initially at a faster rate for lower value of force

but eventually the rate becomes higher for the larger force. ΔS_{tot}, obtained from simulation as well as from Eq.(4.24), shows similar behavior as a function of the force parameter regarding the values at short and long times as shown in Fig.4.8(c). In Fig.4.8(b), we have plotted the variation of ΔS_{sys}. After a small time, ΔS_{sys} reaches a steady value as the reaction system reaches the NESS. With increase in force, it reaches the steady value earlier and the magnitude of ΔS_{sys} decreases with increase in force. As the magnitude of ΔS_{sys} is small compared to the value of ΔS_m, hence the nature of the curve of ΔS_m versus time follows the ΔS_{tot} versus time plot and at the NESS they grow linear in time. At $t \to \infty$, $\Delta S_m \to \Delta S_{tot}$ which is very useful when ΔS_{sys} is not known, for example, when no rate equation is available although the detailed steps of the reaction may be known. Finally, one can see from Fig.4.8(d) that $\langle n(t) \rangle$ decreases significantly with the application of force as the force increases the dissociation rate of the ES-complex. Its variation with time and the force is similar to that of ΔS_{sys}. It is evident from the figures that the transient and NESS characteristics of the reaction are exactly followed by the system entropy production. However, the medium entropy production which is mainly concerned with the flow through the boundaries of the system, actually takes care of the total entropy production at NESS when the system property saturates; one can identify the boundary effect of the system by its size and physical or chemical nature of interactions between the system and surroundings in terms of the medium entropy.
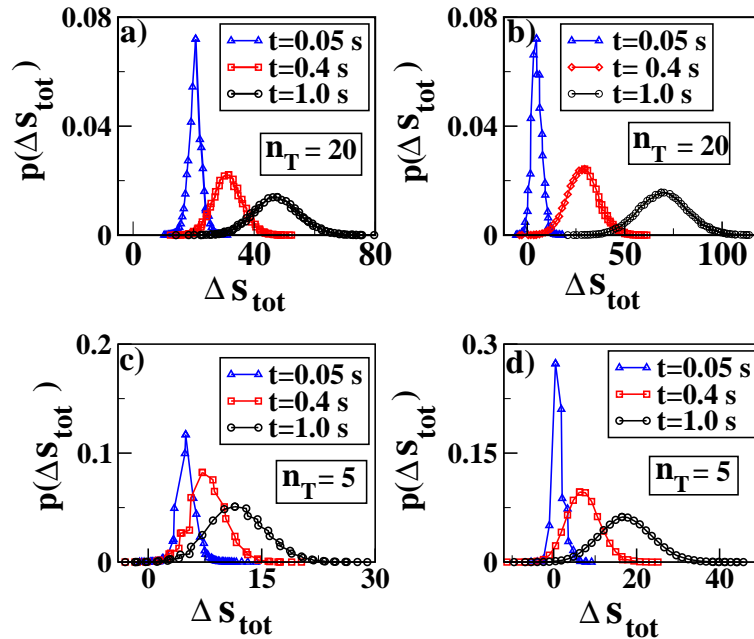
Figure 4.9: The distribution of the total entropy production over trajectories, $p(\Delta s_{tot})$ versus Δs_{tot} is plotted for different times in (a) and (b) with force, F= 0 pN and F=30 pN, respectively with $n_T = 20$. The corresponding plots for $n_T = 5$ are shown in (c) and (d).

The entropy production, Δs_{tot} along a single trajectory is a fluctuating quantity;

it has a distribution, $p(\Delta s_{tot})$, which is shown in Fig.4.9(a) and Fig.4.9(b) at different time intervals for force values F = 0 pN and F = 30 pN, respectively with n_T = 20. At short times, the distribution is non-Gaussian in nature but gradually tends to a Gaussian distribution which is obtained due to the chemiostatic condition of the open system at NESS. It is evident from the figure that initially there is a non-zero probability of observing negative values of Δs_{tot} for a particular trajectory with F = 30 pN whereas for F = 0 pN, such probability is zero for the rate parameters considered here. We have found that with rise in the magnitude of the force, the probability of observing negative values of Δs_{tot} first increases but then saturates (not shown in figures). Although the mean value can be obtained from the master equation, the broadening of the distribution due to the increase in external force can only be realized through the trajectory based method.

By comparing the distributions in Fig.4.9(a) and Fig.4.9(b) at different times, one can see that the overall distribution quickly shifts to the positive zone reaching larger positive values with increased force. These simulation results provide the microscopic basis for the macroscopic result of the initially lower ΔS_{tot} for higher forces and explains how ΔS_{tot} becomes higher for the same higher forces at some later time. The larger probability for negative Δs_{tot} values under the $p(\Delta s_{tot})$ distribution curve at higher forces brings the average value, ΔS_{tot} down at short times. Now similar results are given in Fig.4.9(c) and Fig.4.9(d) for n_T = 5. By comparing these plots with those for n_T = 20 reveals that for lower system size, there is a larger probability to realize entropy consuming trajectories as here the distribution, $p(\Delta s_{tot})$ can initially span larger negative regions, particularly at higher forces. The total entropy production distribution for n_T = 5 is always shifted to the left compared to that for n_T = 20 and this gives the microscopic basis of the extensive nature of the entropy production.

With decrease in the system size the probability of obtaining the entropy consuming trajectories is increased. It is customary to have a finite region of the distribution, $p(\Delta s_{tot})$ with negative values of Δs_{tot} to explicitly show the detailed fluctuation theorem at steady state[97]. Initially, with increase in the value of rate parameter k_2 increases the probability of finding the entropy consuming trajectories. We have observed that in the ideal Michaelis-Menten type enzyme kinetics reaction where k_2 value is very very small, probability of obtaining the entropy consuming trajectories is almost zero. It is also important to note that with increase in the values of force parameters, probability of entropy annihilating trajectories is increased and that's why we have verified the fluctuation theorem at force F=30 pN and F= 50 pN which is shown in Fig.4.10. We have plotted, $\ln\frac{p(\Delta s_{tot})}{p(-\Delta s_{tot})}$ versus Δs_{tot} in the range $-10 < \Delta s_{tot} < 10$ for n_T = 20 in Fig.4.10(a) and (b) at F=30 pN and F= 50 pN, respectively and for n_T = 5 in Fig.4.10(c) and (d) for the same force values. It is evident from the figure that the total entropy production of the reaction system
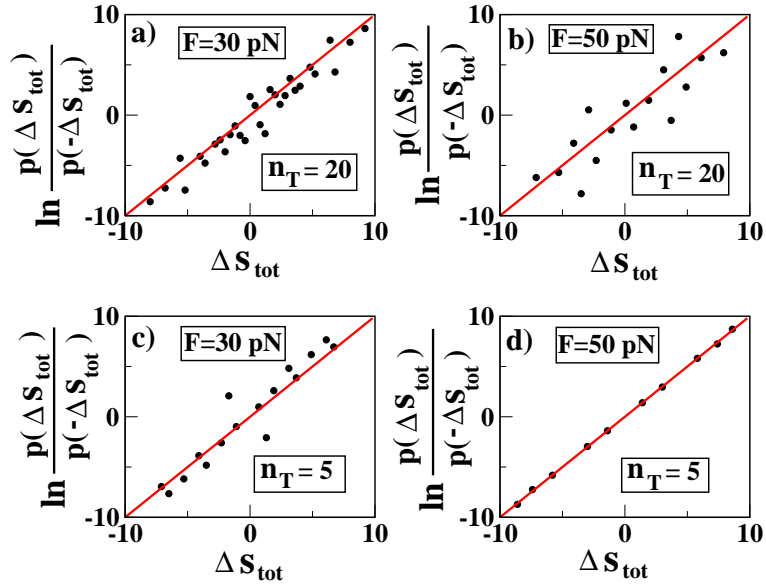
Figure 4.10: $\ln\left(\frac{p(\Delta s_{tot})}{p(-\Delta s_{tot})}\right)$ versus Δs_{tot} is plotted in (a) and (b) for $n_T = 20$ with force, F=30 pN and F=50 pN, respectively. Similar plots are drawn in (c) and (d) for $n_T = 5$ with same force parameters.

satisfy the detailed fluctuation theorem at the steady state.
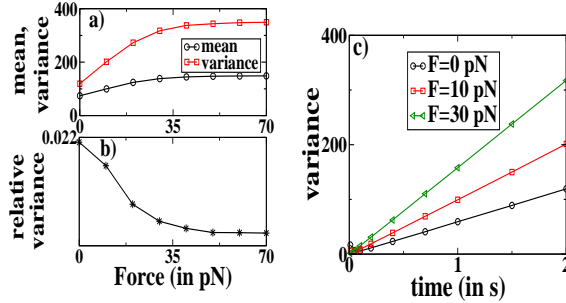
Figure 4.11: (a) The mean and variance of the total entropy production distribution, $p(\Delta s_{tot})$ as a function of the external force determined at the NESS. (b) The relative variance is plotted against applied force at NESS. (c) The evolution of variance of $p(\Delta s_{tot})$ with time for force F = 0, 10 and F = 30 pN.

From the simulation data, we also analyze the variance and the mean of the total entropy production distribution, $p(\Delta s_{tot})$. The mean total entropy production is obviously equal to the results already obtained from the analytical approach. Now from Fig.4.11(a), we see that both the mean and the variance of $p(\Delta s_{tot})$, determined at the NESS, first increases but then saturates with the applied force. The saturation at large force is associated with almost instantaneous dissociation of the ES-complex when the net rate of product formation reaches a limiting value with an activationless transition[12]. The relative variance of the distribution decreases with the external force at the NESS which is shown in Fig.4.11(b). It indicates that

the higher force makes the system more deterministic. Due to the high dissociation rate, a ES-complex breaks readily immediately after formation. So the population of the occupied state mainly oscillates between 0 and 1 and the system behaves more deterministically.

We have also shown the time evolution of the variance in Fig.4.11(c) at three different forces, F = 0 pN, F = 10 pN and F = 30 pN. It is evident that except some transient behavior, the variance increases linearly with time as the system reaches and stays at the NESS. It amounts to the fact that the entropy production distribution obeys a driven diffusion process at the NESS with a time-independent diffusion coefficient which implies the variance of entropy production distribution increases linearly with time for a particular value of applied force. The diffusion coefficient increases with increase in force before going to saturation. The mean and variance of the Gaussian distribution of the total entropy production at NESS behaves almost in a similar fashion with the applied force.
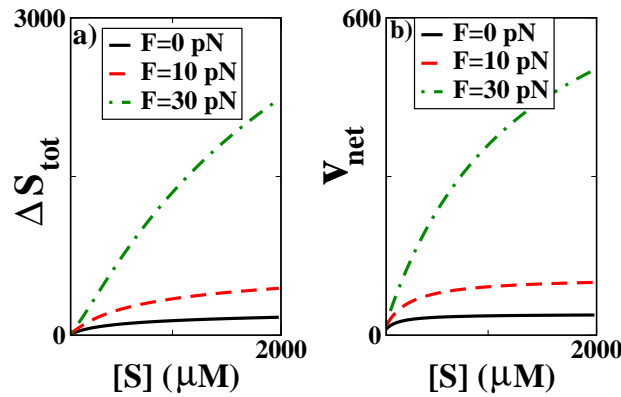
Figure 4.12: (a) Plot of total entropy production versus substrate at NESS with force values F = 0 pN, F = 10 pN and F = 30 pN. (b) The evolution of net velocity, v_{net} with substrate is plotted at NESS for same force values.

We have also calculated the total entropy production(ep) rate at NESS as a function of the substrate population for different force values. The rate increases with substrate population in a hyperbolic fashion as is usually observed both in the bulk and single enzyme catalysis and the rise of force makes the ep rate larger. We have compared this ep rate variation with the corresponding variation of the net velocity of the reaction, v_{net} in Fig.4.12(a) and Fig.4.12(b). It is evident that v_{net} rises with the substrate population and the applied force in a similar manner as that of the ep rate. From Fig.4.8 and Fig.4.12, it is evident that reaction characteristics follow the ΔS_{sys} curve as a function of time whereas at the NESS, they follow the ΔS_{tot} curve as a function of the substrate population.

4.5 Conclusion:

We have provided a master equation description of an immobilized single oligomeric enzyme catalysis in a chemiostatic condition as is usually done in single molecule enzymology. The dynamic and non-equilibrium steady state are characterized in terms of the Michaelis-Menten parameters by the application of the master equation of random hopping of the substrate molecules over the active sites of the single oligomeric enzyme. In contrast to equilibrium solution of chemical master equation for bulk reaction, which is a Poisson distribution with respect to the number of molecules of each reactant, here also we obtain Poisson distribution with respect to the number of active sites of the oligomeric enzyme in chemiostatic condition but in NESS. So in the spirit of single molecule enzymology, single oligomeric enzyme with large number of active sites or a few numbers of active sites with large Michaelis-Menten constant gives a bulk-like analog in NESS.

Effect of external mechanical force on the reaction kinetics is again shown to be another level of catalysis by mechanically manipulating the activation barrier. The net rate of the reaction is not only multiplied by the number of active sites of the oligomeric enzyme but also it is further enhanced by two to three orders of magnitude with the application of external force of $10 - 100$ pN through the techniques of atomic force microscopy. Here the average number of occupied sites decreases with increase in the value of applied force as the force decreases the height of the energy barrier of dissociation process. However, at a critical value of the applied force, the dissociation reaction becomes barrierless and consequently, above this critical value of force, the net velocity of the reaction becomes force independent.

To understand the non-equilibrium thermodynamic behavior of the system, we have also used the single stochastic trajectory approach of calculating the entropy production with Gillespie's stochastic simulation algorithm. We have thoroughly analyzed the effect of the external force on the reaction characteristics like the net velocity and the entropy productions. At the non-equilibrium steady state the rate of the reaction and entropy production rate follow the similar hyperbolic trend with substrate population for various forces. We have found that the time-variation of the system entropy production is qualitatively similar to that of the average substrate binding at different forces. From the single trajectory stochastic simulation data, we have analyzed the evolution of the distribution of the total entropy production as a function of time and the applied force. We have found that with increase in force, an increased probability of entropy consuming trajectories can be obtained which becomes more prominent for lower system-size. All these results are constrained by the detailed fluctuation theorem which maintains the corresponding entropy production distribution.

The mean value of the distribution of entropy production obtained from the en-

semble of single trajectories corresponds to the results obtained from the master equation. However, it indicates a new effect of the external force on the distribution of entropy production which is akin to power broadening of the distribution. The variance of entropy production increases linearly with time for a particular value of applied force indicating that the entropy production distribution obeys a a driven diffusion equation at the NESS. Both the mean and the variance of the Gaussian distribution of entropy production, determined at a particular instant of NESS, first increases but then saturates with the rise in applied force. This is due to the instantaneous dissociation of the ES-complex when the net rate of product formation reaches a limiting value with a 'barrierless' transition. In mechanochemistry, an external force being another controllable thermodynamic variable over the traditional variables of temperature and pressure, which can be used to find out the variance of the entropy production in small systems where the fluctuation is as important as the mean value.

Chapter 5

Entropic estimate of cooperative binding of substrate on a single oligomeric enzyme

In this chapter, we have studied the cooperativity phenomena displayed by a single oligomeric enzyme due to the different substrate binding mechanisms in a chemiostatic condition and estimated the entropy production for the cooperative binding schemes based on single trajectory analysis using a kinetic Monte Carlo technique. To understand the nature of the cooperativity, we have also introduced a cooperativity index defined in terms of the stochastic system entropy. In the introductory section we have discussed about the goal of our study. Then in Section 5.2, we have given the master equations and their steady state solutions to describe the spatial and temporal cooperative binding mechanisms and the corresponding entropy production rates. In Section 5.3, we have discussed on measures of cooperativity and introduced an index of cooperativity. Numerical results of entropy production and cooperative kinetics is discussed in Section 5.4. Finally the chapter is concluded in Section 5.5.

5.1 Introduction

Conventional thermodynamics at or near equilibrium needs serious modification to accommodate the events of single molecular processes as well as nano-systems which are generally in states far away from equilibrium [58, 131, 132, 141, 142, 143, 144, 145, 146, 147]. The single molecule study is very important in biological systems because most of the processes in cell are taking place on the level of a single or a few molecules. The non-equilibrium feature is mainly developed within a cell due to the mechanical or chemical stimuli which runs the metabolism through the driven chemical reactions[80, 136]. Quantitative measure of fluctuations [83, 84, 86, 87, 88, 95, 133] in small system like a cell is possible over short periods of time that allow

88

the thermodynamic concepts to be applied to such finite system. A crucial concept in the statistical description of a non-equilibrium small system is that of a single trajectory or path[83, 88, 84, 131] and defining the entropy of the system for such a single trajectory allows one to formulate the second law of thermodynamics at the stochastic level[80, 85, 134, 135, 136, 148]. Using this concept of trajectory-based entropy production[135, 136, 148], it is now possible to describe the non-equilibrium thermodynamic behavior of the single enzyme kinetics.

Enzyme kinetics is a very important process in cellular metabolism where the non-equilibrium feature is developed due to the imbalanced chemical reactions and the presence of chemiostatic condition which prevents the reaction system to attain equilibrium [12, 64, 65, 66]. In a chemiostatic condition, substrate and product are maintained at constant concentrations by continuous influx of the substrate and withdrawing the product from the system. Under this condition, the reaction system reaches at NESS[64, 65, 66], characterized by a non-zero total entropy production rate. Now most of the enzymes found in enzymology are oligomeric in nature consisting of two or more subunits usually linked to each other by non-covalent interactions[34]. Possibility of interaction between the subunits during the substrate binding process can give rise to positive, negative or no cooperativity phenomena [34, 40, 91, 92, 149, 150].

In this chapter, we have studied the entropy production in the kinetics of a single oligomeric enzyme which shows cooperativity with respect to the substrate binding in the chemiostatic condition. We have classified the cooperativity phenomena according to the nature of the different substrate binding mechanisms, namely, sequential and independent, as detailed by Weiss[151]. In sequential binding, the adjacent sites of the oligomeric enzyme are successively occupied by the substrate molecules. So the substrate-bound states of the system are actually adjacent in space and hence we denote the cooperativity arising out of this binding protocol as the spatial cooperativity. For the sequential mechanism, the first binding site, *i.e*, the first subunit of the oligomeric enzyme must be filled in order for the second site to become occupied by the substrate, as if the substrate molecules have been stacked on top of each other at their binding sites[151]. This type of binding can be relevant to an ion transporter, such as the Na-K pump[152]. The other class is called temporal cooperativity which can occur due to the independent binding of the substrate molecules to any one of the subunits at a particular time without any specific spatial arrangement. Here the substrate-bound sites are not physically neighboring in the enzyme [39] but the global state of the system is defined in terms of the total occupancy of the overall sites at a particular instant of time. This type of binding can be observed in multimeric proteins with individual binding sites located on different subunits, such as ligand gated ion channels or ligand gated enzymes[151]. Here we have theoretically studied the cooperative behavior

solely from the viewpoint of the substrate binding mechanism and not in terms of the active and inactive enzyme conformations or the actual structural details of the enzyme that can lead to such mechanisms [37, 38]. To study the bulk kinetics of allosteric enzymes Monod, Wyman and Changeux (MWC) in 1965 and Koshland, Nemethy and Filmer (KNF) in 1966 put forward models to account for cooperative binding. Generally 'Sequential' is used as a term for a classical distinction between multi-step binding models, as for instance differentiating between the KNF and MWC models in terms of the variation of the substrate binding rates in each successive step. So the term sequential in KNF model should not be confused with the term sequential used in our approach [151, 153].

In what follows, we have constructed the master equations for each class of substrate binding namely, the spatial and temporal model systems. Time evolution of such cooperative systems can be described by suitably applying a kinetic Monte Carlo technique[14, 15]. Here we have applied this algorithm to calculate the total, medium and system entropy production along a single trajectory for such cooperative systems as a function of the substrate concentration over a time interval where finally the system reaches a non-equilibrium steady state (NESS) and then determined the ensemble average quantities over many realizations of such trajectories. We show the correspondence between the evolution of the total and the medium entropy production with the average substrate binding and net velocity of the reaction in the context of detection of the cooperative behavior. Similarly this correspondence is also studied for the total entropy production rate at the NESS. The system entropy production is thoroughly studied in terms of the substrate binding probabilities for the different classes of cooperative systems considered. We have introduced a cooperativity index, C defined in terms of the stochastic system entropy to understand the nature of the cooperativity.

5.2 Cooperative binding, master equation and entropy production rate

In this section, we have first classified the cooperativity of a single oligomeric enzyme on the basis of the nature of the enzyme-substrate binding and then proposed a stochastic description for each class in terms of a one-dimensional random walk problem. Here we have provided a master equation approach for the description of spatial and temporal cooperativity which is suitable for the calculation of entropy production.

5.2.1 Classes of cooperativity: spatial and temporal substrate binding

Here we have considered that the substrate molecules can bind to the subunits of the oligomeric enzyme sequentially or independently as already discussed in the Introduction section of this chapter. In the oligomeric enzyme kinetics, the substrate molecules bind to the subunits of the oligomeric enzyme in a stepwise manner with different affinity which was first proposed by Adair to explain the cooperativity phenomenon observed in the oxygen-binding to the hemoglobin at equilibrium[36]. If an oligomeric enzyme consists of n_T number of homo or hetero type of subunits, then at the chemiostatic condition the substrate-binding scheme of the enzyme can be written as

$$\text{E} \underset{K_2^{(1)}}{\overset{K_1^{(0)}}{\rightleftarrows}} \text{ES}_1 \underset{K_2^{(2)}}{\overset{K_1^{(1)}}{\rightleftarrows}} \ldots \ldots \underset{K_2^{(n)}}{\overset{K_1^{(n-1)}}{\rightleftarrows}} \text{ES}_n \underset{K_2^{(n+1)}}{\overset{K_1^{(n)}}{\rightleftarrows}} \ldots \ldots \underset{K_2^{(n_T-1)}}{\overset{K_1^{(n_T-2)}}{\rightleftarrows}} \text{ES}_{n_T-1} \underset{K_2^{(n_T)}}{\overset{K_1^{(n_T-1)}}{\rightleftarrows}} \text{ES}_{n_T}.$$

$$(5.1)$$
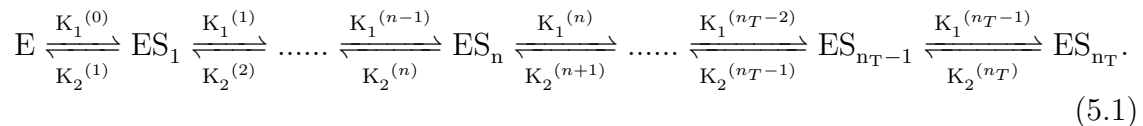
Here ES_n represents the conformational state of the oligomeric enzyme in which n number of subunits are occupied by the substrate molecules. $K_1^{(n-1)}$ and $K_2^{(n)}$ are designated as the total formation and total dissociation rate constants in the n-th reaction step, respectively.

The above scheme of substrate binding of an oligomeric enzyme can be viewed as a generalization of the kinetics of an enzyme having a single subunit given by

$$\text{E} + \text{S} \underset{k_{-1}}{\overset{k_1{}'}{\rightleftarrows}} \text{ES} \underset{k_2{}'}{\overset{k_{-2}}{\rightleftarrows}} \text{E} + \text{P},$$
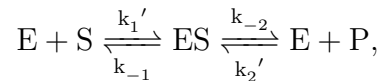
which can be further simplified as

$$\text{E} \underset{K_2}{\overset{K_1}{\rightleftarrows}} \text{ES}. \qquad (5.2)$$

Here $K_1 = (k_1 + k_2)$ and $K_2 = (k_{-1} + k_{-2})$, are designated as the total formation and total dissociation rate constants of ES, respectively. The pseudo first-order rate constants are written as $k_1 = k_1'[\text{S}]$ and $k_2 = k_2'[\text{P}]$ where [S] and [P] are the constant substrate and product concentration in the chemiostatic condition. Hence the site-dependent total formation and dissociation rate constants in the case of the oligomeric enzyme kinetics are similarly defined as $K_1^{(n-1)} = (k_1^{(n-1)} + k_2^{(n-1)})$ and $K_2^{(n)} = (k_{-1}^{(n)} + k_{-2}^{(n)})$ where $k_1^{(n-1)} = k_1'^{(n-1)}[\text{S}]$ and $k_2^{(n-1)} = k_2'^{(n-1)}[\text{P}]$.

The dynamics of the substrate binding mechanisms are quantified by counting the number of occupied sites present in the oligomeric enzyme at a particular instant of time. If at time t, 'n' number of occupied sites are present in the oligomeric enzyme (the state ES_n) then at time t+dt, the number of occupied sites may be increased or decreased by one unit due to the occurrence of a formation or a dissociation reaction. During the time evolution, the number of occupied sites is a fluctuating quantity.
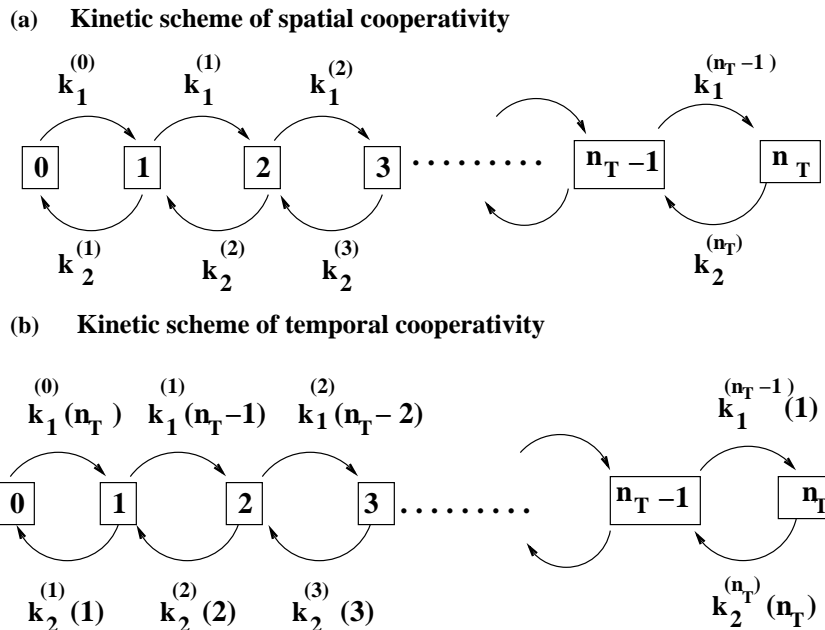
Figure 5.1: Kinetic schemes for (a) spatial and (b) temporal cooperativity with site-dependent binding and dissociation rate constants. The numbers in the square boxes denote the number of occupied sites. In spatial cooperativity (a), the forward and backward transition probabilities depend only on the total formation and dissociation rate constants, respectively. For temporal cooperativity (b), the forward transition probability depends on the total formation rate constant and the number of unoccupied sites, whereas the backward transition probability depends on the total dissociation rate constant and the number of occupied sites.

Therefore, the system performs a one-dimensional random walk along the finite number of states where state-n of the system is equivalent to the conformational state ES_n, as shown in Fig.5.1. The kinetic scheme of the spatially cooperative system is given in Fig.5.1(a). As the subunits get occupied sequentially starting from subunit-1, so when we say that the n-th subunit is occupied it automatically means that n number of sites are occupied in total. Here the forward and the backward transition probabilities depend only on the total formation and dissociation rate constants $K_1^{(n)}$ and $K_2^{(n)}$, respectively which are generally site-dependent. This is so because after the filling of one subunit, there is no other choice for the next substrate molecule but to fill up the next adjacent subunit and as this is true for all the subunits, there is no combinatorial term in the transition probability.

The kinetic scheme for the temporal cooperativity is shown in Fig.5.1(b). Here the substrate molecules can bind independently with any one of the n_T number of

subunits. The state-n of the system represents n-number of occupied sites of the enzyme. In this mechanism, the forward transition probability of the n-th state at time t is given by the product of the total formation rate constant $K_1^{(n)}$ with the number of distinct combinations of unoccupied sites present at that time. Similarly, the backward transition probability of the same state is the product of the total dissociation rate constant, $K_2^{(n)}$ and the number of distinct combinations of occupied sites present at time t (see Fig.5.1(b)). Here these rate constants are taken to be site-dependent in general. If all the rate constants are site-independent, then the system will be non-cooperative. The main difference of the sequential binding scheme from the independent one is as follows: *for the sequential scheme, the system will show spatial cooperativity in substrate binding even when the formation and dissociation rate constants are not site-dependent.*

5.2.2 Master equations

For the time-dependent description of the spatial cooperativity, we have constructed the corresponding master equation for this cooperativity mechanism as

$$\frac{\partial P_{sp}(n,t)}{\partial t} = K_1^{(n-1)}P_{sp}(n-1,t) + K_2^{(n+1)}P_{sp}(n+1,t) - (K_1^{(n)} + K_2^{(n)})P_{sp}(n,t), \quad (5.3)$$

with $K_1^{(-1)} = K_2^{(0)} = K_1^{(n_T)} = K_2^{(n_T+1)} = 0$ to match the boundary terms. Here, $P_{sp}(n,t)$ is the probability of having n number of occupied sites at time t. We have given an analytical expression for the solution of the master equation by setting $\frac{\partial P_{sp}(n,t)}{\partial t} = 0$. The steady state distribution of the spatial cooperativity is given by

$$P_{sp}^{ss}(n) = \frac{\prod_{j=0}^{n-1} X^{(j)}}{\sum_{n=0}^{n_T} \prod_{j=0}^{n-1} X^{(j)}}, \quad (5.4)$$

where $X^{(j)} = \frac{K_1^{(j)}}{K_2^{(j+1)}} = \frac{k_1'^{(j)}[S]+k_2^{(j)}}{k_{-1}^{(j+1)}+k_{-2}^{(j+1)}}$ with $j = 0, 1, ..., (n_T - 1)$. Here the steady state is actually a non-equilibrium steady state (NESS) as already discussed. If $X^{(j)} = X \forall j$, the NESS probability distribution becomes

$$P_{sp}^{ss}(n) = \frac{X^n(1-X)}{1-X^{(n_T+1)}}, \quad (5.5)$$

which is a geometric distribution. The average population of the occupied sites at the NESS for $X^{(j)} = X \forall j$ is given by

$$\langle n \rangle = \sum_{n=0}^{n_T} n P_{sp}^{ss}(n) = \frac{X(1-(n_T+1)X^{n_T}+n_T X^{n_T+1})}{(1-X)(1-X^{n_T+1})}. \quad (5.6)$$

For temporal cooperativity, the master equation is written as

$$\frac{\partial P_{temp}(n,t)}{\partial t} = K_1^{(n-1)}(n_T - n + 1)P_{temp}(n-1,t) + K_2^{(n+1)}(n+1)P_{temp}(n+1,t)$$

$$-K_1^{(n)}(n_T - n)P_{temp}(n, t) - K_2^{(n)}nP_{temp}(n, t), \tag{5.7}$$

again with $K_1^{(-1)} = K_2^{(0)} = K_1^{(n_T)} = K_2^{(n_T+1)} = 0$. Solving this master equation at the NESS, we can obtain the probability distribution as

$$P_{temp}^{ss}(n) = \frac{\binom{n_T}{n} \prod_{j=0}^{n-1} X^{(j)}}{\sum_{n=0}^{n_T} \binom{n_T}{n} \prod_{j=0}^{n-1} X^{(j)}}, \tag{5.8}$$

where $X^{(j)} = \frac{K_1^{(j)}}{K_2^{(j+1)}}$ as already defined with $j = 0, 1, ..., (n_T - 1)$. The average number of occupied sites at the NESS is simply expressed as

$$\langle n \rangle = \frac{\sum_n n \binom{n_T}{n} \prod_{j=0}^{n-1} X^{(j)}}{\sum_{n=0}^{n_T} \binom{n_T}{n} \prod_{j=0}^{n-1} X^{(j)}}. \tag{5.9}$$

Now positive cooperativity in this scenario means a higher affinity of a second substrate molecule to attach with the oligomeric enzyme compared to that of the first substrate molecule which is already bound and so on. Therefore, in this case, the successive binding affinity of the substrate molecule increases. So naturally here we take the binding rate constants, $k_1^{(n)}$ as follows [151, 154]

$$k_1^{(0)} < k_1^{(1)} .... < k_1^{(n)} < k_1^{(n+1)} < .... < k_1^{(n_T-1)}. \tag{5.10}$$

Here the site-dependent overall association rate constant $K_1^{(n)}$ is defined as $K_1^{(n)} = k_1^{(n)} + k_2^{(n)}$ and similarly, the overall site-dependent dissociation rate constant is written as $K_2^{(n)} = k_{-1}^{(n)} + k_{-2}^{(n)}$. We take the rate constants $k_{-1}^{(n)}$, $k_2^{(n)}$ and $k_{-2}^{(n)}$ to be site-independent. This is due to the fact that to get a cooperative behavior for the independent binding case, it is not necessary to take all the rate constants of the reaction system to be site-dependent that will also make the results obtained hard to analyze. Then the site-dependent quantities $X^{(j)}$ for positive cooperativity maintain the relation:

$$X^{(0)} < X^{(1)} .... < X^{(n)} < X^{(n+1)} < .... < X^{(n_T-1)}. \tag{5.11}$$

Similarly, negative cooperativity arises as a second substrate molecule binds to the oligomeric enzyme with a lower affinity than that of the first substrate molecule. Therefore, the substrate binding reaction rate constants for different sites obey the inequalities [34, 93, 149]

$$k_1^{(0)} > k_1^{(1)} .... > k_1^{(n)} > k_1^{(n+1)} > ... > k_1^{(n_T-1)}. \tag{5.12}$$

Then taking the rate constants $k_{-1}^{(n)}$, $k_2^{(n)}$ and $k_{-2}^{(n)}$ as site-independent constants, we have

$$X^{(0)} > X^{(1)} .... > X^{(n)} > X^{(n+1)} > .... > X^{(n_T-1)}. \tag{5.13}$$

If all the association and dissociation rate constants are site-independent, then the enzyme becomes non-cooperative. Thus the steady state distribution, Eq.(5.8) reduces to

$$P^{ss}(n) = \binom{n_T}{n} \frac{X^n}{(1+X)^{n_T}},$$ (5.14)

where $X = \frac{K_1}{K_2}$. By inserting the value of X, the above equation can be written as a binomial distribution given by

$$P^{ss}(n) = \binom{n_T}{n} \left(\frac{K_1}{K_1+K_2}\right)^n \left(\frac{K_2}{K_1+K_2}\right)^{(n_T-n)} = P^{(bino)}(n).$$ (5.15)

This is expected, as in the absence of any cooperativity, the distribution of the occupied sites must follow a binomial distribution. So for a system with no cooperativity, the average number of occupied sites at the NESS is

$$\langle n \rangle = n_T \left(\frac{X}{1+X}\right) = n_T \left(\frac{K_1}{K_1+K_2}\right)$$ (5.16)

and the average number of unoccupied sites is

$$\langle n_T - n \rangle = n_T \left(\frac{K_2}{K_1+K_2}\right).$$ (5.17)

We mention that, in addition to the overall association and dissociation rate constants being site-independent, if the rate constant k_2 is also negligibly small, then the enzyme kinetics becomes simply the Michaelis-Menten type. If $k_2^{(j)}$ $(j = 0, \ldots, (n_T - 1))$ is taken to be much less than the other rate constants, then we have

$$X^{(j)} = \frac{[S]}{K_M^{(j)}},$$ (5.18)

where $K_M^{(j)} = \frac{k_{-1}^{(j+1)}+k_{-2}^{(j+1)}}{k_1'^{(j)}}$ can be described as the stepwise Michaelis-Menten constant.

5.2.3 Entropy production rates

The system entropy is defined in terms of the Shannon entropy as

$$S_{sys}(t) = -k_B \sum_n P(n,t) \ln P(n,t),$$ (5.19)

where $P(n,t)$ is the probability of having n number of occupied states at time t with $P(n,t) \equiv P_{sp}(n,t)$ or $P(n,t) \equiv P_{temp}(n,t)$. Here we set the Boltzmann constant, $k_B = 1$. Using the master equation, one can get the system entropy production rate [13, 74, 100, 101] as

$$\dot{S}_{sys}(t) = \frac{1}{2} \sum_{n,\mu} [w_\mu(n-\nu_\mu|n)P(n-\nu_\mu,t) - w_{-\mu}(n|n-\nu_\mu)P(n,t)]$$

$$\times \ln \frac{P(n - \nu_\mu, t)}{P(n, t)}. \tag{5.20}$$

Here the state of the system can change by any one of the four reactions, denoted with index μ, via which the substrate and the product molecules can bind with the enzyme sites and detach. They are given as: (1) $(ES_n + S) \xrightarrow{k_1^{(n)}} (ES_{n+1})$ ($\mu = 1$), (2)$(ES_n) \xrightarrow{k_{-1}^{(n)}} (ES_{n-1} + S)$ ($\mu = -1$), (3)$(ES_n) \xrightarrow{k_{-2}^{(n)}} (ES_{n-1} + P)$ ($\mu = -2$) and (4)$(ES_n + P) \xrightarrow{k_2^{(n)}} (ES_{n+1})$ ($\mu = 2$). Here ν_μ is designated as the stoichiometric coefficient of the μ-th reaction with rate constant k_μ where $\nu_\mu = 1$ with $\mu > 0$ and $-\nu_\mu = 1$ with $\mu < 0$. The transition probabilities are defined as follows

$$w_\mu(n - \nu_\mu | n) = k_\mu^{(n - \nu_\mu)}(n_T - (n - \nu_\mu)), \mu > 0$$

and

$$w_\mu(n - \nu_\mu | n) = k_\mu^{(n - \nu_\mu)}(n - \nu_\mu), \mu < 0. \tag{5.21}$$

We have assumed ideal reservoir(surroundings) with no inherent entropy production except through the boundaries of the system. The system entropy production rate(epr) can be split as[100]

$$\dot{S}_{sys}(t) = \dot{S}_{tot}(t) - \dot{S}_m(t). \tag{5.22}$$

Here the first term in the r.h.s. of Eq.(5.22) gives the total entropy production rate and the second term denotes the medium entropy production rate due to the entropy flux into the surroundings. Therefore the total and medium entropy production rates are defined as

$$\dot{S}_{tot}(t) = \frac{1}{2} \sum_{n,\mu} [w_\mu(n - \nu_\mu | n)P(n - \nu_\mu, t) - w_{-\mu}(n | n - \nu_\mu)P(n, t)]$$

$$\times \ln \frac{w_\mu(n - \nu_\mu | n)P(n - \nu_\mu, t)}{w_{-\mu}(n | n - \nu_\mu)P(n, t)} \tag{5.23}$$

and

$$\dot{S}_m(t) = \frac{1}{2} \sum_{n,\mu} [w_\mu(n - \nu_\mu | n)P(n - \nu_\mu, t) - w_{-\mu}(n | n - \nu_\mu)P(n, t)]$$

$$\times \ln \frac{w_\mu(n - \nu_\mu | n)}{w_{-\mu}(n | n - \nu_\mu)}. \tag{5.24}$$

At steady state, $\dot{S}_{sys} = 0$ (whether equilibrium or NESS). An NESS is characterized by a non-zero total epr given by

$$\dot{S}_{tot}^{(NESS)} = \sum_n [w_1(n - 1 | n)P(n - 1) - w_{-1}(n | n - 1)P(n)]$$

$$\times \ln \left(\frac{w_1(n - 1 | n)P(n - 1) \times w_{-2}(n | n - 1)P(n)}{w_{-1}(n | n - 1)P(n) \times w_2(n - 1 | n)P(n - 1)} \right). \tag{5.25}$$

This equation is derived using the circular balance condition [11]

$$w_1(n-1|n)P(n-1) - w_{-1}(n|n-1)P(n) =$$

$$w_{-2}(n|n-1)P(n) - w_2(n-1|n)P(n-1). \tag{5.26}$$

Now here we consider two limiting situations.

(i) It is clear that if we do not consider the presence of the product species then there will be just two sets of rate constants, $k_1^{(n)}$ and $k_{-1}^{(n)}$. Then at the steady state, the balance condition that holds is obviously the detailed balance which gives

$$w_1(n-1|n)P(n-1) - w_{-1}(n|n-1)P(n) = 0.$$

Then from Eq.(5.25), we have $\dot{S}_{tot} = 0$ at the steady state which is reduced now to an equilibrium. Now from Eq.(5.18), the quantity $X^{(j)}$ under this condition becomes $X^{(j)} = \frac{k_1^{'(j)}[S]}{k_{-1}^{(j+1)}}$ where $\frac{k_1^{'(j)}}{k_{-1}^{(j+1)}}$ are the stepwise equilibrium (binding) constants. So in this limit, theoretically there is no difference between our model and a protein-ligand binding model which generally does not consider the product formation.

(ii) Another interesting point is that if we consider the case where $k_1^{(n)}, k_{-1}^{(n)} \gg k_{-2}^{(n)}$ (with $k_2^{(n)}$ being already considered negligible) then this corresponds to the pre-equilibrium limit or simply the equilibrium limit. The assumption is valid when fast reversible reactions precede slower reactions in a reaction network. Now in this situation also, the quantity $X^{(j)}$ is defined in terms of the stepwise equilibrium (binding) constants. In this context, we mention that the original derivation of the enzyme catalysis reaction by Michaelis and Menten involved the pre-equilibrium assumption with the equilibrium dissociation constant parameter. The more general derivation by Briggs and Haldane used the steady state approximation and their expression contained the actual Michaelis-Menten constant. In our case also we see the same features in the quantity, $X^{(j)}$ which is the parameter of our model study. In the general non-equilibrium case, $X^{(j)}$ is related to the stepwise Michaelis-Menten constant, $K_M^{(j)}$ (see Eq.(5.18) with $k_2^{(j)}$ considered negligible) whereas in the absence of product species leading to equilibrium or under the pre-equilibrium assumption, $X^{(j)}$ is related to the stepwise equilibrium (binding) constant, $\frac{k_1^{'(j)}}{k_{-1}^{(j+1)}}$.

5.3 Measure of cooperativity

Here we have discussed on the determination of the Hill coefficient from the master equation corresponding to the different binding schemes. We have also introduced an index of cooperativity in terms of the stochastic system entropy associated with the fully bound state of the cooperative and non-cooperative cases. We have analyzed its connection to the Hill coefficient using some relevant experimental data which gives a realistic application of the proposed scheme of measurement of cooperativity.

5.3.1 Hill coefficient

In the traditional enzymology, the characterization of cooperativity is carried out by measuring the Hill coefficient [34]. For positive and negative cooperative cases, the Hill coefficient becomes greater than or less than one, respectively, whereas the non-cooperative case is characterized with Hill coefficient equal to one. Experimentally it is obtained by determining the fractional saturation, $\theta(= \langle n \rangle / n_T)$ at various substrate concentrations [S], constructing the Hill plot ($\ln(\frac{\theta}{1-\theta})$ vs. $\ln[S]$) and then finding the slope at the half-saturation point, $\theta = 0.5$ or at a point where the slope deviates maximum from unity. On the other hand, Hill coefficient is theoretically defined as the ratio of the variances of the binding number of the cooperative and non-cooperative cases at the half-saturation point with the non-cooperative binding case following the binomial distribution[150, 155].

We briefly mention the features of the Hill plot for the model binding schemes studied here. The slope of the Hill plot is generally given by [150]

$$H = \frac{[S] (d\theta/d[S])}{\theta(1-\theta)}. \tag{5.27}$$

For temporal cooperativity, the fractional saturation can be written as (see Eq.(5.9))

$$\theta_{\text{temp}} = \frac{\sum_n n B_n [S]^n}{n_T \sum_n B_n [S]^n}, \tag{5.28}$$

where $B_n = \binom{n_T}{n} \prod_{j=0}^{n-1} (K_M^{(j)})^{-1}$ with $B_0 = 1$. Then one gets

$$H_{\text{temp}} = \frac{\langle n^2 \rangle - \langle n \rangle^2}{n_T \theta(1-\theta)} = \frac{\sigma_{\text{temp}}^2}{\sigma_{\text{bino}}^2}, \tag{5.29}$$

where σ_{temp}^2 and σ_{bino}^2 are the variances of the binding numbers of the temporal and non-cooperative cases, respectively. The Hill coefficient, n_H is given at the half-saturation point as[150] $n_H = \frac{4\sigma_{\text{temp}}^2}{n_T}$. Similar expressions hold for the spatial cooperative binding. We have already mentioned in Sec.IIB that if all the rate constants of the independent binding scheme are site-independent, then the binding is non-cooperative with binomial distribution of the binding probability. Here we discuss the corresponding scenario for the sequential binding (leading to spatial cooperativity) to be non-cooperative in terms of the variance of the binding number. In the case of spatial cooperativity, the variance of the binding number, σ_{sp}^2 is given by

$$\sigma_{\text{sp}}^2 = \left(\frac{1+X}{1-X} \right) \langle n \rangle - \langle n \rangle^2 - \frac{n_T (n_T + 1) X^{n_T+1}}{1 - X^{n_T+1}}, \tag{5.30}$$

where X and $\langle n \rangle$ are as given in Eq.(5.5) and Eq.(5.6). Now for $n_T = 1$, this reduces to

$$\sigma_{\text{sp}}^2 = \frac{X}{(1+X)^2} = \sigma_{\text{bino}}^2. \tag{5.31}$$

and then the slope of the Hill plot becomes $H_{sp} = \frac{\sigma_{sp}^2}{\sigma_{bino}^2} = 1$ for any substrate concentration. So for sequential binding, the cooperative behavior is absent only if the enzyme is monomeric.

5.3.2 Cooperativity index

Here we introduce an index of cooperativity. First we build up the concept from binding probabilities and then demonstrate how this index can indicate the nature of the cooperativity. For positive cooperative binding, one expects that full occupancy of the enzyme is more probable compared to the case of non-cooperativity. Similarly, for negative cooperativity, the full occupancy of the enzyme is less probable. Now, if the probability of an event-n is p_n, then the associated surprisal is given by $-\ln(p_n)$ and more probable the event, the less is its surprisal. So the ratio of the surprisals, associated with the probability of the system to remain in a fully occupied state without and with cooperativity at NESS, should be greater than 1 for positive cooperativity and less than 1 for negative cooperativity. Hence we define the index of cooperativity, denoted by C in terms of the ratio of the surprisals, associated with the probability of the system to remain in a fully occupied state without and with cooperativity at NESS as

$$C = \frac{-\ln(P^{(bino)}(n_T))}{-\ln(Q(n_T))} \qquad (5.32)$$

where the binomial distribution, $P^{(bino)}$ is the reference corresponding to the non-cooperative case and the distribution Q corresponds to the cooperative binding case. The rate constants of the reference non-cooperative system (binomial) must be the same as those of the starting or initial rate constants of the cooperative system for the comparison to be valid. The relation is then independent of the actual value of the (constant) substrate concentration. We point out that the surprisal is equivalent to the single trajectory stochastic system entropy[85, 99] (associated with the fully occupied state). So the index, C is truly an entropic estimate of cooperativity at the microscopic level.

Based on the above argument, next we theoretically analyze the probability to remain in a fully occupied state for different cooperative systems and compare that with the non-cooperative case to formulate the criteria of cooperativity in terms of C. For spatial cooperativity, the ratio of its steady state distribution (Eq.(5.5)) and the reference binomial distribution (Eq.(5.14)) for $n = n_T$ is given by

$$R_{sp} = \frac{P_{sp}^{ss}(n_T)}{P^{(bino)}(n_T)}$$

$$= 1 + \frac{\left[\left(\binom{n_T}{1} - \binom{n_T}{0}\right)X + \left(\binom{n_T}{2} - \binom{n_T}{1}\right)X^2 + \ldots + \left(\binom{n_T}{n_T} - \binom{n_T}{n_T-1}\right)X^{n_T}\right]}{(1 - X^{n_T+1})}. \qquad (5.33)$$

From the above expression it is clear that for all values of X, either greater than or less than 1, the quantity R_{sp} is greater than 1 indicating positive cooperativity. This will lead to the condition $C > 1$ for the case of spatial cooperativity for any substrate concentration. Only in the case of monomeric enzyme, ($n_T = 1$), the system will be non-cooperative with $R_{sp} = C = 1$ as already discussed in terms of variances at the end of Section 5.3.1.

In the case of temporal cooperativity, the corresponding ratio, R_{temp} is given using Eq.(5.8) and Eq.(5.14) at $n = n_T$ as

$$R_{temp} = \frac{P_{temp}^{ss}(n_T)}{P^{(bino)}(n_T)}$$

$$= \left[\frac{\frac{X^{(0)}X^{(1)}...X^{(n_T-1)}}{[1+n_T X^{(0)}+...+(X^{(0)}X^{(1)}...X^{(n_T-1)})]}}{\frac{X^{n_T}}{(1+X)^{n_T}}} \right]$$

$$= \left[\frac{\frac{(X^{(0)})^{n_T} f^{(n_T-1)}}{[1+n_T X^{(0)}+...+(X^{(0)})^{n_T} f^{(n_T-1)}]}}{\frac{(X^{(0)})^{n_T}}{[1+n_T X^{(0)}+...+(X^{(0)})^{n_T}]}} \right], \tag{5.34}$$

with $X^{(0)} = X$. Now both $P_{temp}^{ss}(n_T)$ and $P^{(bino)}(n_T)$ tend to 1 at large $X^{(0)}$ *i.e.* large substrate concentration. But it is clear that for positive cooperative binding with $f > 1$, the last term in the denominator of $P_{temp}^{ss}(n_T)$ dominates the previous terms more readily compared to the case of $P^{(bino)}(n_T)$. Hence at a particular substrate concentration, $P_{temp}^{ss}(n_T)$ is closer to 1 compared to $P^{(bino)}(n_T)$ and so R_{temp} is greater than 1. For negative cooperativity with $f < 1$, the situation is obviously reverse and R_{temp} is less than 1. Therefore, in the light of the above discussions and Eq.(5.32), we write down the condition of cooperativity in terms of C as

$$C \begin{cases} > 1, & \text{positive cooperativity} \\ = 1, & \text{no cooperativity} \\ < 1, & \text{negative cooperativity.} \end{cases} \tag{5.35}$$

This is the same criteria of cooperativity as given in terms of the Hill coefficient. To find out the Hill coefficient, *i.e.,* the variances theoretically, it is necessary to know the probability distribution of the corresponding positive and negative cooperativity cases, respectively. Now our measure of cooperativity, the index C, is also related to the probability distributions; but it is defined in terms of the ratio of a specific term of the distributions, namely the probability of the fully occupied state. So apparently there is no straightforward connection between the Hill coefficient and C. The Hill coefficient is the slope of the binding curve at a particular substrate concentration corresponding to the half-saturation point whereas the index C is defined independent of the substrate concentration and the characterization of cooperativity in terms of C is valid at any substrate concentration.

5.3.3 Estimate of the limiting value of the cooperativity index, C for various cooperative binding

Here the limiting value of the cooperativity index, C for the spatial and temporal cooperative binding are determined at high substrate concentration. The limiting value of the cooperativity index, C for the spatial cooperativity is calculated from Eq.(5.32) by using the steady state probability distribution function of spatial cooperativity, $P_{sp}^{ss}(n)$ (Eq.(5.5)) and that of no cooperativity, $P_{bino}^{ss}(n)$ (Eq.(5.14)) at $n = n_T$. The expression of C then becomes

$$C = \frac{-\ln\left[\left(\frac{X}{1+X}\right)^{n_T}\right]}{-\ln\left[\frac{X^{n_T}(1-X)}{1-X^{(n_T+1)}}\right]}. \tag{5.36}$$

At high substrate concentration, with $X \gg 1$, the above equation can be written as

$$C = \frac{n_T\ln(1+\frac{1}{X})}{-\ln(1-\frac{1}{X})}. \tag{5.37}$$

Now expanding the log terms in the Eq. (5.37) and neglecting the higher order terms, we finally obtain

$$C = n_T. \tag{5.38}$$

Therefore, the limiting value of C in the case of spatial cooperativity, obtained at high substrate concentration, is equal to the total number of sub-units of the oligomeric enzyme.

In a similar fashion, the limiting value of C can be calculated for the temporal cooperativity from Eq.(5.32) by using the steady state probability distribution function of temporal cooperativity, $P_{temp}^{ss}(n)$ (Eq.(5.8)) and that of no cooperativity, $P_{bino}^{ss}(n)$ (Eq.(5.14)) at $n = n_T$. At this value the distribution, $P_{temp}^{ss}(n)$ can be written as

$$P_{temp}^{ss}(n_T) = \frac{X^{(0)}X^{(1)}...X^{(n_T-1)}}{[1 + n_T X^{(0)} + ... + (X^{(0)}X^{(1)}...X^{(n_T-1)})]}. \tag{5.39}$$

Here $X^{(j)} \approx f^{(j)}X^{(0)}$ with $j = 0, ..., (n_T - 1)$. This follows from the definition of $X^{(j)}$ (see Eq.(5.8) and Eq.(5.4)) with the small value of k_{-2} taken in this study. Now at high substrate concentration with $X^{(0)} \gg 1$, the above equation can be written as

$$P_{temp}^{ss}(n_T) = \frac{1}{\left[1 + \frac{n_T}{X^{(0)}f^{(n_T-1)}}\right]}. \tag{5.40}$$

Now, by using the value of $P_{temp}^{ss}(n_T)$ and $P_{bino}^{ss}(n_T)$ into the Eq.(5.32) at high substrate concentration, we obtain

$$C = \frac{n_T\ln(1+\frac{1}{X})}{\ln[1 + \frac{n_T}{X^{(0)}f^{(n_T-1)}}]}. \tag{5.41}$$

For the comparative study of the temporal and non-cooperative cases, the starting value, $X^{(0)}$ is taken equal to X. Then expanding the log terms in the above equation and neglecting the higher order terms, we finally obtain the limiting value of C for temporal cooperativity as

$$C = f^{(n_T-1)} = \frac{k_1^{(n_T-1)}}{k_1^{(0)}}. \tag{5.42}$$

Here we mention that for the negative cooperative binding, $f^{(n_T-1)}$ can be much less than 1 in general. But here we consider the case $X^{(0)}f^{(n_T-1)} \gg 1$.

5.4   Numerical simulation of entropy production

In this section, we have calculated the medium, system and the total entropy production for the spatial and temporal cooperative systems. For a given initial condition, the oligomeric enzyme system reaches NESS at a particular time which depends on the chemiostatic condition, *i.e*, the value of the constant substrate concentration. The initial condition is taken as the fully unbound state of the enzyme with all the subunits being vacant *i.e.*, $P(n, t = 0) = \delta_{n,0}$. This condition leads to zero system entropy at t=0. For the time-dependent system entropy production calculation in general, one needs the time-dependent solution of the master equation, $P(n, t)$. But here the final time in the calculation of the entropy production over the time interval (starting at t = 0 with the specified initial condition above) is taken such that by then the system reaches the NESS and hence steady state solutions are all we need to get the system entropy production over the length of the trajectory. The total entropy production for a single trajectory is calculated over the time interval where the determination of the medium entropy production requires the detailed information of the path and not just the initial and final points. We run the simulations in all the cases up to a fixed point of time taken to be the same for all the binding mechanisms. As the steady state is an NESS (and not an equilibrium), total and medium entropy production increase linearly with time and hence if the final point of time is not the same for all the cases, one can not compare the various entropy production values for the different cooperative systems.

5.4.1   Implementation of the scheme of single trajectory stochastic simulation

Along a single stochastic trajectory the system entropy production can be defined as[135] $\mathbf{S(t)} = -\ln p(n, t)$, where $p(n, t)$ is the solution of the stochastic master equation for a given initial condition, $p(n_0, t_0)$, taken along the specific trajectory $n(t)$. Note that, the single trajectory entropy is denoted by (bold) $\mathbf{S}$ whereas the trajectory-average entropy production (equivalent to ensemble average) is denoted by S. Now at the microscopic level, the number of occupied sites of the oligomeric

enzyme becomes a fluctuating quantity due to the random occurrence of the different reaction events within the random time interval. This develops the concept of different trajectories. Here the state of the system can change by any one of the four reactions (denoted with index μ) as discussed in Sec.IIC.

A stochastic trajectory, $\chi(t)$ starting at the state n_0, jumping at times t_j from the state n_{j-1} to the state n_j and finally ending up at n_l with $t = t_l$ is defined as,

$$n(t) \equiv (n_0, t_0) \xrightarrow{\nu_\mu^{(1)}} (n_1, t_1) \xrightarrow{\nu_\mu^{(2)}} ..... \xrightarrow{\nu_\mu^{(j)}} (n_j, t_j) \to ... \to (n_{l-1}, t_{l-1}) \xrightarrow{\nu_\mu^{(l)}} (n_l, t_l). \quad (5.43)$$

Here $n_j = n_{j-1} + \nu_\mu^{(j)}$ where $\nu_\mu^{(j)}$ is the stoichiometric coefficient of the μ-th reaction along a trajectory and $t_j = t_{j-1} + \tau_j$ where τ_j is the time interval between two successive jumps. During the jump from the $(n_j - 1)$ state to the n_j state, any one of the four reactions will occur (see Eq. (5.1) and Eq. (5.2)). The rate constant of the reaction μ is denoted as k_μ. The time interval τ_j between the two jumps is a random variable following the exponential distribution[14, 15]

$$p(\tau_j) = a \ \exp(-a\tau_j) \quad (5.44)$$

with $a = \sum_{\mu=\pm1}^{\pm2} w(n_j - 1; \nu_\mu^j)$. Here $w(n_{j-1}; \nu_\mu^{(j)})$ denotes the forward transition probability from the state $(n_j - 1)$ to the state n_j through a reaction channel μ with the stoichiometric coefficient $\nu_\mu^{(j)}$.

Now a time reversed trajectory can be defined as,

$$n^R(t) \equiv (n_l, t_l) \xrightarrow{-\nu_\mu^{(l)}} (n_{l-1}, t_{l-1}) \xrightarrow{-\nu_\mu^{(l-1)}} ... \to (n_j, t_j) \xrightarrow{-\nu_\mu^{(j)}} ... \to (n_1, t_1) \xrightarrow{-\nu_\mu^{(1)}} (n_0, t_0). \quad (5.45)$$

This time reversed trajectory is generated due to the occurrence of a reaction channel whose state changing vector $-\nu_\mu^{(j)}$ is exactly opposite to the state changing vector $\nu_\mu^{(j)}$ of the forward reaction channel.

The time-dependent total entropy production, ΔS_{tot} along a trajectory can be split into a system part, ΔS_{sys} and a medium contribution, ΔS_m. Hence the change of total entropy along a trajectory can be written as [135]

$$\Delta S_{tot} = \Delta S_m + \Delta S_{sys} \quad (5.46)$$

where

$$\Delta S_{sys} = \ln\frac{p(n_0, t_0)}{p(n, t)} \quad (5.47)$$

and

$$\Delta S_m = \sum_j \ln\frac{w(n_{j-1}; \nu_\mu^{(j)})}{w(n_j; -\nu_\mu^{(j)})}. \quad (5.48)$$

Here $w(n_{j-1}; \nu_\mu^{(j)})$ denotes the forward transition probability as already defined. Similarly, $w(n_j; -\nu_\mu^{(j)})$ denotes the backward transition probability from the state n_j to the $(n_j - 1)$ state through a reaction channel μ with the exactly opposite stoichiometric coefficient $-\nu_\mu^{(j)}$.

5.4.2   Cooperative kinetics

To simulate the spatial cooperativity associated with the sequential binding, we have taken the site-independent reaction rate constants as $k_1^{'} = 0.015 \ \mu M^{-1}s^{-1}$ and $k_{-1} = 7.0$, $k_{-2} = 2.0$, $k_2 = 0.001$, all in s^{-1}. The substrate concentration is taken in μM unit. The total number of subunits present in the oligomeric enzyme is taken as $n_T = 3$. We have calculated the various entropy productions using the stochastic simulation for single trajectories over a time interval starting from the initial condition to a final time as mentioned above. We have taken 2×10^5 trajectories to get the ensemble average of the entropy production values. We have calculated the average binding number, $\langle n \rangle$ for this case from Eq.(5.6) and the net product formation rate by using the formula, $v_{net} = k_{-2}\langle n \rangle - k_2 \langle n_T - n \rangle$, at the final time where the system resides at the NESS. We have plotted these quantities as a function of the substrate concentration in Fig.5.2(a) and (b). It is clear from the plots that both the quantities grow with a sigmoidal shape as a function of substrate concentration indicating positive cooperativity in substrate binding. According to Eq.(5.6), this is due to the higher power (> 1) dependence of $\langle n \rangle$ on the factor X which is proportional to the substrate concentration. As the rate constants are taken as site-independent, the positive cooperativity generated in the system is inherent in the binding mechanism. Now we have plotted ΔS_{tot} and ΔS_m, both being ensemble averages taken over the 2×10^5 realizations of the trajectories, in Fig.5.2(c) and (d), respectively, against the substrate concentration. Interestingly, we find the nature of both the curves to be sigmoidal.

Next we come to the case of independent substrate binding that can give rise to the case of temporal cooperativity with site-dependent reaction rate constants. To simulate the entropy production for the positive cooperative system, we take the rate constants of successive substrate binding steps as (see Eq.(5.10)): $k_1^{(1)} = f^{(1)}k_1^{(0)}$ and $k_1^{(2)} = f^{(2)}k_1^{(0)}$, where $k_1^{(0)} = k_1^{'(0)}[S]$ with $k_1^{'(0)} = 0.015 \ \mu M^{-1}s^{-1}$. The set $\{k_1^{'(0)}, k_{-1}, k_{-2}, k_2\}$ is called the starting or initial rate constants of the cooperative system. For the simulation, here we take $f^{(1)} = 10$ and $f^{(2)} = 100$, *i.e.*, a 10-fold increase in substrate binding rate constants in each step. The other rate constants are site-independent and taken to be the same as in the case of the spatial cooperativity. We also calculate the average binding number using Eq.(5.9) and the net product formation rate, at the NESS. They are shown in Fig.5.3(a) and (b) along with the total and the medium entropy production in Fig.5.3(c) and (d), respectively, all as a function of the substrate concentration. It is evident from the figure that all the curves show a significant sigmoidal behavior indicating the positive cooperativity. We have also given the corresponding quantities in the case of non-cooperativity in the same plot for comparison. The non-cooperative case is simulated with site-independent rate constants same as in the case of the spatial cooperativity. In this case $\langle n \rangle$ is determined using Eq.(5.16). We see that in this case also, the nature of
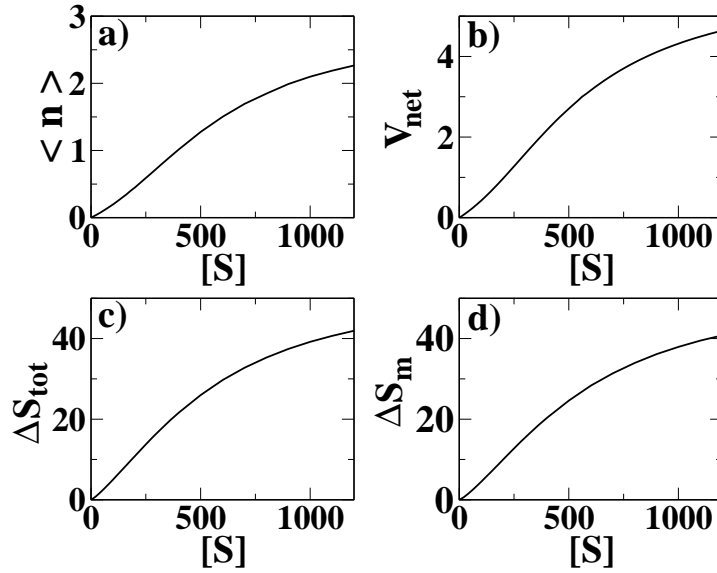
Figure 5.2: (a) $\langle n \rangle$ and (b) v_{net} for the spatial cooperative (sequential) binding as a function of substrate concentration, [S] (in μM unit) at the NESS. (c) and (d) exhibit the corresponding ΔS_{tot} and ΔS_m variations with [S]. The entropy productions are calculated over a time interval that starts with the given initial condition (see text) and ends with the system at the NESS.

variation of $\langle n \rangle$, v_{net}, ΔS_m and ΔS_{tot} with the substrate concentration is the same, hyperbolic to be specific.

Now we come to the last case in this category, $i.e.$, the negative cooperativity. In this case, the rate constants of the substrate binding reaction are taken as (see Eq.(5.12)): $k_1^{'(0)} = 1.5 \ \mu M^{-1}s^{-1}$, $k_1^{(1)} = f^{(1)}k_1^{(0)}$ and $k_1^{(2)} = f^{(2)}k_1^{(0)}$ with the values of the factors being $f^{(1)} = 0.1$ and $f^{(2)} = 0.01$, $i.e.$, a 10-fold decrease in substrate binding rate constant in each step. The other rate constants are taken as in the previous cases. The value of $k_1^{'(0)}$ is taken to be 100 times greater compared to the cases of spatial and positive cooperativity. This is only for the demonstration of the negative cooperativity effect on the binding curves of the reaction. We have plotted $\langle n \rangle$ against substrate concentration in Fig.5.4(a) for the negative as well as the non-cooperative case. Here for the non-cooperative case also we have taken $k_1^{'(0)} = 1.5 \ \mu M^{-1}s^{-1}$. Both the curves show the hyperbolic nature. The two cases are distinguished by plotting $\frac{1}{\langle n \rangle}$ versus $\frac{1}{[S]}$ which is the Lineweaver-Burk plot. For non-cooperative enzyme, this plot gives a straight line whereas the curve for the negative cooperative binding starts at a higher value on the y-axis and becomes nonlinear when it comes close to the curve of the non-cooperative system at high substrate concentration. This feature is shown in Fig.5.4(b). Now we have plotted similar curves for ΔS_{tot} in Fig.(5.4(c) and (d). One can see the same hyperbolic nature in the plot of ΔS_{tot} versus substrate concentration (Fig.5.4) for both the cases and
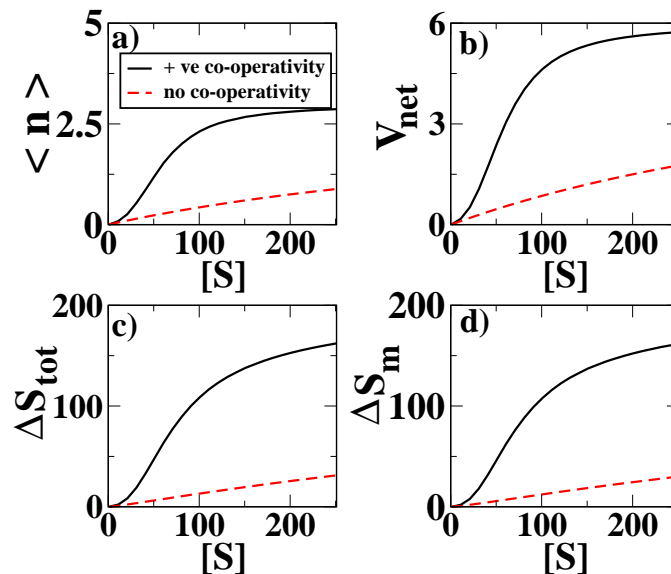
Figure 5.3: (a) $\langle n \rangle$ and (b) v_{net} for the temporally cooperative (independent) binding with positive cooperativity against substrate concentration, [S] (in μM unit) at the NESS. (c) and (d) give the corresponding ΔS_{tot} and ΔS_m variations with [S]. The entropy productions are calculated over a time interval as described in the caption of Fig.5.2. It is evident from the figure that all the curves show a significant sigmoidal behavior indicating the positive cooperativity.

the nonlinearity in the plot of $\frac{1}{\Delta S_{tot}}$ versus $\frac{1}{[S]}$ at high substrate concentration for the negative cooperativity (Fig.5.4(d)). So from the above discussion and the plots, we conclude that the familiar indications of the cooperative behavior in substrate binding, given in terms of the nature of variation of the average binding number and the net velocity of the reaction as a function of the substrate concentration, are all reflected in the same manner in the corresponding variation of the total as well as the medium entropy production.

We have also calculated the total entropy production rate, $\dot{S}_{tot}$ at the NESS using Eq.(5.25) for all the cases of cooperativity . Here we have taken the same set of rate constants as we have already considered to calculate the various entropy productions. The variations of $\dot{S}_{tot}$ with substrate concentration, [S] for different binding schemes are shown in Fig.5.5. It is evident from the figure that the features of cooperative binding are also reflected in a similar fashion on the variation of $\dot{S}_{tot}$ with substrate concentration.
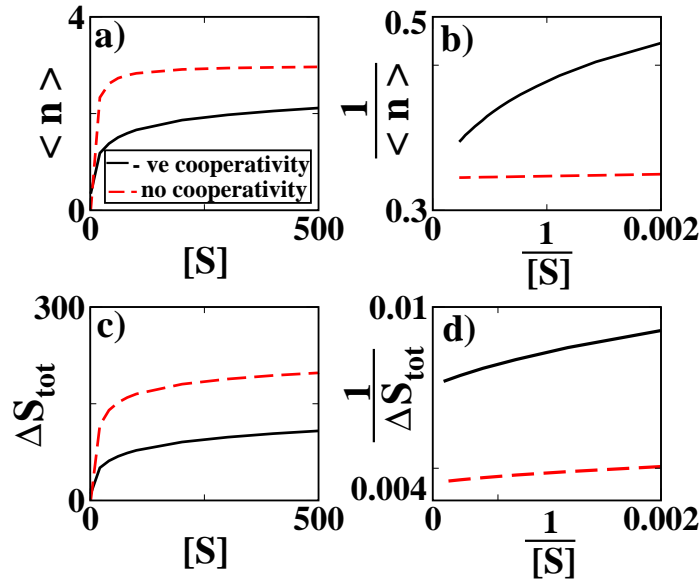
Figure 5.4: Plots of (a) $\langle n \rangle$ vs. [S] (in μM unit) and (b) $\frac{1}{\langle n \rangle}$ vs. $\frac{1}{[S]}$ at the NESS. (c) ΔS_{tot} vs. [S] and (d) $\frac{1}{\Delta S_{\text{tot}}}$ versus $\frac{1}{[S]}$ for negative cooperative (temporal) as well as non-cooperative binding. The entropy productions are calculated over a time interval as described in the caption of Fig.5.2.
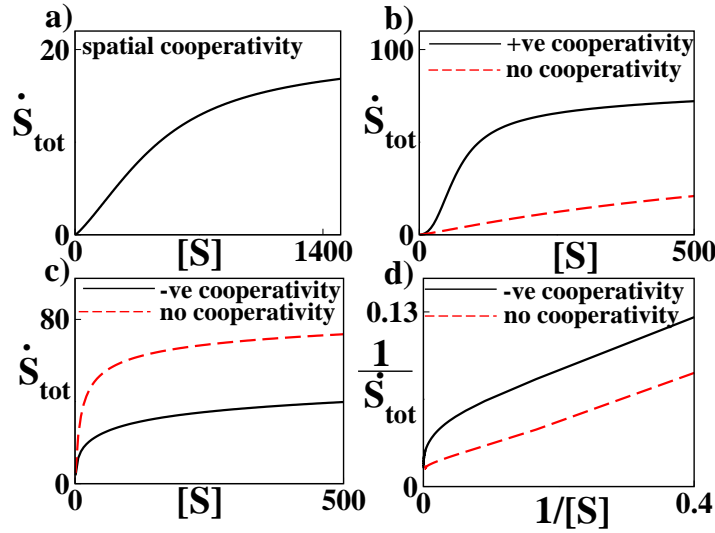
Figure 5.5: (a) Plot of $\dot{S}_{\text{tot}}$ against substrate concentration, [S] (in μM unit) for spatial cooperativity. In (b) and (c), the same quantity is plotted for positive and negative cooperative cases, respectively. The non-cooperative case is also shown for comparison. (d) Plot of $\frac{1}{\dot{S}_{\text{tot}}}$ vs. $\frac{1}{[S]}$, which is a Lineweaver-Burk type plot, for negative and non-cooperative cases.
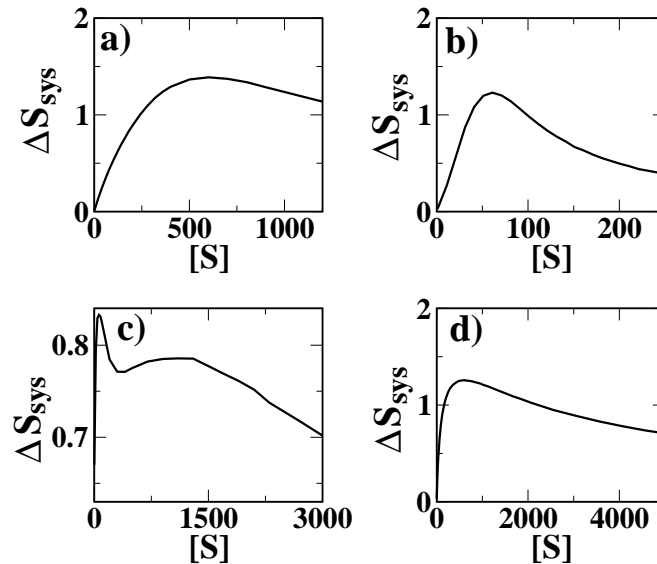
Figure 5.6: Plot of ΔS_{sys} against substrate concentration, [S] (in μM unit) for (a) spatial cooperative binding, (b) positive (temporal) cooperative binding, (c) negative (temporal) cooperative binding and (d) non-cooperative binding. In all the cases, the final time of observation is the same, set as such that the system reaches the NESS.

5.4.3 System entropy production and binding characteristics

The ensemble or trajectory average system entropy production over the time interval can be written as

$$\Delta S_{sys} = S_{sys}^{final} - S_{sys}^{initial} = -\sum_{n=0}^{n_T} P^{ss}(n)\ln P^{ss}(n), \qquad (5.49)$$

where the initial condition (time t = 0) of the fully unbound enzyme gives $S_{sys}^{initial} = 0$ and the final state of the system is an NESS characterized by the distribution $P^{ss}(n)$. We have plotted the ensemble average system entropy production, ΔS_{sys} as a function of the substrate concentration in Fig.5.6 for all the cases. In Fig.5.6(a), ΔS_{sys} is plotted for spatial cooperativity and in Fig.5.6(b-d) it is shown for the positive, negative and non-cooperative cases, respectively which belong to the class of temporal cooperativity. The first thing evident from the plots is that ΔS_{sys} passes through a global maximum for all the cases and in the case of negative cooperativity, there is also a local maximum with the parameters of our system.

We have plotted $P^{ss}(n)$ as a function of the substrate concentration in Fig.5.7(a-d) with the steady state ('ss') superscript being dropped for simplicity. Fig.5.7(a) shows the curves for spatial cooperativity. We can see that they all cross almost exactly at the same point, [S] $\sim 600\,\mu$M giving rise to the maximum in ΔS_{sys} for spatial cooperativity at this point (see Fig.5.7(a)). In Fig.5.7(b), we have shown the

curves for the positively cooperative system. At $[S] \sim 60\,\mu M$, the curves cross in a pairwise fashion; curves of P(0) and P(3) cross each other at this point as well as curves for P(1) and P(2). This particular substrate concentration corresponds to the maximum of ΔS_{sys} in this case (see Fig.5.7(b)).

The case of negative cooperativity requires a bit more attention. There is again pairwise curve crossing of the two sets of probabilities same as in the case of positive cooperativity at the same substrate concentration shown in Fig.5.7(c). This gives rise to the global maximum in the curve of ΔS_{sys} for this type of binding shown in Fig.5.6(c). The local maximum can be explained as follows. Unlike the plots in Fig.5.7(a) and (b), the probability curves P(2) and P(3) remain at significant values over the substrate range studied and the dominance of these two probability curves in Fig.5.7(c) (actually when P(2) and P(3) cross, they are close to 0.5 at $[S] \sim 1800\,\mu M$) over a large substrate range gives rise to an increase of ΔS_{sys}, albeit slow. Finally we come to the case of non-cooperativity in Fig.5.7(d) where again there is the pairwise crossing of the same set of probabilities as in Fig.5.7(b) but at $[S] \sim 600\,\mu M$ that again gives rise to the maximum of ΔS_{sys} shown in Fig.5.6(d). In this case too, there are more than one dominating probability curves before and after the pairwise crossing over similar substrate range as in Fig.5.7(c). But the ΔS_{sys} in this case shows a slow but steady decrease with substrate concentration after passing through the maximum without any unusual behavior. This may be due to the fact that here at least three of the four probabilities are significant (with comparable values) over a large substrate range and so they do not cross the value of 0.5 in this range unlike the case in Fig.5.7(c). It is clear that arbitrary variation of the rate constants of the system in each binding step can make life more complicated and then the maxima in the ΔS_{sys} curve may or may not be associated with the binding probability curve crossings.

We can justify the curve crossings, whether they all cross or cross pairwise at a particular substrate concentration, by inspecting the expressions of the steady state probability distributions. We see from the steady state distribution for the spatial cooperativity, Eq.(5.5), that if one of the probabilities, say P(0) is approximately equal to any other probability, say P(3), then $X \sim 1$ (but obviously not exactly equal to 1) and this automatically leads to the near equality of all the probabilities at this value of X. This is true for all the probabilities and hence in this case the probabilities can only cross simultaneously at $X \sim 1$. As the probabilities are equal at this point which corresponds to $[S] \sim 600\,\mu M$, this obviously gives the maximum system entropy production in this case. Now we take the steady state distribution of the non-cooperative case, Eq.(5.14). It can be easily seen that here only P(0) = P(3) leads to the equality P(1) = P(2) at $X = 1$ giving the maximum of ΔS_{sys} again at $[S] \sim 600\,\mu M$. So in the context of the system entropy production the spatial cooperative system shows some similarity with the non-cooperative system.
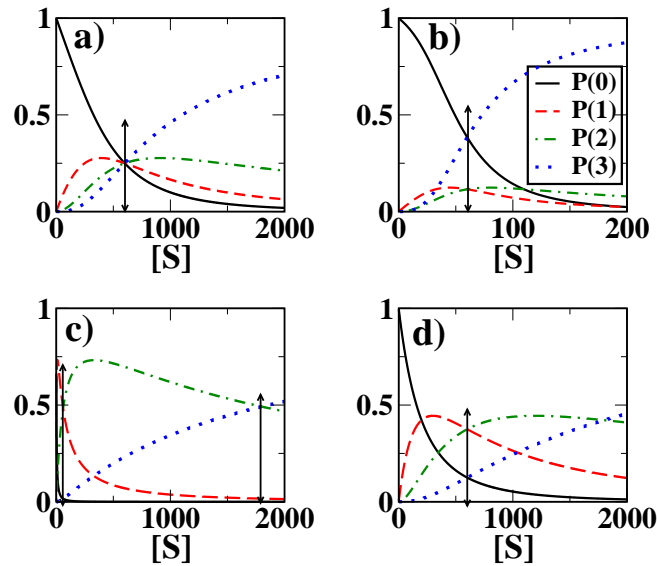
Figure 5.7: Plot of the steady state distributions, $P^{ss}(n)$ against [S] (in μM unit) for (a) spatial cooperative binding, (b) positive (temporal) cooperative binding, (c) negative (temporal) cooperative binding and (d) non-cooperative binding. In the plots, the 'ss' superscript is dropped for simplicity. The arrows indicate the curve crossing points.

With the same set of site-independent rate constants, the spatial cooperative system is also associated with larger system entropy production compared to that of the non-cooperative case. This is because all the binding probabilities become equal for the spatial cooperativity whereas they become equal pairwise for non-cooperative binding.

The cases of positive and negative cooperativity belonging to the class of temporal cooperativity are a bit complicated. We have considered a 10-fold increase of the substrate binding rate constant for each successive binding in the case of positive cooperativity whereas a 10-fold decrease in the corresponding rate constant for each successive binding for negative cooperativity. This symmetry ensures that in both the cases only $P(0) = P(3)$ leads to the equality $P(1) = P(2)$ at $X^{(1)} = 1$. This can be easily proved from Eq.(5.8). But if the rise or fall of the value of the substrate binding rate constant in each successive step of binding is not by the same factor, then the pairwise equality of the binding probabilities is not possible at a given substrate concentration.

We have plotted the quantity, C in Fig.5.8 for positive cooperative system (independent binding) and also for the spatial cooperative binding for different values of n_T as a function of substrate concentration. For the positive cooperativity case, the substrate binding rate constants, $k_1^{(n)}$ increase by a factor of 2 in each step. The value of C grows with substrate concentration, starting just above 1.0 and finally
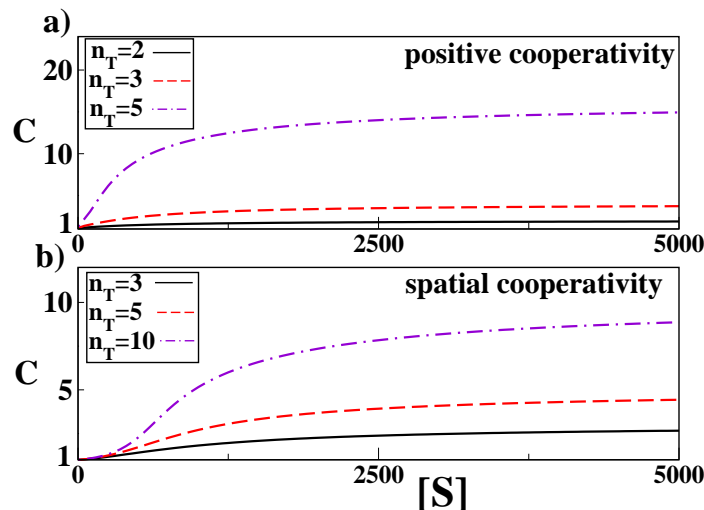
Figure 5.8: Plot of the cooperativity index, C against substrate concentration, [S] (in μM unit) for different values of the number of subunits of the oligomeric enzyme, n_T in the case of (a) positive (temporal) cooperativity and 5(b) spatial cooperativity.

saturates. One can see from Eq.(5.32), that the limiting value of C (obtained at high substrate concentration) in case of spatial cooperativity is n_T whereas for temporal cooperativity it is given by $f^{(n_T-1)}$ where $f^{(n_T-1)} = \frac{k_1^{(n_T-1)}}{k_1^{(0)}}$. Here we specifically mention the case of $n_T = 5$ for the positive cooperativity where the limiting value of C is $f^{(4)} = \frac{k_1^{(4)}}{k_1^{(0)}} = 2^4 = 16$. It is evident from Fig.5.8(a) that this is indeed the case.

5.4.4 Characterization of cooperativity: a case study with stepwise Aspartate receptor binding

Although apparently there is no straightforward connection between the Hill coefficient, n_H and C, first of all it is clear that the well-known criteria of cooperativity in terms of n_H is exactly the criteria we have given in terms of the cooperativity index, C in Eq.(5.35). Both the measures are equal to 1 in the absence of cooperativity whereas for cooperative binding, the criteria are the same although the actual values of n_H and C will be generally different. Here we will try to illustrate this point using some experimental data from the work of Kolodziej *et al.* [154] regarding the production of positive, negative as well as non-cooperativity by mutations at a serine 68 residue located at the subunit interface in the dimeric aspartate receptor of *Salmonella typhimurium*. Due to unavailability of experimental data of the stepwise Michaelis-Menten constants, $K_M^{(j)}$, we use the stepwise binding constants reported in their study in the place of $(K_M^{(j)})^{-1}$ of the independent binding model with $n_T = 2$ and $j = 0, 1$. Now the parameter $X^{(j)}$ in our study is related to

$K_M^{(j)}$ in the general non-equilibrium condition and reduces to stepwise equilibrium (binding) constants under the conditions already discussed at the end of Sec.IIC. For experimental testability of C at NESS, one needs the stepwise Michaelis-Menten constants, $K_M^{(j)}$. We choose the independent binding model as the experimental result reports both positive and negative cooperativity. We calculate the fractional saturation θ as a function of substrate concentration, [S] using Eq.(5.9) and find out the Hill coefficient, n_H at the half-saturation point ($\theta = 0.5$). Then we determine the cooperativity index, C at the substrate concentration where $\theta = 0.5$. The results are given in Table. 1. The Hill coefficients derived by us for different cases tally very well with the experimental data[154]. The cooperativity index, C detects the presence and absence of cooperativity successfully. Also the extent or degree of positive or negative cooperative behavior is equally well characterized by the index, C. This can be seen by comparing the values of n_H and C for the cases of serine and cysteine showing negative cooperativity as well as for threonine and isoleucine showing positive cooperativity.

Table 5.1: The stepwise Aspartate binding constants, K_1' and K_2' (in μM^{-1}) for different amino acid residues at position 68 of Aspartate receptor taken from the experimental study of Kolodziej *et al*[154]. Here we have taken the values of the inverse of the stepwise Michaelis-Menten constants, $K_M^{(j)}$ in our model to be equal to the binding constants. The values of the Hill coefficient, n_H in the parentheses are from the experimental work, given for comparison with the values determined here. The cooperativity index, C characterizes the cooperative behavior successfully as can be seen by comparing it with n_H.

Amino acid	$\frac{1}{K_M^{(0)}}(= K_1')$	$\frac{1}{K_M^{(1)}}(= K_2')$	n_H	C
serine	0.7	0.2	0.7(0.7)	0.491
cysteine	0.5	0.2	0.776(0.8)	0.598
threonine	0.4	0.9	1.197(1.2)	1.519
isoleucine	0.4	2.8	1.446(1.4)	2.558
aspartate	0.1	0.1	1.0(1.0)	1.0

The cooperativity index, C is related to the probability of fully bound state of the single enzyme. So another possibility of experimentally determining C, apart from the measurement of the stepwise Michaelis-Menten constants, will be to detect this fully bound state by electrical or optical means in a single molecule experiment and then to fit the resulting probability with some model distribution.

5.5 Conclusion

We have classified the cooperative substrate binding phenomena of a single oligomeric enzyme on the basis of the binding mechanism and the nature of the substrate-bound

states of the system in a chemiostatic condition. Both the binding mechanisms are modelled in terms of master equation. The sequential binding of the substrate molecules leads to spatial cooperativity whereas the independent binding scheme leads to temporal cooperativity. We have determined the various entropy productions due to the enzyme kinetics over a time interval where at the final point of time the system is in a non-equilibrium steady state (NESS) that can be arbitrarily far away from equilibrium. We have used kinetic Monte Carlo simulation algorithm applied on a single trajectory basis to calculate the entropy production. In this context, the interesting finding is that the total as well as the medium entropy production show the same diagnostic signatures for detecting the cooperativity as is well known in terms of the average binding number or the net velocity of the reaction. More specifically, ΔS_{tot} as well as ΔS_m for positive cooperative kinetics show sigmoidal variation as a function of substrate concentration whether the class being spatial or temporal. They also show the non-linearity in the inverse plot of Lineweaver-Burk type demonstrating the case of negative cooperativity. The signs of cooperative behavior is also reflected in a similar fashion on the variation of the total entropy production rate (epr) with substrate concentration determined at the NESS for different binding schemes. That the features of cooperativity are reflected similarly on the variations of both the total epr at the NESS and the total (and medium) entropy production over a time interval up to the NESS is a highly interesting fact and gives deep insight on the role of the binding mechanism in governing the total entropy production in a general non-equilibrium setup.

We have thoroughly analyzed the system entropy production for all the cases in terms of the steady state binding probability distributions. For a spatial and a non-cooperative system, the maximum value of the system entropy production due to the non-equilibrium processes in the reaction appears at the same substrate concentration with the value of the entropy production being greater for the spatial cooperativity. We have explained this in terms of the different binding probability curve-crossings that helps to understand how the binding characteristics affect the entropy production of the system, *i.e,* the single oligomeric enzyme. Similarly, the distinct features of the evolution of system entropy production for the positive and negative cooperative binding give valuable insights on its connection to the binding mechanism.

We have introduced an index of cooperativity, C defined as the ratio of the surprisal or equivalently, the stochastic system entropy associated with the fully bound state of the cooperative and non-cooperative cases. The criteria of cooperativity in terms of C is identical to that of the Hill coefficient. We have analyzed its connection to the Hill coefficient using some relevant experimental data. This index is truly an entropic estimate of cooperativity and gives a microscopic insight on the cooperative binding of substrate on a single oligomeric enzyme instead of realizing cooperativity

in terms of macroscopic reaction rate.

Chapter 6

Kinetic and thermodynamic description of voltage-gated single Potassium ion channel

In this chapter we have studied the non-equilibrium thermodynamic response of a voltage-gated single *Shaker* Potassium ion channel using a master equation. After giving a brief introduction about the goal of our study in Section 6.1, we have described the ion channel kinetic scheme in section 6.2, both for constant and oscillating voltage. For constant voltage case, we have discussed about the Hodgkin-Huxley equation for the probability of the ion-conducting state and in the case of time-dependent voltage, an analytical expression is given in terms of the probability of the ion-conducting state. Expressions of the total, medium and system entropy production rates are also given in this section for the non-equilibrium characterization. In section 6.3, we have extended the kinetic result of single ion channel to a system of finite number of ion channels. We have determined the various entropy production rates as well as the ionic current for constant and oscillating voltage and studied the hysteretic behavior to characterize the non-equilibrium response properties of the system in section 6.4. Finally the chapter is concluded in section 6.5.

6.1 Introduction

Study of ion channel plays an important role in understanding the propagation of nerve impulse and a wide variety of phenomena associated with excitable tissue of neural as well as non-neural nature[5, 45, 46, 47]. Ion channels maintain a controlled exchange of ions between the cells and the extra-cellular medium through ion-permeable pores with the rearrangement of the tertiary structure of channel proteins. A great deal of understanding about the function of the ion channel owes its origin in the experiments using voltage clamp method[5, 47, 48, 53, 54, 55, 156, 157, 158]. In

a traditional voltage clamp technique, ion flow across a cell membrane is measured as electric current, while the membrane voltage is held under experimental control with a feedback circuit[5, 47, 48, 54, 55, 156]. Current due to single ion channel can also be measured using patch clamp experiment based on the similar principle[5]. Recently non-equilibrium response spectroscopy [56, 57] has added a new dimension in the field of ion channel experiments using oscillating voltage protocol. This technique has been used for the selection of the appropriate Markov model from various possible schemes of ion channel kinetics[4, 56, 57, 69, 159]. From the kinetic studies, it has been found qualitatively that the oscillating voltage drives the ion channel out of equilibrium and resists the system to relax back to equilibrium [4, 56, 57, 69]. The oscillating voltage protocol[159] thus offers an opportunity to explore non-equilibrium response properties of the ion channel such as hysteresis[160] at non-equilibrium steady state(NESS).

Hysteresis has a long history[160] in its wide manifestation in various magnetic[161, 162] and other condensed matter systems[163, 164] as well as in biological processes[50, 159, 165]. In voltage-gated ion channels, hysteresis can occur when the time period of the oscillating external voltage is comparable to the characteristic relaxation time of the conformational transitions between conducting and non-conducting states [165, 166, 167, 168]. The channel hysteresis has several biological relevance, for example, it plays an important functional role in regulating physiological phenomena and is also a governing factor in maintaining the action of a neuron pacemaker[167]. A detailed theoretical description of hysteresis in ion channel for oscillating voltage was given by Pustovoit *et al.*[168] by considering a simple two-state model. Recently, Andersson described the hysteresis of ionic conductance[70] for oscillating voltage by considering the analysis of Pustovoit *et al.*[168] and then they have extended the study of the channel gating schemes for multiple states with independent as well as cooperative gating. Their studies[70, 168] reveal that the probability-voltage as well as the current-voltage hysteresis is dynamic in nature. The hysteresis loop area vanishes at the low and high frequency limits of the external oscillating voltage due to the wide time scale separation. Now, particularly for time-dependent external voltage, the system can go arbitrarily far away from equilibrium. Hence, along with the kinetic properties, the non-equilibrium thermodynamic features of the ion channel must also be explored. In this perspective, we have raised the following questions. (i) Are these low and high frequency limiting situations equivalent from the thermodynamic viewpoint or does the vanishing of an out-of-equilibrium phenomenon like hysteresis ensure that the system is at thermodynamic equilibrium? (ii) At non-equilibrium steady state(NESS), how the supplied energy is utilized for the production of ionic current? To address the above issues coherently, we have given a detailed non-equilibrium thermodynamic analysis of a voltage-gated *Shaker* Potassium ion channel. The ion channel kinetics is described by a master equation

constructed on the basis of a most suited Markov process proposed in an experimental work[4]. Starting from the model consisting of five states, we have discussed about how the stochastic conformational states are connected with the essential features of traditional Hodgkin-Huxley equation at constant voltage. Then we have explored the non-equilibrium thermodynamic features due to oscillating voltage.

6.2 Markov model of a voltage-gated Potassium ion channel

In this section, first we have provided the master equation describing the voltage-gated Potassium ion channel kinetics. For constant voltage case, the connection of the master equation with the Hodgkin-Huxley equation and results of the probability of ion-conduction are discussed. The time-dependent solution of the ion-conducting state probability is then given for oscillating voltage for a five-state model with one conducting and four non-conducting states. Then the corresponding expressions of the system, medium and total entropy production rates are provided.

6.2.1 Kinetic scheme of a Potassium ion channel and the master equation

Various experimental results reveal that a Potassium ion channel is comprised of four independent homologous subunits [169, 170, 171] where each subunit remains in several conformational states. For simplicity, here we have considered only two conformational states of each subunit, *i.e.,* inactive and active[172, 173, 174]. The dynamics of the Potassium channel can be described in terms of the number of subunits in active state at a particular instant of time. An optimum kinetic scheme of the activation of voltage-gated Potassium ion channel[4, 48] can be written as

$$
C_0 \underset{k_{-1}^{(1)}(V(t))}{\overset{4\,k_1^{(0)}(V(t))}{\rightleftharpoons}} C_1 \underset{2\,k_{-1}^{(2)}(V(t))}{\overset{3\,k_1^{(1)}(V(t))}{\rightleftharpoons}} C_2 \underset{3\,k_{-1}^{(3)}(V(t))}{\overset{2\,k_1^{(2)}(V(t))}{\rightleftharpoons}} C_3 \underset{4\,k_{-1}^{(4)}(V(t))}{\overset{k_1^{(3)}(V(t))}{\rightleftharpoons}} C_4 \tag{6.1}
$$
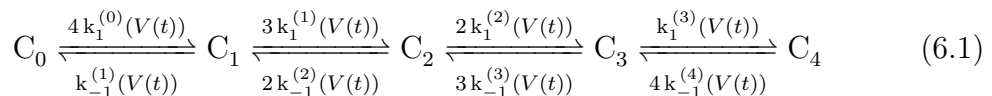
where C_n represents the n-th conformational state of the ion channel with n number of subunits in active state, where $n = 0, 1, \ldots, 4$. The number of subunits in active state can increase or decrease by one unit due to the occurrence of a forward or a backward reaction with voltage-dependent rate constants $k_1^{(n)}(V(t))$ and $k_{-1}^{(n)}(V(t))$, respectively. Here $V(t)$ is the time-dependent external voltage. The rate constants are explicitly defined as[4]

$$
k_1^{(n)}(V(t)) = k_1^{(n)}(0)\exp\left(\frac{q^+ V(t)}{k_B T'}\right)
$$

and

$$
k_{-1}^{(n)}(V(t)) = k_{-1}^{(n)}(0)\exp\left(\frac{q^- V(t)}{k_B T'}\right), \tag{6.2}
$$

where $q^{\pm}$ are the gating charges associated with each forward and backward transitions, respectively. $k_1^{(n)}(0)$ and $k_{-1}^{(n)}(0)$ are the forward and backward rate constants of the n-th conformational state at zero voltage, T' is the absolute temperature and k_B is the Boltzmann constant. During the time evolution, the number of subunits in active state becomes a fluctuating quantity[12, 13, 16] for a single ion channel. Therefore, the system performs a one-dimensional random walk along these dynamical states[12, 16]. The state, C_4 has been considered here as the ion-conducting state where all the subunits are simultaneously in active state. To describe the time evolution of the single ion channel, we have constructed a stochastic master equation[13, 74, 173, 175] in terms of the number of subunits in active state at a particular instant of time, t. The master equation can be written as

$$\frac{dP_n(t)}{dt} = \sum_{\mu=\pm1} [w_{\mu}^{(n-\nu_{\mu})}(n-\nu_{\mu}|n)(t)P_{(n-\nu_{\mu})}(t) - w_{-\mu}^{(n)}(n|n-\nu_{\mu})(t)P_n(t)], \qquad (6.3)$$

where ν_{μ} is the stoichiometric coefficient of the μ-th reaction and $\nu_1 = 1$ for forward process and $\nu_{-1} = -1$ for backward process. $P_n(t)$ is the probability of having n number of subunits in active state at time t where n runs from 0 to n_T. Here n_T is the total number of subunits with $n_T = 4$. The forward process, say $\mu = 1$, transforms the state $(n-1)$ to n and the reverse process, $\mu = -1$, transforms the state n to $(n-1)$. The corresponding transition probabilities are defined as

$$w_1^{(n-1)}(n-1|n)(t) = k_1^{(n-1)}(V(t))(n_T - (n-1)),$$

and

$$w_{-1}^{(n)}(n|n-1)(t) = k_{-1}^{(n)}(V(t))(n). \qquad (6.4)$$

Now putting the transition probabilities in Eq.(6.3) we obtain the simplified form of master equation as

$$\frac{dP_n(t)}{dt} = k_1^{(n-1)}(V(t))(n_T - n + 1)P_{(n-1)}(t) + k_{-1}^{(n)}(V(t))(n+1)P_{(n+1)}(t)$$

$$-k_1^{(n-1)}(V(t))(n_T - n)P_n(t) - k_{-1}^{(n)}(V(t))nP_n(t). \qquad (6.5)$$

6.2.2 Constant voltage case: Hodgkin-Huxley results from master equation

Traditionally the ion channel kinetics is studied using the voltage clamp technique where the voltage is varied, say from one holding potential to another, by matching the voltage value to a variable control voltage[48, 54, 55, 70]. Thereby the ion channel

conductance relaxes towards its new equilibrium[70]. In the constant voltage case, the steady state solution of Eq.(6.5) can be written as

$$P_n^c = \frac{\binom{n_T}{n} \prod_{j=0}^{n-1} K^{(j)}(V)}{\sum_{n=0}^{n_T} \binom{n_T}{n} \prod_{j=0}^{n-1} K^{(j)}(V)}, \tag{6.6}$$

where $K^{(j)}(V) = \frac{k_1^{(j)}(V)}{k_{-1}^{(j+1)}(V)}$. Here we take $K^{(j)} = f^j K^{(0)}$ with $j = 0, 1, ..., (n_T - 1)$. For $f > 1$, the successive equilibrium constants continue to increase giving rise to positive cooperativity whereas for $f < 1$, they go on decreasing resulting in negative cooperativity. For $f = 1$ *i.e.*, $K^{(j)}(V) = K^{(0)}(V) = K(V)$, the system is noncooperative where the probability distribution reduces to a binomial as

$$P_n^{nc} = \binom{n_T}{n} \frac{(K(V))^n}{(1 + K(V))^{n_T}}, \tag{6.7}$$

where $K(V) = \frac{k_1(V)}{k_{-1}(V)}$. By inserting the value of $K(V)$, the above equation can be written as a binomial distribution given by

$$P_n^{nc} = \binom{n_T}{n} \left(\frac{k_1(V)}{k_1(V) + k_{-1}(V)} \right)^n \left(\frac{k_{-1}(V)}{k_1(V) + k_{-1}(V)} \right)^{(n_T-n)}. \tag{6.8}$$

For noncooperative case, the time-dependent solution of Eq.(6.5) gives[12, 16, 173, 176, 177, 178, 153] as

$$P_n(t) = \binom{n_T}{n} X(t)^n (Y(t))^{n_T-n}. \tag{6.9}$$

Here

$$X(t) = \frac{k_1(V)(1 - \exp(-(k_1(V) + k_{-1}(V))t))}{k_1(V) + k_{-1}(V)}, \tag{6.10}$$

$$Y(t) = (1 - X(t)) = \frac{k_{-1}(V) + k_1(V)\exp(-(k_1(V) + k_{-1}(V))t)}{k_1(V) + k_{-1}(V)}, \tag{6.11}$$

assuming that initially all the subunits are in inactive state, C_0 *i.e*, the $n = 0$ state. This solution is well-known for the independent conformational transitions of the ion channel subunits[173, 179]. So the overall dynamics of the ion channel having $n_T = 4$ number of independent subunits can be expressed in terms of the dynamics of a single subunit described by the variables, $X(t)$ and $Y(t)$. This idea has been put forward by a number of authors in the context of ion-channels[173], enzyme kinetics[177, 178] and receptors[153, 179]. The combinatorial factor appearing in front of Eq.(6.9) gives the number of ways to choose n active states from n_T.

The average number of subunits in active state is expressed as $\langle n(t) \rangle = n_T X(t)$ and the average number of subunits in inactive state is $\langle n_T - n(t) \rangle = n_T Y(t)$. The parameter X satisfies the differential equation[47, 173]

$$\frac{dX(t)}{dt} = k_1(V)(1 - X(t)) - k_{-1}(V)(X(t)). \tag{6.12}$$

This equation is identical to the equation for the 'open probability' originally introduced by Hodgkin and Huxley to model the Potassium ion channel conductance[47, 173]. However, they did not consider the details of the conformational dynamics of the channel subunits as described here in the master equation.

Furthermore, the probability of ion conducting state, $P_{n_T}(t)$ $(n_T = 4)$ at steady state can be obtained from Eq.(6.9) as

$$P_{n_T}^{(ss)} = [X^{(ss)}]^{n_T}, \tag{6.13}$$

where $X^{(ss)}$ is the steady state value of $X(t)$ given from Eq.(6.10) as $X^{(ss)} = \frac{k_1(V)}{k_1(V)+k_{-1}(V)}$. Using the value of $X^{(ss)}$ in Eq.(6.13), we get

$$P_{n_T}^{(ss)} = \left[\frac{k_1(V)}{k_1(V) + k_{-1}(V)}\right]^{n_T}. \tag{6.14}$$

Now substituting the expressions of $k_1(V)$ and $k_{-1}(V)$ from Eq.(6.2) into Eq.(6.14), we finally obtain the steady state probability of the ion-conducting state[48],

$$P_{n_T}^{(ss)} = \left[\frac{1}{1 + K_{eq}(0)\exp(\frac{-qV}{k_B T'})}\right]^{n_T}, \tag{6.15}$$

with $q = (q^+ - q^-)$ and $K_{eq}(0)$ is the equilibrium constant defined as $K_{eq}(0) = \left(\frac{k_{-1}(0)}{k_1(0)}\right)$. The above probability is of the form of Boltzmann distribution of power n_T, usually used for calculating the probability of ion-conducting state in voltage clamp experiments where n_T is the number of independent and identical transitions[48]. Therefore, at constant voltage the probability of ion-conducting state becomes a powered Boltzmann distribution.

6.2.3   Solution of Ion channel kinetics for oscillating voltage

Here we have described the kinetics of a single Potassium ion channel for oscillating voltage based on the reaction scheme in Eq.(6.1). To get some analytical understanding, we have expressed the overall reaction in terms of the ion-conducting state which is designated as C_4 in the reaction scheme. The probability rate equation for this state can be easily obtained from Eq.(6.3) as

$$\frac{dP_4(t)}{dt} = k_1(V(t))P_3(t) - n_T k_{-1}(V(t))P_4(t). \tag{6.16}$$

By using the normalization condition $\sum_{n=0}^{4} P_n(t) = 1$, we can rewrite Eq.(6.16) as

$$\frac{dP_4(t)}{dt} = \chi(t) - K(t)P_4(t), \tag{6.17}$$

where $\chi(t) = k_1(V(t))\left[1 - \{P_0(t) + P_1(t) + P_2(t)\}\right]$ and $K(t) = [k_1(V(t)) + n_T k_{-1}(V(t))]$.

The solution of the above equation can be written as

$$P_4(t) = P_4(t_0) \exp[-\int_{t_0}^{t} K(t')dt'] + \int_{t_0}^{t} \chi(t') \exp[-\int_{t'}^{t} K(t'')dt'']dt'. \qquad (6.18)$$

Using Eq.(6.18) one can write $P(4, t)$ for $mT < t < (m+1)T$ as[168]

$$P_4(mT + t) = P_4(mT) \exp[-\int_{mT}^{t} K(t')dt'] + \int_{mT}^{t} \chi(t') \exp[-\int_{t'}^{t} K(t'')dt'']dt',$$
$$(6.19)$$

where T is the time period of the oscillating voltage and m ($= 0, 1, 2, ...$) is the index of oscillation period. Now, using Eq.(6.18), one can write a recursion formula connecting the probabilities $P_4(mT)$ and $P_4((m+1)T)$ as

$$P_4((m+1)T) = \phi P_4(mT) + \Delta_0, \qquad (6.20)$$

where ϕ and Δ_0 are given by

$$\phi = \exp\left[-\int_0^T K(t)dt\right] \qquad (6.21)$$

and

$$\Delta_0 = \int_0^T \chi(t') \exp\left[-\int_{t'}^T K(t'')dt''\right] dt'. \qquad (6.22)$$

Above recursion relation gives the value of $P_4(mT)$ as

$$P_4(mT) = \phi^m P_4(0) + \frac{1 - \phi^m}{1 - \phi}\Delta_0, \qquad (6.23)$$

where $P_4(0)$ is the initial probability of the ion-conducting state. When $m \to \infty$, the probability $P_4(mT)$ approaches its asymptotic value,

$$\lim_{m\to\infty} P_4(mT) = \frac{\Delta_0}{1 - \phi}. \qquad (6.24)$$

By substituting the above equation into Eq.(6.19) and taking the asymptotic long time limit of the probability, $P_4(mT + t)$ which is denoted as $P_4^{(ss)}(t)$, we obtain

$$P_4^{(ss)}(t) = \lim_{m\to\infty} P_4(mT + t) = \frac{\Delta(t)}{1 - \phi}. \qquad (6.25)$$

Here the function $\Delta(t)$ is given by

$$\Delta(t) = \int_t^{t+T} \chi(t') \exp\left[-\int_{t'}^{t+T} K(t'')dt''\right] dt'. \qquad (6.26)$$

At very low frequency limit when $T \to \infty$, ϕ defined in Eq.(6.21) vanishes. Therefore, $P_4^{(ss)}(t)$ in Eq.(6.25) can be written as

$$P_4^{(ss)}(t) = \int_0^T \chi(t - t') \exp[-\int_0^{t'} K(t - t'')dt'']dt'. \qquad (6.27)$$

As $\chi(t')$ and $K(t')$ are slowly varying functions in the low frequency limit, we can take the following approximation

$$\chi(t - t') \approx \chi(t) - t'\dot{\chi}(t'), K(t - t'') \approx K(t) - t''\dot{K}(t'')$$

and

$$\exp[-\int_0^{t'} K(t - t'')dt''] \approx \left(1 + \frac{1}{2}\dot{K}(t)t'^2\right)\exp[-K(t)t']. \tag{6.28}$$

Neglecting the term proportional to the product $\chi(t)K(t)$, we obtain

$$P_4^{(ss)}(t) \approx Q(t) - \frac{\dot{Q}(t)}{K(t)}, \tag{6.29}$$

where $Q(t) = \frac{\chi(t)}{K(t)}$. Then for slowly varying voltage, $P_4^{(ss)}(t)$ finally becomes

$$P_4^{(ss)}(t) = \frac{\chi(t)}{K(t)}. \tag{6.30}$$

Similarly, in the high frequency limit when $T \to 0$, ϕ defined in Eq.(6.21) can be written as

$$\phi = 1 - T\langle K \rangle. \tag{6.31}$$

Here $\langle f \rangle = \frac{1}{T}\int_0^T f(t)dt$ where f can be $\chi(t)$ or $K(t)$. Hence $P_4^{(ss)}(t)$ in Eq.(6.25) takes the form

$$P_4^{(ss)}(t) = \frac{1}{T\langle K \rangle}\int_t^{t+T}\chi(t')\exp\left[-\int_{t'}^{t+T}K(t'')dt''\right]dt'. \tag{6.32}$$

In the high frequency limit we can take the following approximation

$$\exp\left[-\int_{t'}^{t+T}K(t'')dt''\right] \approx 1 - \int_{t'}^{t+T}K(t'')dt''. \tag{6.33}$$

Using this approximation, Eq.(6.32) can be written as

$$P_4^{(ss)}(t) = \frac{\int_t^{t+T}\chi(t')dt' - \int_t^{t+T}\chi(t')dt'\int_{t'}^{t+T}K(t'')dt''}{\int_t^{t+T}K(t')dt'}$$

$$= \frac{\langle\chi(t)\rangle}{\langle K(t)\rangle} - \delta(t). \tag{6.34}$$

Here we define $\delta(t) = \frac{\xi}{\int_t^{t+T}K(t')dt'}$ where $\xi = \int_t^{t+T}\chi(t')(\int_{t'}^{t+T}K(t'')dt'')dt'$. Here the limit t' varies in the range, $t \leq t' \leq t+T$ and t'' varies in the range, $t' \leq t'' \leq t+T$. In the double integration, ξ in the limit of $T \to 0$, one can approximate $(\int_{t'}^{t+T}K(t'')dt'')$ as $(T+t-t')K(t')$ where $0 \leq (T+t-t') \leq T$. This makes $\xi \approx T\int_t^{t+T}\chi(t')K(t')dt'$ and consequently $\delta(t) \to 0$ in the high frequency limit. This ensures that in the high frequency limit, $P_4^{(ss)}(t)$ in Eq.(6.34) becomes

$$P_4^{(ss)}(t) = \frac{\langle\chi(t)\rangle}{\langle K(t)\rangle}. \tag{6.35}$$

The fact that the value of $\delta(t)$ tends to 0 with increase in frequency is also supported by the direct numerical evaluation of $P_4^{(ss)}(t)$ and $\frac{\langle \chi(t) \rangle}{\langle K(t) \rangle}$. One must also note that although the equations (6.30) and (6.35) give the steady state ion-conducting probability, $P_4^{(ss)}(t)$ in compact form, it is not possible to evaluate analytically as $\chi(t)$ depends on $P_0(t), P_1(t)$ and $P_2(t)$. To determine these probabilities, we resort to numerical solution of the general master equation, Eq.(6.3) with time-dependent transition probabilities for oscillating voltage. The numerically determined time-dependent probabilities, $P_n(t)$ are used to obtain the ionic current and entropy production rates for further studies. The details are given in section 6.4.

6.2.4 Entropy production rates: non-equilibrium characterization of ion channel

To explore the non-equilibrium thermodynamic features of the Potassium ion channel, here we discuss on the entropy production rates due to the channel kinetics. We start from the definition of the entropy of the system in terms of the Shannon entropy as[16, 100, 101]

$$S_{sys}(t) = -k_B \sum_n P_n(t) \ln P_n(t). \tag{6.36}$$

Using the master equation, Eq.(6.3) we get the system entropy production rate (epr) as

$$\dot{S}_{sys}(t) = \frac{1}{2} \sum_{n,\mu=\pm 1} [w_\mu(n-\nu_\mu|n)(t)P_{(n-\nu_\mu)}(t) - w_{-\mu}(n|n-\nu_\mu)(t)P_n(t)]$$

$$\times \ln \left(\frac{P_{(n-\nu_\mu)}(t)}{P_n(t)} \right), \tag{6.37}$$

where we set the Boltzmann constant, $k_B = 1$. Here the voltage-dependent transition probabilities are functions of time due to the explicit time-dependence of the voltage as given in Eq.(6.4). We have assumed ideal reservoir (surroundings) with no inherent entropy production except through the boundaries of the system. The system epr can be split as[100, 101, 102, 103, 104, 180]

$$\dot{S}_{sys}(t) = \dot{S}_{tot}(t) - \dot{S}_m(t). \tag{6.38}$$

Here the first term in the r.h.s. of Eq.(6.38) gives the total epr and the second term denotes the medium epr due to the entropy flux into the surroundings. They are defined as

$$\dot{S}_{tot}(t) = \frac{1}{2} \sum_{n,\mu=\pm 1} [w_\mu(n-\nu_\mu|n)(t)P_{(n-\nu_\mu)}(t) - w_{-\mu}(n|n-\nu_\mu)(t)P_n(t)]$$

$$\times \ln \left(\frac{w_\mu(n-\nu_\mu|n)P_{(n-\nu_\mu)}(t)}{w_{-\mu}(n|n-\nu_\mu)P_n(t)} \right) \tag{6.39}$$

124

and

$$\dot{S}_m(t) = \frac{1}{2} \sum_{n,\mu=\pm 1} [w_\mu(n-\nu_\mu|n)(t)P_{(n-\nu_\mu)}(t) - w_{-\mu}(n|n-\nu_\mu)(t)P_n(t)]$$

$$\times \ln\left(\frac{w_\mu(n-\nu_\mu|n)}{w_{-\mu}(n|n-\nu_\mu)}\right). \tag{6.40}$$

Using the values of forward and backward transition probabilities from Eq.(6.4) into Eq.(6.39) and considering the boundary conditions $P_{(n-1)} = 0$ for $n = 0$ and $P_{(n+1)} = 0$ for $n = n_T$, we finally obtain the expression of $\dot{S}_{tot}(t)$ for ion channel as

$$\dot{S}_{tot}(t) = \sum_{n=0}^{n_T-1} \left[k_1(V(t))(n_T-n)P_n(t) - k_{-1}(V(t))(n+1)P_{(n+1)}(t)\right]$$

$$\times \ln\left(\frac{k_1(V(t))(n_T-n)P_n(t)}{k_{-1}(V(t))(n+1)P_{(n+1)}(t)}\right). \tag{6.41}$$

From the above Eq.(6.41) we can calculate the total entropy production rate at constant voltage as well as at high and low frequency limits of oscillating voltage.

Calculation of total entropy production rate at constant voltage

To calculate the total entropy production rate at equilibrium, we have substituted the time-dependent probability value, $P_n(t)$ from Eq.(6.9) into Eq(6.41) and obtain

$$\dot{S}_{tot}(t) = [k_1(V)\langle n_T - n(t)\rangle - k_{-1}(V)\langle n(t)\rangle]\ln\left(\frac{k_1(V)Y(t)}{k_{-1}(V)X(t)}\right). \tag{6.42}$$

At steady state from Eq.(6.10) and (6.11) we have $X^{(ss)} = \left(\frac{k_1(V)}{k_1(V)+k_{-1}(V)}\right)$ and $Y^{(ss)} = \left(\frac{k_{-1}(V)}{k_1(V)+k_{-1}(V)}\right)$. Then it follows easily from Eq.(6.42) that $\dot{S}_{tot}(t)$ becomes zero at equilibrium for a constant external voltage.

Estimation of total entropy production rate at low and high frequency limit

Here we have estimated the entropy production rate in the low and high frequency limit from Eq.(6.41). It is quite obvious that in the low frequency limit, the steady state value of $P_4(t)$, $P_4^{(ss)}(t)$ tends to its equilibrium value where the condition of detailed balance is satisfied as in the case of constant voltage. Therefore, at steady state the total entropy production rate, $\dot{S}_{tot}^{(ss)}(t)$ becomes zero in the low frequency limit.

To estimate the total entropy production rate, $\dot{S}_{tot}^{(ss)}(t)$ at high frequency limit, we have considered that at this limit the values of $P_0(t), P_1(t)$ and $P_2(t)$ becomes zero. Our consideration is justified from the numerical analysis which is thoroughly discussed in the section 6.4. From this consideration, $\chi(t)$ in Eq.(6.17) can be written

as $\chi(t) \approx k_1(V(t))$ and $\dot{S}_{tot}^{(ss)}(t)$ in Eq.(6.41) can be expressed in terms of the steady state probability of ion-conducting state, $P_4^{(ss)}(t)$ as

$$\dot{S}_{tot}^{(ss)}(t) = \left[k_1(V(t))(1 - P_4^{(ss)}(t)) - k_{-1}(V(t))n_T P_4^{(ss)}(t) \right] \ln \frac{k_1(V(t))(1 - P_4^{(ss)}(t))}{k_{-1}(V(t))n_T P_4^{(ss)}(t)}. \tag{6.43}$$

Therefore, in the high frequency limit, the steady state value of $\dot{S}_{tot}^{(ss)}$ can be easily calculated by substituting the value of $P_4^{(ss)}(t)$ from Eq.(6.35) into Eq.(6.43) whereby we get

$$\dot{S}_{tot}^{(ss)}(t) = n_T \left[\frac{k_1(V(t))\langle k_{-1}(V(t))\rangle - k_{-1}(V(t))\langle k_1(V(t))\rangle}{\langle K(t)\rangle} \right] \ln \frac{k_1(V(t))\langle k_{-1}(V(t))\rangle}{k_{-1}(V(t))\langle k_1(V(t))\rangle}. \tag{6.44}$$

Here $K(t) = k_1(V(t)) + n_T k_{-1}(V(t))$. When $\omega \to \infty$, $\langle k_1(V(t))\rangle$ and $\langle k_{-1}(V(t))\rangle$ can be written as

$$\langle k_1(V(t))\rangle = f_1 \, k_1(0)$$

and

$$\langle k_{-1}(V(t))\rangle = f_{-1} \, k_{-1}(0), \tag{6.45}$$

where $f_1 = \langle \exp[x_1 V(t)]\rangle$ with $x_1 = \frac{q^+}{k_B T'}$ and $f_{-1} = \langle \exp[x_{-1} V(t)]\rangle$ with $x_{-1} = \frac{q^-}{k_B T'}$. As the value of $q^+ \approx -q^-$, we have taken $q^+ = q^- = q$. So we can write $x_1 = x$ and $x_{-1} = -x$. Therefore, $f_{\pm 1}$ can be written as

$$f_{\pm 1} = 1 \pm \langle xV(t)\rangle + \frac{(\langle xV(t)\rangle)^2}{2} \pm \frac{(\langle xV(t)\rangle)^3}{3!} + \cdots,$$

where $\langle xV(t)\rangle^n = \left[\frac{1}{T} \int_0^T x(V_0 \sin\omega t) dt \right]^n$ with $n = \{0, 1, 2....\}$. When n is odd, $\langle xV(t)\rangle^n = 0$ and for even values of n, $\langle xV(t)\rangle^n$ becomes independent of frequency, ω. Hence we can write $\langle k_1(t)\rangle = f \, k_1(0)$ and $\langle k_{-1}(t)\rangle = f \, k_{-1}(0)$, where $f_{\pm} = f$. Using these relations, Eq.(6.44) can be written as

$$\dot{S}_{tot}^{(ss)}(t) = n_T \left[\frac{k_1(0)k_{-1}(0)2\sinh(V'(t))}{k_1(0) + n_T k_{-1}(0)} \right] 2V'(t), \tag{6.46}$$

where $V'(t) = xV(t)$ with $x = \frac{q}{k_B T'}$. The value of $\dot{S}_{tot}^{(ss)}(t)$ calculated from Eq.(6.46) is an approximate one, however, from this analytic expression we can obtain the limiting value of $\langle \dot{S}_{tot}^{(ss)}(t)\rangle$ in the high frequency limit ($\omega \to \infty$).

Now from Eq.(6.46) it can be easily shown that in the high frequency limit, $\dot{S}_{tot}^{(ss)}(t)$ oscillates with a time-period which is half of that of the external voltage, $V(t)$. To prove this first we note that $V(t+\frac{T}{2}) = V_a \sin\omega(t+\frac{T}{2}) = -V_a \sin\omega t = -V(t)$ and thus $\sinh(V'(t + \frac{T}{2})) = -\sinh(V'(t))$. Then it follows from Eq.(6.46) that

$$\dot{S}_{tot}^{(ss)}\left(t + \frac{T}{2}\right) = n_T \left[\frac{k_1(0)k_{-1}(0)2\sinh(V'(t + \frac{T}{2}))}{k_1(0) + n_T k_{-1}(0)} \right] 2V'\left(t + \frac{T}{2}\right) = \dot{S}_{tot}^{(ss)}(t). \tag{6.47}$$

Therefore, in the high frequency limit $\dot{S}_{tot}^{(ss)}(t)$ versus time curve becomes symmetric and it completes a cycle at $T/2$.

6.3 Markov model for many Potassium ion channels

Here we have discussed about how the single ion channel results can be extended for L_T number of *Shaker* channels. In Eq.(6.1), we have already discussed the kinetic scheme of a single ion channel, where an ion channel remains in any one of the five conformational states (C_0 to C_4) at a particular instant of time. For L_T number of channels, the kinetic scheme can be written as[53]

$$m_0 \underset{W(m_1|m_0)(t)}{\overset{W(m_0|m_1)(t)}{\rightleftharpoons}} m_1 \underset{W(m_2|m_1)(t)}{\overset{W(m_1|m_2)(t)}{\rightleftharpoons}} m_2 \underset{W(m_3|m_2)(t)}{\overset{W(m_2|m_3)(t)}{\rightleftharpoons}} m_3 \underset{W(m_4|m_3)(t)}{\overset{W(m_3|m_4)(t)}{\rightleftharpoons}} m_4, \tag{6.48}$$
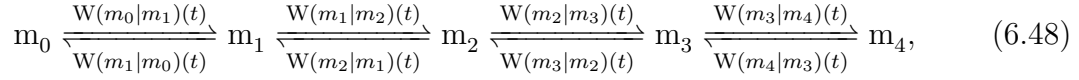
where the transition probabilities are given as $W(m_n|m_{(n-1)})(t) = m_n w_{-1}(n|n-1)(t)$ and $W(m_{(n-1)}|m_n)(t) = m_{(n-1)} w_1(n-1|n)(t)$. Here $w_{-1}(n|n-1)(t)$ and $w_1(n-1|n)(t)$ are defined as in Eq.(5.21). Here m_n specifies the number of channels in the C_n conformational state (n varies from 0 to 4) at time t with $\sum_{n=0}^{4} m_n = L_T$. The corresponding master equation can be written as[53]

$$\frac{\partial Q(\mathbf{m}, t)}{\partial t} = \sum_{n=1}^{4} (m_n+1) w_{-1}(n|n-1)(t) Q(m_{(n-1)}-1, m_n+1, t) + (m_{(n-1)}+1) w_1(n-1|n)(t)$$

$$Q(m_{(n-1)}+1, m_n-1, t) - m_n w_{-1}(n|n-1)(t) Q(\mathbf{m}, t) - m_{(n-1)} w_1(n-1|n)(t) Q(\mathbf{m}, t). \tag{6.49}$$

Here $Q(\mathbf{m}, t)$ is the probability of having the population state vector $\mathbf{m}$ at time t where $\mathbf{m} \equiv (m_1, m_2, m_3, m_4)$ with $m_0 = L_T - \sum_{n=1}^{4} m_n$. For analytical simplicity, we have considered the two-state Markov model instead of a five-state one by assuming that all the ion channels are either in inactive or active state. Therefore, for the two-state Markov model the kinetic scheme can be written as

$$\text{Close} \underset{k_{-1}(V(t))}{\overset{k_1(V(t))}{\rightleftharpoons}} \text{Open.} \tag{6.50}$$

These 'Close' and 'Open' states are similar to the conformational states, m_0 and m_4 in Eq.(6.48) where all the subunits in an ion channel remain in inactive and active state, respectively. For this two-state case, the master equation can be constructed in terms of the number of channels in open state at a particular instant of time as

$$\frac{dQ(m,t)}{dt} = k_1(V(t))(L_T - m + 1)Q(m-1, t) + k_{-1}(V(t))(m+1)Q(m+1, t)$$

$$-k_1(V(t))(L_T - m)Q(m, t) - k_{-1}(V(t))mQ(m, t). \tag{6.51}$$

Here $Q_{(m, t)}$ is the probability of having m number of channels in open state at time t where the total number of channels. The master equation described in Eq.(6.51) looks similar to that in Eq.(6.5) for a single ion channel consisting of five conformational states. At constant voltage, solution of Eq.(6.51) becomes a binomial

distribution as described in Eq.(6.9) and the average number of channels in open state is given by $\langle m(t)\rangle = L_T X(t)$ where $X(t)$ is defined similarly as in Eq.(6.10). At steady state, the value of $X(t)$ becomes $X^{(ss)} = \frac{k_1(V)}{k_1(V)+k_{-1}(V)}$ and the probability distribution becomes $Q^{(ss)}(m) = \frac{L_T!}{m!(L_T-m)!}(X^{(ss)})^m(Y^{(ss)})^{L_T-m}$. If L_T is very large and $X^{(ss)}$ is very small, $\frac{L_T!}{(L_T-m)!}$ becomes $(L_T)^m$ and $(1-X^{(ss)})^{(L_T-m)} \approx \exp(-X^{(ss)}L_T)$. Then the probability distribution becomes Poissonian given as

$$Q^{(ss)}(m) = \frac{(L_T X^{(ss)})^m}{m!}\exp(-X^{(ss)}L_T) \qquad (6.52)$$

where $X^{(ss)}L_T$ is the average number of ion channels in open state. At a particular time, t the ionic current can be calculated as

$$I(t) = g_0 \times g(V) \times (V - V_r)\langle m(t)\rangle = g_0 \times g(V) \times (V - V_r)L_T Q_o(t), \qquad (6.53)$$

where $Q_o(t)$ is the open state probability of a single channel for the two-state case. g_0 is the overall scaling factor representing the cell expression rate, $g(V)$ is the nonlinear conductance of an ion channel. V_r is the reversal potential at which no ionic current can pass from the cell. From numerical analysis of Eq.(6.51), we can also obtain the total epr, $\dot{S}_{tot}(t)$ and other non-equilibrium thermodynamic quantities.

6.4 Numerical study of voltage-gated *Shaker* Potassium ion channel

In this section, using the numerical solution of the master equation given in Eq.(6.5) for ion channel kinetics with time-dependent voltage, we determine the ionic current described below as well as the various entropy production rates with dynamical hysteresis phenomenon. Eq.(6.5) is numerically solved using the Heun's algorithm with constant time steps. We have taken the rate parameters from the experimental work of Kargol *et al.*[4] obtained for the *Shaker* Potassium ion channel expressed in mammalian cells, tsA 201. The rate constants at zero voltage are taken as $k_1(0) = 124.8 s^{-1}$ and $k_{-1}(0) = 4.74 s^{-1}$. The gating charges associated with each forward and backward transition rates are $q^+ = 0.66e$ and $q^- = -0.64e$, respectively and the temperature is $12^0 C$. The externally applied oscillating voltage is considered here as sinusoidal.

Here our main aim is to study the case of oscillating voltage. However, for completeness of the study and as a theoretical support of a physiologically important experimental system[4], at first we have briefly discussed about the case of constant voltage where the master equation is analytically solvable.
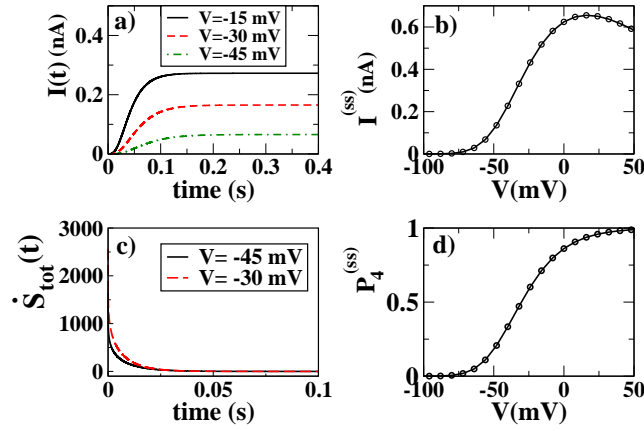
Figure 6.1: (a) Ionic current, I(t) in nanoAmpere(nA) is plotted against time (in s) at constant depolarizing voltages, V=-15,-30 and -45 mV, respectively. In (b) and (d), the steady state ionic current, $I^{(ss)}$ and probability of ion-conducting state, $P_4^{(ss)}$ are plotted as a function of voltage at steady state. In (c), the total entropy production rate(epr), $\dot{S}_{tot}(t)$ is plotted as a function of time at depolarizing voltages, V=-30 and -45 mV, respectively. At constant voltage, system reaches equilibrium characterized by vanishing total epr.

6.4.1 Kinetics and thermodynamics at constant voltage

Experimentally, kinetic description is usually carried out by measuring the ionic current, I(t) which is calculated using the expression

$$I(t) = g_0 \times g(V) \times (V - V_r)P_4(t). \tag{6.54}$$

Here g_0 is the overall scaling factor representing the cell expression rate taken as $g_0 = 1.013$ [4]. The functional form of the nonlinear conductance, g(V) (in microSiemens, μS) is taken from the experimental paper of Kargol $et\ al.$[69] and given as $g(V) = 1.340 \times 10^{-9}(V)^3 - 7.30 \times 10^{-8}(V)^2 - 3.35 \times 10^{-5}(V) + 4.470 \times 10^{-3}$. V_r is the reversal potential at which no ionic current can pass from the cell and taken here as $V_r = -90$mV. From Fig.6.1(a) it is observed that the ionic current, I(t) first increases with time and then saturates at a constant value. The magnitude of I(t) increases with increase in constant (depolarizing) voltage, V. The conductance, g(V) as a function of voltage, V is an inverted basin passing through a maximum. The probability of ion-conducting state at steady state, $P_4^{(ss)}$ shows a sigmoidal rise with increasing depolarizing voltage and goes to saturation at high (positive) voltage values as is evident from the plot Fig.6.1(d). The current at steady state, $I^{(ss)}$ shows similar behavior; however, at high (positive) depolarizing voltages it exhibits a small decay as shown in Fig.6.1(b). This is due to the nonlinear voltage dependence of the conductance, g(V). The nature of the steady state current-voltage curve follows
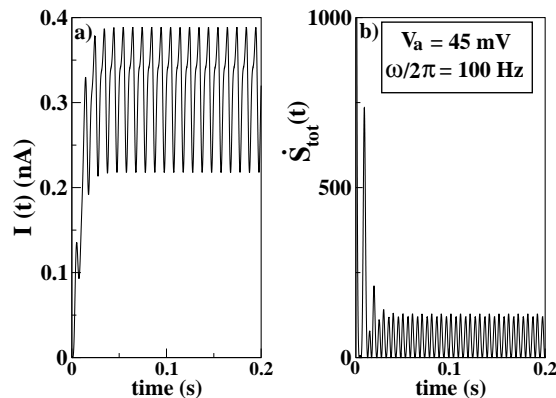
Figure 6.2: The ionic current, I(t) and entropy production rate, $\dot{S}_{tot}(t)$ are plotted as a function of time. The bold line in (b) denotes the mean value of $\dot{S}_{tot}(t)$ at NESS.

similar qualitative trend as that of the experimental results of Kargol *et al.* for the voltage clamp study. From Fig.6.1(c) it is observed that the steady state value of $\dot{S}_{tot}(t)$ becomes zero which indicates that at constant voltage the system goes to equilibrium.

To investigate the thermodynamic nature of the steady state at constant voltage, The analytical result is supported by the numerical result shown in Fig.6.1(c).

6.4.2 Nonequilibrium behavior for oscillating Voltage: Dynamic entropy hysteresis

Now we come to the more interesting case of the time-dependent external voltage. We take a sinusoidal voltage variation $V(t) = V_0 + V_a \sin \omega t$ with mean V_0, amplitude V_a and frequency ω. We numerically solve the master equation, Eq.(6.5) to get the probability of the ion-conducting state, $P_4(t)$ and to calculate the ionic current, I(t) and various entropy production rates. The ionic current, I(t) is calculated according to Eq.(6.54) by considering the time-dependent voltage variation. For oscillating external voltage, the ionic current reaches a time-periodic steady value, $I^{(ss)}(t)$. The steady state is actually a non-equilibrium steady state(NESS) characterized by a non-zero total epr, $\dot{S}_{tot}(t)$ shown in Fig. 6.2(b). $\dot{S}_{tot}(t)$ oscillates around a non-zero mean value which is indicated in the figure with a bold line.

In Fig.6.3(a) and (b), $I^{(ss)}(t)$ vs voltage and $P_4^{(ss)}(t)$ vs voltage plots are shown for three different frequency values (low, medium and high) of the external voltage at steady state over a period. The hysteresis is evident in both the cases which tends to vanish at very low and at very high frequencies with the hysteresis loop area disappearing in these two limits. Here we want to point out the nature of the $P_4^{(ss)}(t)$-voltage plot specifically at the two limiting situations; at low frequency

of the external voltage, $P_4^{(ss)}(t)$ oscillates significantly whereas in high frequency the amplitude of oscillation is much less and $P_4^{(ss)}(t)$ deviates maximum from its instantaneous steady state (equilibrium) value, *i.e,* the value $P_4^{(ss)}(t)$ will take if the time-dependent voltage is frozen at the value taken at that instant.
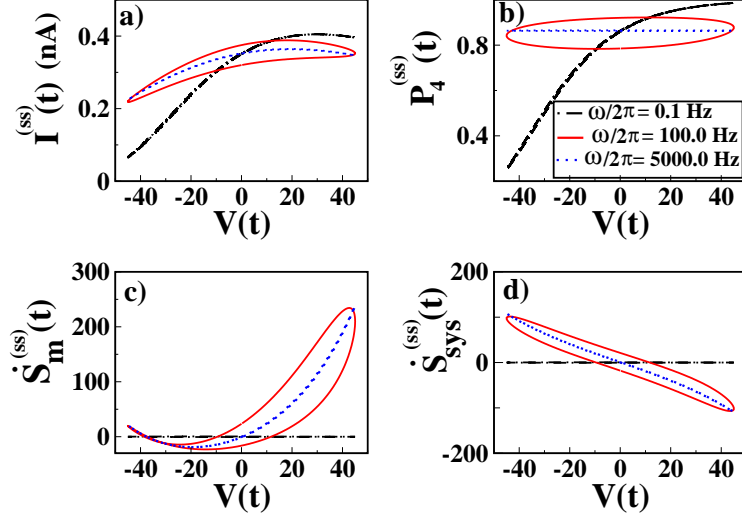
Figure 6.3: In figures (a)-(d), ionic current, $I^{(ss)}(t)$, probability of ion conducting state, $P_4^{(ss)}(t)$, medium entropy production rate, $\dot{S}_m^{(ss)}(t)$ and system entropy production rate, $\dot{S}_{sys}^{(ss)}(t)$ are plotted against oscillating voltage (sinusoidal) with frequency $\omega/2\pi = 0.1, 100.0$ and 5000.0 Hz, respectively at NESS over a time period. In all cases hysteretic behavior is observed which vanishes at low and high frequency domains.

Now similar kind of hysteretic behavior is present in the medium epr, $(\dot{S}_m^{(ss)}(t))$-voltage and also for the system epr$(\dot{S}_{sys}^{(ss)}(t))$-voltage plots as shown in Fig.6.3(c) and (d) at the non-equilibrium steady state for the same frequency values. Apart from the vanishing hysteresis loop area at the limiting situations of low and high frequencies, one can see from these plots that the values of both $\dot{S}_m^{(ss)}(t)$ and $\dot{S}_{sys}^{(ss)}(t)$ tend to zero as $\omega \to 0$ (shown here with $\omega/2\pi = 0.1$ Hz). However, at the high frequency limit, these quantities have finite values although the corresponding hysteresis disappears. $\dot{S}_m^{(ss)}(t)$-voltage plot becomes highly asymmetric in this limit whereas $\dot{S}_{sys}^{(ss)}(t)$-voltage plot is almost symmetric. This amounts to a finite value of total epr implying that the steady state is a non-equilibrium steady state (NESS). This is also true for any intermediate frequency value of the external voltage. Only at $\omega \to 0$ limit, all the entropy production rates tend to zero and the NESS tends to equilibrium.

For thorough analysis, we have plotted the total epr, $(\dot{S}_{tot}^{(ss)}(t))$ vs voltage at the NESS in Fig.6.4 at the frequencies mentioned in Fig.6.3. At the low frequency case
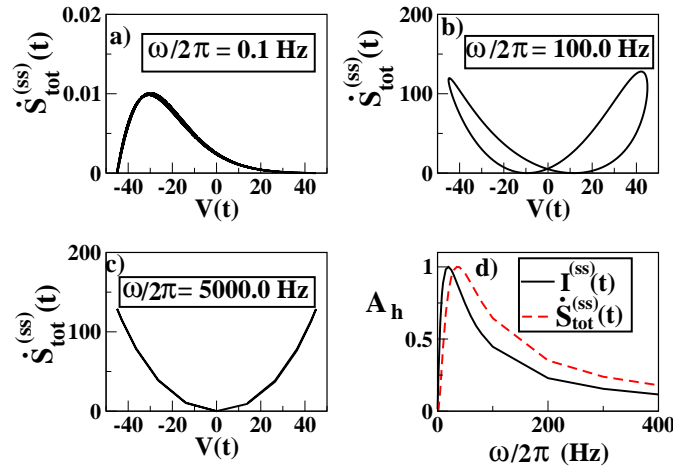
Figure 6.4: Total entropy production rate, $\dot{S}_{tot}^{(ss)}(t)$ is plotted against oscillating voltage, $V(t)$ at low, medium and high frequency values at steady state over a time period which are depicted in figures (a), (b) and (c), respectively. In figure (d), the normalized hysteresis loop area, A_h of current-voltage and $\dot{S}_{tot}^{(ss)}(t)$-voltage curves are plotted which passes through a maximum indicating that hysteresis is dynamic in nature.

with the vanishing hysteresis loop area, $\dot{S}_{tot}^{(ss)}(t)$ becomes almost zero at the extremum points of the voltage, $V_e = \pm V_a (= \pm 45$ mV$)$ as shown in Fig.6.4(a). Hence at these two points the system is only infinitesimally away from the equilibrium. Now at very low frequency of the external voltage variation, the system can always adjust to the instantaneous value of the voltage. Hence one can roughly picturize the points $V_e = \pm 45$ mV as the classical turning points of a simple pendulum where the pendulum becomes stationary momentarily. With increase in the frequency of $V(t)$, the response of the system to the external driving starts to lag. This is reflected in the plot with $\omega/2\pi = 100$ Hz in Fig.6.4(b) where $\dot{S}_{tot}^{(ss)}(t)$ becomes close to zero at points $0 < |V_e| < V_a$. At $\omega \to \infty$, the system totally fails to sense the ultrafast voltage variation and sees only the average voltage value, V_0. In this limiting case, the two points mentioned above merge at $V_e = V_0 = 0$ mV as shown in Fig.6.4(c) for $\omega/2\pi = 5000$ Hz. We have also shown the variation of the hysteresis loop area, A_h for the $\dot{S}_{tot}^{(ss)}(t)$ -voltage as well as the current-voltage hysteresis plots at the NESS in Fig.6.4(d). The $\dot{S}_{tot}^{(ss)}(t)$ -voltage and current-voltage hysteresis loop area is calculated numerically by integrating the value of $\dot{S}_{tot}^{(ss)}(t)$ and $I^{(ss)}(t)$ over a complete period of oscillating voltage, $V(t)$ according to the formula[181] $A_h = \oint \alpha(V(t))dV$, where α is $\dot{S}_{tot}^{(ss)}(t)$ or $I^{(ss)}(t)$. It is clear that the hysteresis loop area for the two plots maximize at close but different frequency values whereas at $\omega \to 0$ as well as at $\omega \to \infty$ limits, the hysteresis loop area goes to zero. Therefore, the hysteresis observed in $\dot{S}_{tot}^{(ss)}(t)$-voltage and $I^{(ss)}(t)$-voltage curves are dynamic in nature. Interestingly, a

close inspection of the $\dot{S}_{tot}^{(ss)}(t)$-voltage plot reveals that these two frequency limits of vanishing hysteresis are thermodynamically different as evident from the variation of total epr with dynamic values of $V(t)$. For the $\omega \to 0$ limit, the amplitude of $\dot{S}_{tot}^{(ss)}(t)$ tends to zero as already mentioned whereas in the $\omega \to \infty$ limit, its amplitude tends to a finite value.
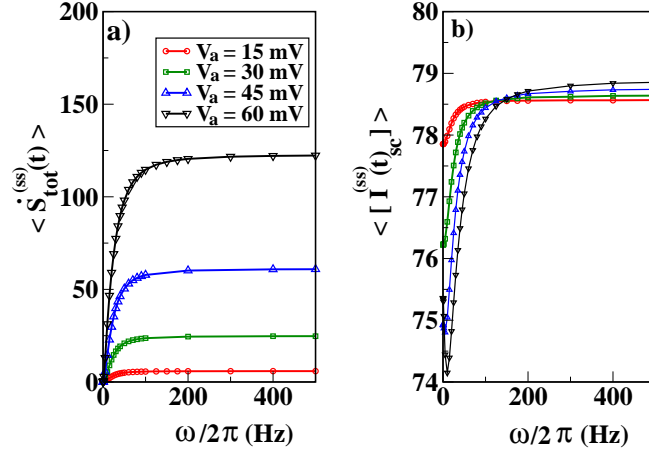
Figure 6.5: (a) Average entropy production rate over a period, $\langle \dot{S}_{tot}^{(ss)}(t) \rangle$ is plotted against frequency, $\omega/2\pi$ with amplitude, $V_a = 15, 30, 45$ and 60 mV. The value of $\langle \dot{S}_{tot}^{(ss)}(t) \rangle$ saturates at higher frequency values. (b) $\langle [I^{(ss)}(t)]_{sc} \rangle$ indicates the ionic current over a period scaled with $g(v)$ and is plotted against frequency, $\omega/2\pi$ with the same amplitudes. With increasing the amplitude values, $\langle [I^{(ss)}(t)]_{sc} \rangle$ becomes almost constant in the high frequency, however, $\langle \dot{S}_{tot}^{(ss)}(t) \rangle$ increases with increase in the value of amplitude, V_a. We have also plotted the values of $\langle \dot{S}_{tot}^{(ss)}(t) \rangle$ in the high frequency limit $(\omega \to \infty)$ obtained from Eq.(6.46) at various amplitudes denoted with the label 'theory' and compared with the numerical results.

For more clarification of the above statement, we have plotted the average total epr over a time period, $\langle \dot{S}_{tot}^{(ss)}(t) \rangle$ in Fig.6.5(a) at NESS as a function of the frequency of the external voltage with the average being defined as $\langle \dot{S}_{tot}^{(ss)}(t) \rangle = \frac{1}{T} \int_0^T \dot{S}_{tot}^{(ss)}(t) dt$. From the figure one can see that the average total epr increases steadily from zero at very low frequency to saturation at high frequency values. Therefore, the non-equilibrium steady state reached by the system is infinitesimally close to equilibrium at the $\omega \to 0$ limit whereas it is farthest from equilibrium at the $\omega \to \infty$ limit for the given parameters of the model system and the amplitude of the external voltage. This plot clearly shows that the low and high frequency limits associated with vanishing hysteresis are indeed thermodynamically distinct. Furthermore, in Fig.6.5(b), we have plotted the average current over a period, $\langle [I^{(ss)}(t)]_{sc} \rangle$ versus frequency at different voltage amplitudes. Here the 'sc' superscript indicates that the ionic current is scaled with the nonlinear conductance, $g(v)$. As the form of $g(V)$

is an experimentally determined empirical equation that can vary from experiment to experiment, so to obtain the general behavior of ionic current we have calculated the scaled current. From Fig. 6.5(b), it is observed that the average ionic current, $\langle [I^{(ss)}(t)]_{sc} \rangle$ increases to saturation with increase in the frequency value. It can be seen from Fig.6.5(b) that in the high frequency limit, $\langle [I^{(ss)}(t)]_{sc} \rangle$ becomes almost independent of amplitude. However, from Fig.6.5(a) it is evident that the high frequency limiting value of $\langle \dot{S}_{tot}^{(ss)}(t) \rangle$ increases sharply with increasing amplitude. In Fig.6.5(a) we have also shown this limiting value of $\langle \dot{S}_{tot}^{(ss)}(t) \rangle$ in the high frequency limit $(\omega \to \infty)$ obtained from the Eq.(6.46).
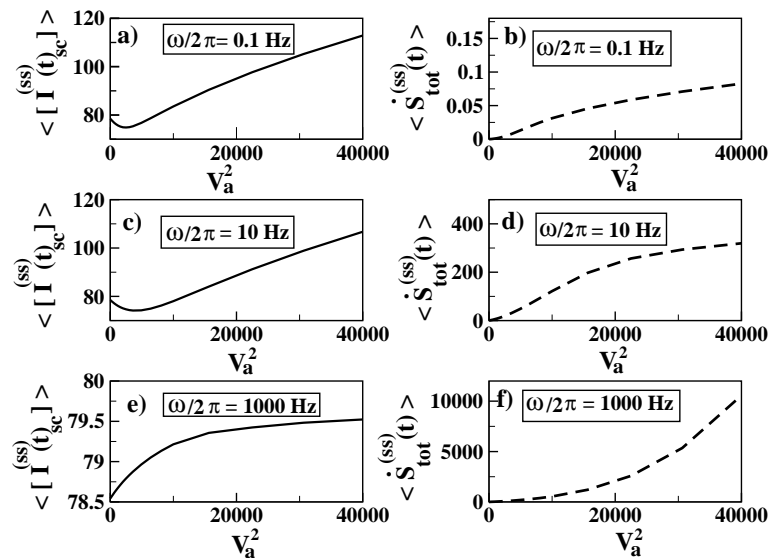
Figure 6.6: In figures (a),(c) and (e), average Ionic current over a period at steady state, $\langle [I^{(ss)}(t)]_{sc} \rangle$ is plotted against square of the amplitude, V_a^2 at low $(\omega/2\pi = 0.1$ Hz), medium $(\omega/2\pi = 10$ Hz) and high frequency $(\omega/2\pi = 1000$ Hz), respectively. Average entropy production rate over a period at steady state, $\langle \dot{S}_{tot}^{(ss)}(t) \rangle$ is plotted against V_a^2 with the same frequency values which are depicted in (b),(d) and (f), respectively.

For a clear understanding of the amplitude dependence of $\langle \dot{S}_{tot}^{(ss)}(t) \rangle$ and $\langle [I^{(ss)}(t)]_{sc} \rangle$, we have plotted these quantities as a function of V_a^2 for low, medium and high frequency values at long time limit which is shown in Fig 6.6. For oscillating voltage, V_a^2 is proportional to the energy supplied to the system and $\dot{S}_{tot}$ is a measure of dissipative flux from the system. From Fig 6.6(a) and (c) it is observed that at low and medium frequency, $\langle [I^{(ss)}(t)]_{sc} \rangle$ increases with increase in the value of V_a^2 after passing through a minima. Such behavior is generated due to the consideration of the current equation described in Eq.(6.54). However, at high frequency limit this tendency vanishes and $\langle [I^{(ss)}(t)]_{sc} \rangle$ saturates with increase in the value of V_a^2 which is shown in Fig 6.6(c). In Fig 6.6(b),(d) and (f), we have plotted $\langle \dot{S}_{tot}^{(ss)}(t) \rangle$ as a func-
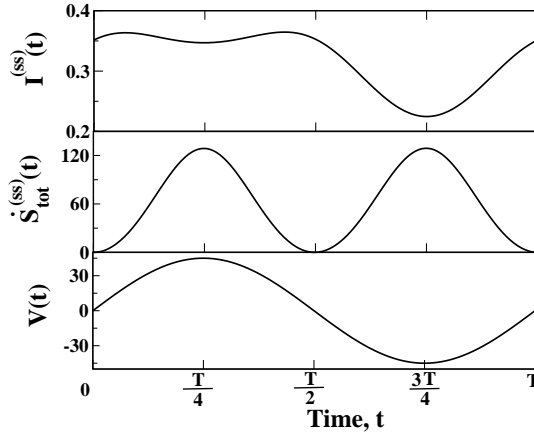
Figure 6.7: The ionic current, $I^{(ss)}(t)$, total entropy production rate, $\dot{S}_{tot}^{(ss)}(t)$ and oscillating voltage, $V(t)$ are plotted with time at $\omega/2\pi = 5000$Hz over an oscillation period at NESS. Time required to complete an oscillation cycle is same for $I^{(ss)}(t)$ but half for $\dot{S}_{tot}^{(ss)}(t)$ compared to that of voltage $V(t)$.

tion of V_a^2 at low, medium and high frequency, respectively. From close inspection, one can observe an interesting difference between the variations of $\langle[I^{(ss)}(t)]_{sc}\rangle$ and $\langle\dot{S}_{tot}^{(ss)}(t)\rangle$ as a function of V_a^2. In the low and medium frequency regions, $\langle[I^{(ss)}(t)]_{sc}\rangle$ goes on increasing with V_a^2 whereas $\langle\dot{S}_{tot}^{(ss)}(t)\rangle$ increases to a saturation. This is evident from Fig. 6.6(a),(b),(c),(d). However, in the high frequency limit the situation gets reversed as shown in Fig. 6.6(e),(f). Here $\langle\dot{S}_{tot}^{(ss)}(t)\rangle$ increases nonlinearly with V_a^2 but $\langle[I^{(ss)}(t)]_{sc}\rangle$ ultimately saturates. So the steep rise of the dissipation function with the input power is associated with a limiting ionic current whereas when the dissipation function gets saturated the current increases almost linearly as a function of input power. Hence the fraction of input energy that goes out from the system as unavailable energy governs the efficiency of the ion conduction.

We report another intriguing observation. We have plotted the ionic current, $I^{(ss)}(t)$, the total entropy production rate, $\dot{S}_{tot}^{(ss)}(t)$ and oscillating voltage, $V(t)$ at high frequency, $\omega/2\pi = 5000$Hz, over a period at steady state in Fig.6.7. In section 6.2.4, we have analytically shown that at high frequency limit $\dot{S}_{tot}^{(ss)}(t)$ oscillates with a time period which is half of the external voltage, $V(t)$. This analytical results is now verified by numerical analysis which is depicted in Fig.6.7(b). However, the time period of ionic current, $I^{(ss)}(t)$ is same as that of the external voltage which is depicted in Fig.6.7(a).

6.5   Conclusion

In view of the physiological significance of the hysteretic response, here we have given a non-equilibrium thermodynamic description of a voltage-gated *Shaker* Potas-

sium ion channel expressed in mammalian cells using the stochastic master equation. Starting from an experimentally proposed most suited five-state Markov process of a *Shaker* Potassium ion channel, here the traditional single parameter Hodgkin-Huxley equation is shown to be connected with the master equation corresponding to the stochastic transitions between the five conformational states at fixed voltage. The powered Boltzmann distribution of the steady state probability of ion-conducting state is also obtained from the master equation in this case. Now from thermodynamic analysis it is observed that for constant external voltage, the system reaches equilibrium, indicated by the vanishing total entropy production rate.

For oscillating voltage, the current as well as the entropy production rates show dynamic hysteresis with vanishing hysteresis loop area for very low and and very high frequency of the external voltage. However, by analyzing the total entropy production rate we have shown that the two limiting situations are thermodynamically different. At very low frequency limit, system remains close to equilibrium whereas, at high frequency it goes far away from equilibrium associated with a finite amount of dissipation. To find the efficiency of the ion current production, the non-equilibrium steady state(NESS) is characterized by the nonlinear dependence of the dissipation function with the power of the external field. A strong nonlinear dependence of unavailable energy flux with the input power dictates that an optimum limit of frequency of the oscillating voltage is necessary for a reasonable steady ionic current to appear. Another intriguing aspect is that the total entropy production rate oscillates at NESS with half of the time period of the external voltage in the limit of high frequency. We have also discussed on the extension of the present analysis to multiple ion channels which is easier to tackle experimentally. The non-equilibrium thermodynamical analysis done here for a Potassium-ion channel is also generically valid for other Markov processes of similar ion conduction problems, namely, sodium ion channels, ryanodine receptor and IP_3 receptors[179].

Bibliography

[1] M. Gudmand, S. Rocha, N. S. Hatzakis, K. Peneva, K. Mullen, D. Stamou, H. Uji-i, J. Hofkens, T. Bjornholm and T. Heimburg, Biophys. J., 98, 1873 (2010).

[2] S. Rocha, J. A. Hutchison, K. Peneva, A. Herrmann, K. Mullen, M. Skjot, C. I. Jorgensen, A. Svendsen, F. C. De Schryver, J. Hofkens and H. Uji-i, ChemPhysChem., 10, 151 (2009).

[3] O. G. Berg, and M. K. Jain, *Interfacial enzyme kinetics*, 1st ed., Wiley., New-York (2002).

[4] A. Kargol, A. Hosein-Sooklal, L. Constantin, and M. Przestalski, Gen. Physiol. Biophys., 23, 53 (2004).

[5] B. Sakmann, and E. Neher, *Single-Channel Recording* 2nd ed., Plenum Press, New York, (1995).

[6] H. Gumpp, E. M. Puchner, J. L. Zimmermann, U. Gerland, H. E. Gaub, and K. Blank, Nano Lett., 9, 3290 (2009).

[7] O. G. Berg, B.-Z. Yu, J. Rogers, and M. K. Jain, Biochemistry, 30, 7283 (1991).

[8] D. A. McQuarrie, J. Chem. Phys, 38, 433 (1963).

[9] D. A. McQuarrie, C. J. Jachimowski, and M. E. Russell, J. Chem. Phys, 40, 2914 (1964).

[10] D. A. McQuarrie, J. Appl. Prob., 4, 413 (1967).

[11] M. Vellela, and H. Qian, J. R. Soc. Interface, 6, 925 (2009).

[12] B. Das, and G. Gangopadhyay, J. Chem. Phys., 132, 135102 (2010).

[13] D. Andrieux, and P. Gaspard, J. Chem. Phys., 121, 6167 (2004).

[14] D. T. Gillespie, J. Comput. Phys. 22 (1976) 403.

[15] D. T. Gillespie, J. Phys. Chem. 81 (1977) 2340.

[16] B. Das, and G. Gangopadhyay, Chem. Phys., 393, 58 (2012).

[17] B. Das, K. Banerjee, and G. Gangopadhyay, J. Math. Chem., 50, DOI 10.1007/s10910-012-0099-2 (2012).

[18] K. Banerjee, B. Das, and G. Gangopadhyay, J. Chem. Phys., 136, 154502 (2012).

[19] O. G. Berg, M. H. Gelb , M. -D. Tsai, and M. K. Jain, Chem. Rev., 101, 2613 (2001).

[20] M. K. Jain, J. Rogers, O. Berg, and M. H. Gelb, Biochemistry, 30, 7340 (1991).

[21] F. Ghomashchi, T. O'Hare, D. Clary, and M. H. Gelb, Biochemistry, 30, 7298 (1991).

[22] F. Ghomashchi, B.-Z. Yu, O. Berg, M. K. Jain, and M. H. Gelb, Biochemistry, 30, 7318 (1991).

[23] T. Honger, K. Jorgensen, R. L. Biltonen, and O. G. Mouritsen, Biochemistry, 35, 9003 (1996).

[24] K. Jorgensen, and O. G. Mouritsen, Biophys. J., 95, 942 (1995).

[25] A. Halperin, O. G. Mouritsen, Eur. Biophys. J. 34 (2005) 967.

[26] I. Tinoco Jr., and C Bustamante, Biophys. Chem., 101, 513 (2002).

[27] C. Bustamante, Y. R. Chemla, N. R. Forde, and D Izhaky, Annu. Rev. Biochem., 73, 705 (2004).

[28] S. R. Koti Ainavarapu, A. P. Wiita, L. Dougan, E. Uggerud, and J. M. Fernandez, J. Am. Chem. Soc, 130, 6479 (2008).

[29] A. P. Wiita, R. K. Ainavarapu, H. H. Huang, J. M. Fernandez, Proc. Natl. Acad. Sci. U. S. A, 103, 7222 (2006).

[30] R. Szoszkiewicz, R. K. Ainavarapu, A. P. Wiita, R. Perez-Jimenez, J. M. Sanchez-Ruiz, J. M. Fernandez, Langmuir, 24, 1356 (2008).

[31] G. Bell, Science, 200, 618 (1978).

[32] G. Hummer, A. Szabo, Biophys. J, 85, 5 (2003)

[33] I. V. Gopich, A. Szabo, J. Chem. Phys, 124, 154712 (2006).

[34] T. Palmer, and P. Bonner, *Enzymes: Biochemistry, Biotechnology, and Clinical Chemistry*, 2nd ed., Horwood Publishing, West Sussex (2007).

[35] D. Voet and J. G. Voet, Biochemistry, 3rd ed., Wiley international Edition, USA (2004).

[36] G. S. Adair, J. Biol. Chem., 63, 529 (1925).

[37] J. Monod, J. Wyman, and J. P. Changeux, J. Mol. Biol., 12, 88 (1965).

[38] D. E. Koshland Jr., G. Nemethy, and D. Filmer, Biochemistry, 5, 365 (1966).

[39] H. Qian, and J. A. Cooper, Biochemistry, 47, 2211 (2008).

[40] J. Ricard, and A. Cornish-Bowden, Eur. J. Biochem., 166, 255 (1987).

[41] H. Qian, Biophys. J., 95, 10 (2008).

[42] A. Cornish, and A. L. Cardenas, J. Theor. Biol., 124, 1 (1987).

[43] C. Frieden, Annu. Rev. Biochem., 48, 471 (1979).

[44] K. E. Neet, and G. R. Ainslie, Methods Enzymol., 64, 192 (1980).

[45] D. L. Nelson, and M. M. Cox, *Lehninger Principles of Biochemistry*, 4th ed., Worth Publishers, New York (2004).

[46] G. M. Shepherd, *Neurobiology*, 3rd ed., Oxford university press, New York, Oxford (1994).

[47] A. L. Hodgkin, and A. F. Huxley, J. Physiol., 117, 500 (1952).

[48] W. N. Zagotta, T. Hoshi, and R. W. Aldrich, J. Gen. Physiol., 103, 321 (1994).

[49] E. Skaugen, and L. Walloe, Physiol. Scand., 107, 343 (1979).

[50] B. Hille, *Ion channels of excitable membranes*, 2nd Ed., Sinauer Associates, Sunderland, MA (1992).

[51] R. Nossal, and H. Lecar, *Molecular and cell Biophysics*, Addison- Wesley, Redwood City, CA (1991).

[52] L. J. DeFelice, and A. Isaac, J. Stat. Phys., 70, 339 (1992).

[53] R. F. Fox, and Y. Lu, Phys. Rev. E, 49, 3421 (1994).

[54] T. Hoshi, W. N. Zagotta, and R. W. Aldrich, J. Gen. Physiol., 103, 249 (1994).

[55] W. N. Zagotta, T. Hoshl, J. Dittman, and R. W. Aldrich, J. Gen. Physiol., 103, 279 (1994).

[56] M. M. Millonas, and D. A. Hanck, Phys. Rev. Lett., 80, 401 (1998).

[57] M. M. Millonas, and D. A. Hanck, Biophys. J., 74, 210 (1998).

[58] C. Bustamante, J. Liphardt, and F. Ritort, Physics Today, 58, 43 (2005).

[59] K. Singer, J. R. Statist. Soc. B, 15, 92 (1953).

[60] H. P. Lu, L. Xun, and X. S. Xie, Science, 282, 1877 (1998).

[61] B. P. English, W. Min, A. M. van Oijen, K. T. Lee, G. Luo, H. Sun, B. J. Cherayil, S. C. Kou, and X. S. Xie, Nat. Chem. Biol., 2, 87 (2006).

[62] J. Cao, Phys. Rev. E, 63, 041101 (2001).

[63] S. C. Kou, B. J. Cherayil, W. Min, B. P. English, and X. S. Xie, J. Phys. Chem. B, 109, 19068 (2005).

[64] H. Qian, and E. L. Elson, Biophys. Chem, 101, 565 (2002).

[65] W. Min, L. Jiang, J. Yu, S. C. Kou, H. Qian, and X. S. Xie, Nano Lett., 5, 2373 (2005).

[66] H. Qian, Annu. Rev. Phys. Chem., 58, 113 (2007).

[67] H. Qian, J.Phys Chem B, 110, 15063 (2006).

[68] H. Ge, and M. Qian, J. Chem. Phys., 129, 015104 (2008).

[69] A. Kargol, and K. Kabza, Phys. Biol., 5, 026003 (2008).

[70] T. Andersson, Math. Biosci., 226, 16 (2010).

[71] M. Delbruck, J. Chem. Phys. 8, 120 (1940).

[72] K. Ishida, Bull. Chem. Soc. Japan, 33, 1030 (1960).

[73] A. Bartholomay, Bull. Math. Biophys., 20,175 (1958).

[74] P. Gaspard, J. Chem. Phys., 120, 8898 (2004).

[75] H. A. Kramers, Physica, 7, 284 (1940).

[76] H. A. Kramers, Adv. Chem. Phys., 1, 361 (1958).

[77] A. Renyi, Magyar Tud. Akad. Alkalm. Mat. Int. Kozl., 2, 93 (1954).

[78] D. T. Gillespie, Physica A, 188, 404 (1992).

[79] D. T. Gillespie, Annu. Rev. Phys. Chem., 58, 35 (2007).

[80] T. Schmiedl, T. Speck, U. Seifert, J. Stat. Phys., 128, 77 (2007).

[81] T. J. Xiao, Z. Hou, H. Xin, J. Chem. Phys., 129, 114506 (2008).

[82] J. Luo, N. Zhao, B. Hu, Phys. Chem. Chem. Phys., 4, 4149 (2002).

[83] G. E. Crooks, J. Stat. Phys., 90, 1481 (1998).

[84] D. J. Evans, E. G. D. Cohen, and G. P. Morriss, Phys. Rev. Lett., 71, 2401 (1993).

[85] U. Seifert, Phys. Rev. Lett., 95, 040602 (2005).

[86] T. Hatano, and S. I. Sasa, Phys. Rev. Lett., 86, 3463 (2001).

[87] G. Gallavotti, Phys. Rev. Lett., 77, 4334 (1996).

[88] C. Jarzynski, Phys. Rev. Lett., 78, 2690 (1997).

[89] C. W. Gardiner, *Handbook of stochastic methods for physics, chemistry and the natural sciences* 2nd edn., New York, NY, Springer, (1985).

[90] J. Cao, Chem. Phys. Lett. 327 38(2000).

[91] G. G. Hammes, and C. W. Wu, Annu. Rev. Biophys. Bioeng., 3, 1 (1974).

[92] A. Goldbeter, Biophys. Chem., 4, 159 (1976).

[93] G. Weber, and S. R. Anderson, Biochemistry, 4, 1942 (1965).

[94] S. B. Long, E. B. Campbell, and R. MacKinnon, Science, 309, 897 (2005).

[95] E. M. Sevick, R. Prabhakar, S. R. Williams, and D. J. Searles, Annu. Rev. Phys. Chem., 59, 603 (2008).

[96] G. E. Crooks, Phys. Rev. E, 60, 2721 (1999).

[97] S. Lahiri, and A. M. Jayannavar, Eur. Phys. J. B, 69, 87 (2009).

[98] C. Maes, Sem. Poincare, 2, 29 (2003).

[99] M. Esposito, and C. Van den Broeck, Phys. Rev. E, 82, 011143 (2010).

[100] L. Jiu-li, C. Van den Broeck, and G. Nicolis, Z. Phys. B **56**, 165 (1984).

[101] G. Nicolis, and I. Prigogine, *Self-Organization in nonequilibrium Systems*, 1st ed., Willey, New York (1977).

[102] G. Nicolis, and I. Prigogine, Proc. Natl. Acad. Sci. (USA) **68**, 2102 (1971).

[103] G. Nicolis, J. Stat. Phys., 6, 195 (1972).

[104] M. Malek-Mansour, and G. Nicolis, J. Stat. Phys. **13**, 197 (1975).

[105] I. Sitkiewicz, K. E. Stockbauer, and J. M. Musser, Trends Microbiol., 15, 63 (2007).

[106] M. H. Gelb, M. K. Jain, A. M. Hanel, and O. G. Berg, Annu. Rev. Biochem., 64, 653 (1995) .

[107] T. Bayburt, B.-Z. Yu, H. -K. Lin, J. Browning, M. K. Jain, and M. H. Gelb, Biochemistry, 32, 573 (1993).

[108] D. P. Cherney, G. A. Myers, R. A. Horton, and J. M. Harris, Anal. Chem., 78, 6928 (2006).

[109] C. Leidy, L. Linderoth, T. L. Andresen, O. G. Mouritsen, K. Jorgensen, and G. H. Peters, Biophys. J., 90, 3165 (2006).

[110] R. Morales, E. Zavala, and M. S. Fernandez, Biochemistry and Molecular Biology International., 44, 1111 (1998).

[111] W. Xu, J. S. Kong, and P. Chen, J. Phys. Chem. C, 113, 2393 (2009).

[112] J. Martins, K. R. Naqvi, and E. Melo, J. Phys. Chem. B, 104, 4986 (2000).

[113] W. H. Press, S. A. Teukolsky, W. T. Vetterling, and B. P. Flannery, *Numerical Recipes in Fortran*, 2nd Ed., Cambridge university Press (1992).

[114] X. S. Xie, and H. P. Lu, J. Biol. Chem., 274, 15967 (1999).

[115] C. Bai, C. Wang, X. S. Xie, and P. G. Wolynes, Proc. Natl. Acad. Sci. USA., 96, 11075 (1999).

[116] A. Molski, Chem. Phys., 352, 276 (2008).

[117] J. Cao, and R. J. Silbey, J. Phys. Chem. B, 112, 12867 (2008).

[118] S. Yang, and J. Cao, J. Chem. Phys., 117, 10996 (2002).

[119] V. Namasivayam, R. G. Larson, D. T. Burke, and M. A. Burns, Anal. Chem., 75, 4188 (2003).

[120] J. Lin, R. Qi, C. Aston, J. Jing, T. S. Anantharaman, B. Mishra, O. White, M. J. Daly, K. W. Minton, J. C. Venter, and D. C. Schwartz, Science, 285, 1558 (1999).

[121] H. -W. Li, and E. S. Yeung, Anal. Chem., 77, 4374 (2005).

[122] M. Z. Kellermeyer, S. B. Smith, H. L. Granzier, and C. Bustamante, Science, 276, 1112 (1997).

[123] L. Tskhovrebova, J. Trinick, J. A. Sleep, and R. M. Simmons, Nature, 387, 308 (1997).

[124] M. Rief, M. Gautel, F. Oesterhelt, J. M. Fernandez, and H. E. Gaub, Science, 276, 1109 (1997).

[125] A. F. Oberhauser, P. E. Marszalek, H. P. Erickson, and J. M. Fernandez, Nature, 393, 181 (1998).

[126] U. Bockelmann, B. Essevaz-Roulet, and F. Heslot, Phys. Rev. E, 58, 2386 (1998).

[127] B. Essevaz-Roulet, U. Bockelmann, and F. Heslot, Proc. Natl. Acad. Sci. USA, 94, 11935 (1997).

[128] J. A. Spudich, Nature, 372, 515 (1994).

[129] H. Yin, M. D. Wang, K. Svoboda, R. Landick, S. M. Block, and J. Gelles, Science, 270, 1653 (1995).

[130] R. J. Davenport, G. J. L. Wuite, and R. Landick, Science, 287, 2497 (2000).

[131] M. Manosas, A. Mossa, N. Forns, J. M. Huguet, and F. Ritort, J. Stat. Mech., P02061 (2009).

[132] F. Ritort, Adv. Chem. Phys., 137, 31 (2008).

[133] J. L. Lebowitz, and H. Spohn, J. Stat. Phys., 95, 333 (1999).

[134] T. Schmiedl, and U. Seifert, J. Chem. Phys., 126, 044101 (2007).

[135] V. Blickle, T.Speck, L. Helden, U. Seifert, and C. Bechinger, Phys. Rev. Lett., 96, 070603 (2006).

[136] U. Seifert, Europhys. Lett., 70 (1), 36 (2005).

[137] I. Migneault, C. Dartiguenave, M. J. Bertrand, and K. C. Waldron, BioTechniques, 37, 790 (2004).

[138] N. G. Vankampen, *Stochastic processes in physics and chemistry*, Amsterdam, The Netherlands, Elsevier (1992).

[139] M. J. Buehler, and T. Ackbarow, *Computer Methods in Biomechanics and Biomedical Engineering*, 11, 595 (2008).

[140] J. J. Sines, and D. D. Hackney, Biochem. J., 243, 159 (1987).

[141] D. Collin, F. Ritort, C. Jarzynski, S. B. Smith, I. Tinoco Jr., and C. Bustamante, Nature, 437, 231 (2005).

[142] C. Jarzynski, Nature Phys., 7, 591 (2011).

[143] J. Liphardt, S. Dumont, S. B. Smith, I. Tinoco. Jr., and C. Bustamante, Science, 296, 1832 (2002).

[144] H. Wang, and G. Oster, Nature, 396, 279 (1998).

[145] D. M. Carberry, M. A. B. Baker, G. M. Wang, E. M. Sevick, and D. J. Evans, J. Opt. A: Pure Appl. Opt., 9, S204 (2007).

[146] A. Mossa, S. De Lorenzo, J. M. Huguet, and F. Ritort, J. Chem. Phys., 130, 234116 (2009).

[147] F. Ritort, C. Bustamante, and I. Tinoco Jr., Proc. Natl. Acad. Sci. USA, 99, 13544 (2002).

[148] C. Tietz, S. Schuler, T.Speck, U. Seifert, and J. Wrachtrup, Phys. Rev. Lett., 97, 050602 (2006).

[149] A. Levitzki, and D. E. Koshland Jr., Proc. Natl. Acad. Sci. USA, 62, 1121 (1969).

[150] H. Abeliovich, Biophys. J., 89, 76 (2005).

[151] J. N. Weiss, FASEB J., 11, 835 (1997).

[152] D. C. Gadsby, R. F. Rakowski, and P. Deweer, Science, 260, 100 (1993).

[153] N. Bindslev, *Drug-acceptor interactions: modeling theoretical tools to test and evaluate experimental equilibrium effects*, 1st ed., Co-Action Publishing, Sweden, (2008).

[154] A. F. Kolodziej, T. Tan, and D. E. Koshland Jr., Biochemistry, 35, 14782 (1996).

[155] J. J. Wyman, Adv. Protein Chem., 19, 223 (1964).

[156] F. Bezanilla, IEEE Transactions on Nanobioscience, 4, 34 (2005).

[157] Y. Pichon, L. Prime, P. Benquet, and F. Tiaho, Eur. Biophys. J., 33, 211 (2004).

[158] O. Yifrach, Biophys. J., 87, 822 (2004).

[159] M. C. Menconi, M. Pellegrini, M. Pellegrino, and D. Petracchi, Eur. Biophys. J., 27, 299 (1998).

[160] G. Bertotti, and I. D. Mayergoyz, *The Science of Hysteresis: Mathematical modeling and applications*, 1st ed., Academic Press, (2006).

[161] C. N. Luse, and A. Zangwill, Phys. Rev. E, 50, 224 (1994).

[162] Y. L. He, and G. C. Wang, Phys. Rev. Lett., 70, 2336 (1993).

[163] B. K. Chakrabarty, and M. Acharyya, Rev. Mod. Phys., 71, 847 (1999).

[164] M. C. Mahato, and S. R. Shenoy, Phys. Rev. E, 50, 2503 (1994).

[165] W. Zhou, F. S. Cayabyab, P. S. Pennefather, L. C. Schlichter, and T. E. DeCoursey, J. Gen. Physiol., 111, 781 (1998).

[166] D. Fologea, E. Krueger, Y. I. Mazur, C. Stith, R. Henry, Y. Okuyama, and G. J. Salamo, Biomembranes, 1808, 12 (2011).

[167] R. Mannikko, S. Pandey, H. P. Larsson, and F. Elinder, J. Gen. Physiol., 125, 305 (2005).

[168] M. A. Pustovoit, A. M. Berezhkovskii, and S. M. Bezrukov, J. Chem. Phys., 125, 194907 (2006).

[169] Y. Jiang, A. Lee, J. Chen, V. Ruta, M. Cadene, B. T. Chait, and R. MacKinnon, Nature, 423, 33 (2003).

[170] A. Nekouzadeh, J. R. Silva, and Y. Rudy, Biophys. J., 95, 3510 (2008).

[171] L. M. Mannuzzu, M. M. Moronne, and E. Y. Isacoff, Science, 271, 213 (1996).

[172] W. R. Silverman, B. Roux, and D. M. Papazian, Proc. Natl. Acad. Sci. USA., 100, 2935 (2003).

[173] J. P. Keener, J. Math. Biol., 58, 447 (2009).

[174] I. Goychuk, and P. Hanggi, Physica A, 325, 9 (2003).

[175] J. P. Keener, J. Math. Biol., 60, 473 (2010).

[176] T. L. Hill, J. Chem. Phys., 54, 34 (1971).

[177] L. W. Shapiro, and D. Zeilberger, J. Math. Biol., 15, 351 (1982).

[178] T.L. Hill, *Cooperativity Theory in Biochemistry-Steady-State and Equilibrium Systems*, Springer-Verlag, New York, (1985).

[179] J. P Keener and J. Sneyd *Mathematical Physiology*, 1st ed., Springer, New York, (1998).

[180] J. Schnakenberg, Rev. Mod. Phys., 48, 571 (1976).

[181] M. Das, D. Mondal, and D. S. Ray, J. Chem. Phys., 136, 114104 (2012).

List of Publications

1. **Master equation approach to single oligomeric enzyme catalysis: Mechanically controlled further catalysis**,
   B. Das and G. Gangopadhyay,
   J. Chem. Phys., **132**, 135102 (2010).

2. **Stochastic theory of interfacial enzyme kinetics: A kinetic Monte Carlo study**,
   B. Das and G. Gangopadhyay,
   Chem. Phys., **393**, 58 (2012).

3. **Entropic estimate of cooperative binding of substrate on a single oligomeric enzyme: An index of cooperativity**
   K. Banerjee, B. Das and G. Gangopadhyay,
   J. Chem. Phys.,**136**, 154502 (2012).

4. **Entropy production of a mechanically driven single oligomeric enzyme: a consequence of fluctuation theorem**,
   B. Das, K. Banerjee and G. Gangopadhyay,
   J. Math. Chem., (in press)
   Online: Doi 10.1007/s 10910-012-0099-2 (2012).

5. **Entropy hysteresis and nonequilibrium thermodynamic efficiency of ion conduction in voltage-gated potassium ion channel**,
   B. Das, K. Banerjee and G. Gangopadhyay,
   Phys. Rev. E, (in press).

6. **On the cooperativity of ion channel dynamics: activation free energy of Shaker potassium ion channel**
   K. Banerjee, B. Das and G. Gangopadhyay (**Communicated**)*.

7. **Memory of voltage-gated potassium ion channel: dynamic and thermodynamic features**,
   K. Banerjee, B. Das and G. Gangopadhyay (**Communicated**)*.

   * not included in the thesis